DEPARTAMENTO DE GEOGRAFÍA – UNIVERSIDAD DE ALCALÁ

BURN SEVERITY ESTIMATION FROM REMOTELY SENSED DATA USING SIMULATION MODELS

Tesis doctoral presentada por

Angela DE SANTIS

bajo la dirección del

Dr. Emilio CHUVIECO SALINERO

Catedrático de Análisis Geográfico Regional

Programa de Doctorado en Cartografía, S.I.G. y Teledetección del Departamento de Geografía

Alcalá de Henares, abril de 2008

Ai miei genitori e a zio Renato con tutto il mio affetto

AGRADECIMIENTOS

En primer lugar quiero agradecer a mi director de tesis, ***Emilio Chuvieco****, por haberme dado la posibilidad de formar parte del grupo de investigación del Departamento de Geografía hace cuatro años. Sin temor a exagerar, puedo decir que esta decisión cambió toda mi vida. En estos años me ha demostrado siempre un gran apoyo y ha sido para mí una guía y un ejemplo a seguir.*

Otro agradecimiento especial es para ***Javier Salas****. Gracias a su ayuda he podido conseguir mi beca/contrato y he sobrevivido al "largo y tedioso" proceso de homologación de mi título de licenciada. Además le agradezco su amistad y disponibilidad infinita.*

Gracias a ***Pilar Martín****, por "los juguetes radiométricos", las imágenes SPOT de Galicia, y sobre todo por estar a mi lado.*

También me gustaría agradecer al resto de ***los profesores del Departamento*** *por hacerme sentir parte de este maravilloso grupo de profesionales.*

Siempre en el ámbito de la Universidad, quiero agradecer de corazón a ***todos mis compañeros (más conocidos como el "comando tupper"),*** *por compartir conmigo alegrías y angustias, trabajo de campo y "momentos tupper". Gracias chicos!*

Además me gustaría dar las gracias a ***José Ángel****, el forestal que ha sido mi "ángel de la guarda" en el trabajo de campo en el incendio de Guadalajara, y os puedo asegurar que lo necesitaba!*

Ya a nivel personal, quiero agradecer a ***mis padres y a toda mi familia*** *todos sus esfuerzos. Siempre han estado a mi lado, anteponiendo mi felicidad a las ganas de tenerme cerca. Han seguido cada paso de mi vida, apoyándome pero dejándome libre de decidir. Lo que soy y lo que estoy consiguiendo se lo debo a ellos. No creo que existan palabras que puedan expresar del todo lo que significan para mí.*

A livello personale, voglio ringraziare ***i miei genitori e tutta la mia famiglia*** *per i loro sforzi che hanno permesso la realizzazione del mio sogno. Sono stati al mio fianco sempre, anteponendo la mia felicitá alla voglia di avermi vicino. Hanno seguito ogni passo della mia vita, appoggiandomi peró lasciandomi libera di decidere. Quello che sono e gli obiettivi che sto raggiungendo, lo devo a loro. Non credo che esistano parole che possano esprimere tutto quello che significano per me.*

Un lugar especial en estos agradecimientos es para ***Patrick.*** *Gracias por estar a mi lado siempre, por tus ánimos en los momentos difíciles, por alegrarte conmigo en los buenos momentos, por tus consejos personales y profesionales, por las revisiones de los artículos, por tu ayuda en el trabajo de campo y laboratorio, por aguantar mis nervios (..y han sido muchos!) en las fases críticas del Doctorado, por creer en mí y sobre todo por quererme.*

Y por último un agradecimiento a mi mejor amiga ***Elena.*** *Desde hace más de diez años, lo hemos compartido todo y nos hemos apoyado en las decisiones difíciles. Gracias Elena por estar presente siempre y "con cualquier medio disponible". Eres un ejemplo de fuerza de ánimo y de positividad. Leg on! Leg on!*

Es difícil resumir en pocas páginas los agradecimientos a todas las personas que han influido en mi vida en este momento tan importante. Así que pido disculpas por no mencionarlos a todos o por no hacerlo con la intensidad que se merecen.

Gracias a todos los que han compartito conmigo una parte de este largo camino.

De corazón,

Angela

"El coraje de imaginar

alternativas es nuestro

recurso más grande"

Daniel J. Boorstin

INDEX

RESUMEN

Estimación de los niveles de severidad de los incendios forestales mediante la utilización de modelos de simulación e imágenes de satélite

Los incendios forestales representan un importante factor de estrés para los ecosistemas, especialmente cuando se altera su frecuencia y/o intensidad. Sus principales efectos negativos son: la pérdida de biomasa vegetal, la degradación del suelo (Doerr *et al.*, 2006), y las emisiones de gas de efecto invernadero (Andreae and Merlet, 2001).

La gestión de las áreas quemadas tiene como objetivos principales la minimización de la erosión (mitigación) y la disminución del tiempo de recuperación del ecosistema afectado por el fuego (recuperación) (Miller and Yool, 2002). Después de la estación de incendios de verano, las lluvias otoñales pueden empeorar los efectos negativos de los incendios, reforzando la erosión y la degradación del suelo. Por estas razones, conviene que la evaluación de daños se haga pocas semanas después del incendio. Lógicamente, en este contexto es fundamental poder concentrar los recursos en las zonas de alta prioridad (Miller and Yool, 2002). Debido a que los incendios afectan un amplio rango de escalas espaciales y temporales, la interpretación de los factores causales, de los efectos del incendio y de la respuesta del ecosistema representan un reto actual para investigadores y gestores (Lentile *et al.*, 2006).

Para aclarar la compleja interacción entre incendios y ecosistemas, se pueden describir dos diferentes ordenes de efectos del fuego (Key, 2006). Justo después de la extinción del incendio, los efectos a corto plazo (*first-order effects*) hacen referencia a las consecuencias ecológicas en los componentes biofísicos que existían antes del incendio (Key and Benson, 2005), mientras que los efectos a largo plazo (*second-order effects*) describen cómo el ecosistema se recupera del impacto del fuego (Kasischke *et al.*, 2007). Ambos efectos a corto y largo plazo sobre vegetación y suelo, pueden ser estimados en términos de **severidad** (*burn severity* en la terminología anglosajona) (Jain, 2004; Key and Benson, 2005; Lentile *et al.*, 2006; van Wagtendonk *et al.*, 2004; White *et al.*, 1996). El conocimiento detallado de los niveles de daño y de su distribución dentro del área quemada (*burn severity map*) representa un factor clave para: cuantificar el impacto del fuego sobre el ecosistema (van Wagtendonk *et al.*, 2004), seleccionar y dar orden de prioridad a los tratamientos aplicados en campo (Bobbe *et al.*, 2001; Patterson and Yool, 1998), planificar y monitorear la restauración y la recuperación de la

vegetación y procurar información que se utilizará como referencia para futuros análisis (Brewer *et al.*, 2005).

La severidad de un incendio está directamente relacionada con la intensidad y el tiempo de residencia del fuego. En incendios muy intensos, con una elevada liberación de energía en el frente de llamas, o en aquellos que se propagan lentamente y cuentan con periodos largos de quema, se destruyen buena parte de los elementos vitales de las plantas y de la materia orgánica del suelo, lo que supone una pérdida de protección del suelo y una regeneración posterior más lenta. Las estrategias de reproducción de las plantas son también claves en la evolución posterior al fuego, ya que las germinadoras requieren disponer de un banco de semillas en buen estado, mientras las rebrotadoras están mejor adaptadas a fuegos periódicos (Calvo *et al*., 2003; Díaz-Delgado *et al.*, 2003; Generalitat, 1988; Moreno and Oechel, 1991; Navarro *et al*., 1996) .

Habitualmente, la severidad del fuego se evalúa según el grado de carbonización de los diferentes estratos vegetales, y la proporción carbón/ceniza en la capa más superficial del suelo. Existen varios métodos de estimación disponibles en la literatura, principalmente apoyados en trabajo de campo (Moreno and Oechel, 1989; Pérez and Moreno, 1998). El inventario de campo puede realizarse poco después del fuego (evaluación inmediata), o varios meses después (evaluación a medio plazo). La dificultad para abarcar un amplio territorio a partir de observaciones de campo ha llevado a diversos autores a plantearse el empleo de imágenes de satélite en la cartografía de niveles de severidad, de cara a garantizar una cobertura actualizada y completa del territorio afectado (Cocke *et al.*, 2005; Díaz-Delgado *et al.*, 2003; Parra and Chuvieco, 2005; van Wagtendonk *et al.*, 2004). El principal reto en el empleo de la teledetección en los estudios de severidad del fuego es demostrar que los niveles de daño están asociados a la variación espectral que pueda recoger el sensor. Esto supone explorar la discriminabilidad teórica entre distintos niveles de severidad, por ejemplo usando modelos de transferencia radiativa (Chuvieco *et al.*, 2006; Pereira *et al.*, 2004). Una vez que se demuestra la sensibilidad teórica de las distintas bandas de reflectividad, habría que constatar si disponemos de sensores con el suficiente nivel de detalle (resolución espacial y espectral) para evaluar la severidad de una manera más o menos automática.

La mayor parte de los estudios de teledetección y severidad del fuego actualmente disponibles están basados en ajustes empíricos, apoyados en parcelas de campo tomadas poco después del incendio (Cocke *et al.*, 2005; Epting *et al.*, 2005; Miller and Yool, 2002; van Wagtendonk *et al.*, 2004). Los modelos empíricos son relativamente sencillos de calcular, pero tienen poca capacidad de generalización, ya que consideran las condiciones locales donde se ajustó el modelo.

Por esta razón, planteamos como **objetivo general** de esta tesis doctoral desarrollar una metodología alternativa a los estudios empíricos, que fuera semi-automática y generalizable de cara a estimar los niveles de severidad a corto plazo a partir de datos de satélite. La metodología propuesta se basa en el uso de modelos de simulación de transferencia radiativa (RTM), que intentan estimar la reflectividad procedente de una determinada cubierta a partir una serie de asunciones físicas (Jacquemoud *et al.*, 1996).

Cuando estos modelos se usan de modo directo, pueden variarse los parámetros de entrada del modelo para simular el efecto que esos parámetros tienen sobre la reflectividad que medimos con teledetección. Esto ayuda a entender mejor la acción de esos factores (características bioquímicas de la hoja, cantidad, distribución geométrica, reflectividad del suelo, etc.). Estos modelos también pueden usar en modo inverso, lo que permite estimar los mismos factores de entrada a partir de la reflectividad observada por el sensor, habitualmente manteniendo algunos constantes o extrayéndolos de otras fuentes (Jacquemoud *et al.*, 2000).

Hasta el momento, los RTMs no se han aplicado extensamente al análisis de áreas quemadas, orientándose los pocos trabajos publicados a la determinación de quemado/no quemado (Pereira *et al.*, 2004; Roy *et al.*, 2002). Solo Chuvieco *et al.* (2006) plantearon el uso de modelos de simulación en modo directo para la cartografía de niveles de severidad, mediante un enlace entre dos modelos, de hoja (PROSPECT; Jacquemoud, 1990) y de dosel (Kuusk; Kuusk, 2001), empleados para simular diversos escenarios de daño.

Continuando en esta línea, iniciamos nuestra tesis doctoral, que pretendía explorar las posibilidades de inversión de estos modelos, y compararlos con los resultados de ajustes empíricos sobre zonas de vegetación mediterránea. Para abordar este objetivo general, se definieron cinco objetivos específicos, tal como se detallan en la tabla 1. En primer lugar (objetivo I, tabla 1), se comparó la precisión en la estimación de la severidad de los modelo empíricos tradicionales con el modelo de simulación propuesto por Chuvieco *et al.* (2006, *primer escenario*). Este estudio confirmó que los modelos de simulación permiten una mejor estimación de la severidad sobre todo para valores de daño muy bajo y muy altos. Sin embargo, para valores intermedios ambas técnicas presentaban errores considerables.

En consecuencia, planteamos como segundo objetivo (tabla 1) intentar mejorar el modelo de simulación existente, para mejorar la estimación de los rangos intermedios de severidad. Para ello, se extendió la simulación presentada en Chuvieco et. al. (2006) incluyendo un rango más amplio de escenarios y condiciones de entrada. Se simularon cinco escenarios distintos:

1- *Sencillo*: se asume que el incendio provoca simultáneamente la consumición de las hojas y su cambio de color (de verde a marrón).

2- *Extendido*: se supone que el fuego puede o consumir las hojas, o hacerles cambiar de color o las dos cosas al mismo tiempo.
3- *Multitemporal*: se modelan cambios en color de las hojas y cobertura a partir de condiciones iniciales fijadas.
4- *Supervisado*: se seleccionan las combinaciones de parámetros de entrada más comunes, basándose en la experiencia de campo.

Los mejores resultados se obtuvieron con este último escenario, aunque todavía se registraron importantes errores de sub-estimación.

Para intentar resolver estos problemas, se siguieron, por lo tanto, dos líneas paralelas:

a. Por un lado (objetivo III, tabla 1), se modificó el índice de campo para que se ajustara mejor a la validación/calibración de métodos que utilizan imágenes de satélite.
b. Por otro (objetivo IV, tabla 1), se propuso emplear un nuevo modelo de simulación, con un componente geométrico (GeoSail; Huemmrich, 2001).

Se comprobó que el nuevo índice de referencia para estimar severidad (que denominamos GeoCBI) se ajusta mejor a la reflectividad registrada por los sensores remotos y representa una buena referencia para poder validar las técnicas de estimación de severidad que utilizan imágenes de satélite.

Por su parte, las nuevas simulaciones basadas en el modelo Prospect-Geosail muestran un muy buen ajuste en tres áreas de estudio, recientemente afectadas por grandes incendios, lo que confirma que la inversión del modelo de simulación es la técnica más adecuada para estimar la severidad en el rango continuo del índice de campo (entre 0 y 3).

Por último (objetivo V, tabla 1), se identificó del sensor comercial más adecuado para la estimación de la severidad. Para ello, se llevó a cabo un ensayo con imágenes de cinco distintos sensores (SPOT 5, Landsat TM, AWIFS, MERIS y MODIS) en el mismo incendio. Finalmente, el Landsat TM resultó ser el sensor más adecuado, ya que representa el mejor compromiso entre resolución espectral y espacial.

Cada objetivo específico ha dado lugar a publicaciones en revistas con sistema de revisión externo (tabla 1).

En conclusión, en esta tesis doctoral se ha identificado y desarrollado una nueva técnica que permite estimar la severidad con mejor ajuste respecto a las técnicas tradicionales, además se ha validado en tres aéreas distintas (en España y Portugal), se ha propuesto un nuevo índice de campo y se ha identificado el sensor comercial más apropiado para la estimación de la severidad, por lo que estimo que la contribución realizada es relevante para el grado académico al que aspiro.

Tabla 1. Esquema descriptivo del desarrollo del proyecto de tesis y de las publicaciones realizadas.

OBJETIVO ESPECÍFICO	PUBLICACIÓN CORRESPONDIENTE (*)
I. Comparar las técnicas empíricas tradicionales con la inversión de los modelos de transferencia radiativa.	De Santis, A. and Chuvieco, E. (2007). Burn severity estimation from remotely sensed data: Performance of simulation versus empirical models. *Remote Sensing of Environment.* Vol. 108, pag. 422-435.
II. Intentar mejorar la estimación del modelo de simulación.	Chuvieco, E., De Santis A., D. Riaño and K. Halligan (2007). Simulation approaches for burn severity estimation using remotely sensed images. Fire Ecology 3(1): 129-150.
III. Mejorar el índice de campo para ajustarlo a la validación/calibración de métodos que utilizan imágenes de satélite.	De Santis, A. and Chuvieco, E. (2008). GeoCBI: a modified version of the Composite Burn Index to estimate burn severity for remote sensing applications. *Remote Sensing of Environment, under review.*
IV. Propuesta de un nuevo modelo de simulación (geométrico), validado en tres áreas distintas.	De Santis, A., Chuvieco, E. and Vaughan P.J. (2008). Short-term assessment of burn severity using the inversion of the GeoSail model. *Remote Sensing of Environment, under review.*
V. Identificación del sensor comercial más adecuado para la estimación de la severidad: ensayo con imágenes de cinco distintos sensores correspondientes al mismo incendio.	De Santis, A. and Chuvieco, E. (2008). Análisis comparativo de sensores espaciales para la cartografía de la severidad en el incendio de Riba de Saelices (Guadalajara). *Revista de Teledetección*, aceptado.

(*) Angela De Santis es el autor de los artículos citados y ha llevado a cabo todas las fases de los estudios. Excepción hecha por el articulo II en el cual: Emilio Chuvieco ha sido el responsable del planteamiento y de la metodología; Angela De Santis ha colaborado en el planteamiento y ha realizado las inversiones de los modelos y la verificación; David Riaño se ha ocupado de la generación de los modelos de simulación y Kerry Halligan ha programado una rutina que ha permitido automatizar algunas tareas. En el artículo IV, Patrick Vaughan ha colaborado en la revisión del artículo.

Referencias

Andreae, M.O. and Merlet, P. (2001), Emission of trace gases and aerosols from biomass burning, *Global Biogeochemical Cycles*. 15(4): 955-966.

Bobbe, T., Finco, M.V., Quayle, B., Lannom, K., Sohlberg, R., Parsons, A. (2001). Field Measurements for the Training and Validation of Burn Severity Maps from Spaceborne, Remotely Sensed Imagery, USDA Forest Service, Remote Sensing Applications Center, Salt Lake City, Utah.

Brewer, C.K., Winne, J.C., Redmond, R.L., Opitz, D. W., Mangrich, M.V. (2005), Classifying and Mapping Wildfire Severity: A Comparison of Methods, *Photogrammetric Engineering and Remote Sensing*. 71(11): 1311-1320.

Calvo, L., Santalla, S., Marcos, E., Valbuena, L., Tárrega, R. and Luis, E. (2003), Regeneration after wildfire in communities dominated by Pinus pinaster, an obligate seeder, and in others dominated by Quercus pyrenaica, a Typical resprouter, *Forest Ecology and Management*. 184: 209-223.

Chuvieco, E., Riaño, D., Danson, F.M., Martín, P. (2006), Use of a radiative transfer model to simulate the post-fire spectral response to burn severity, *Journal of Geophysical Research*. 111(G04S09): doi: 10.1029/2005JG000143.

Cocke, A.E., Fule, P.Z. and Crouse, J.E. (2005), Comparison of burn severity assessments using Differenced Normalized Burn Ratio and ground data, *International Journal of Wildland Fire*. 14: 189-198.

Díaz-Delgado, R., Lloret, F., Pons, X. (2003), Influence of fire severity on plant regeneration by means of remote sensing imagery, *International Journal of Remote Sensing*. 24(8): 1751-1763.

Doerr, S.H., Shakesby, R.A., Blake, W.H., Chafer, C.J., Humphreys, G.S., Wallbrink, P.J. (2006), Effects of differing wildfire severities on soil wettability and implications for hydrological response, *Journal of Hydrology*. 319: 295-311.

Epting, J., Verbyla, D.L. and Sorbel, B. (2005), Evalation of remotely senses indices for assessing burn severity in interior Alaska using Landsat TM and ETM+, *Remote Sensing of Environment*. 96: 328-339.

Generalitat, V. (1988), Respuesta y adaptación de la vegetación al fuego. In: *Los incendios forestales en la Comunidad Valenciana.* Generalitat Valenciana, Conselléria d'agricultura, Valencia, pp. 49-55.

Huemmrich, K.F. (2001), The GeoSail model: a simple addition to the SAIL model to describe discontinuous canopy reflectance, *Remote Sensing of Environment*. 75: 423-431.

Jacquemoud, S. (1990), PROSPECT: a model to leaf optical properties spectra, *Remote Sensing of Environment*. 34: 74-91.

Jacquemoud, S., Ustin, S.L., Verdebout, J., Schmuck, G., Andreoli, G. and Hosgood, B. (1996), Estimating Leaf Biochemistry Using the PROSPECT Leaf Optical Properties Model, *Remote Sensing of Environment*. 56: 194-202

Jacquemoud, S., Bacour, C., Poilve, H. and Frangi, J.P. (2000), Comparison of Four Radiative Transfer Models to Simulate Plant Canopies Reflectance: Direct and Inverse Mode, *Remote Sensing of Environment*. 74: 471-481.

Jain, T.B. (2004), Confused meanings for common fire terminology can lead to fuels mismanagement. A new framework is needed to clarify and communicate the concepts, *Wildfire*. july-aug: 22-26.

Kasischke, E., Hoy, E.E., French, N.H.F., Turetsky, M.R., (2007). Post-fire evaluation of the effects of fire on the environment using remotely-sensed data. In: C.C.-M. Ioannis Z. Gitas (Editor), 6th International Workshop of the EARSel Special Interest Group on Forest Fires: Advances in Remote Sensing and GIS applications in forest fire managment. Torwards an operational use of Remote Sensing in Forest Fire Managment. European Communities, Thessaloniki, Greece, pp. 34-52.

Key, C.H. (2006), Ecological and sampling constraints on defininf landscape fire severity, *Fire Ecology*. 2(2): 34-59.

Key, C.H. and Benson, N. (2005), Landscape Assessment: Ground measure of severity, the Composite Burn Index; and Remote sensing of severity, the Normalized Burn Ratio. In: *FIREMON: Fire Effects Monitoring and Inventory System* (D.C. Lutes, R.E. Keane, J.F. Caratti, C.H. Key, N.C. Benson and L.J. Gangi, Eds.), USDA Forest Service, Rocky Mountain Research Station, Gen. Tech. Rep. RMRS-GTR-164, Ogden, UT, pp. CD:LA1-LA51.

Kuusk, A. (2001), A two-layer canopy reflectance model, *Journal of Quantitative Spectroscopy & Radiative Transfer*. 71: 1 –9.

Lentile, L.B., Holden, Z. A., Smith, A.M.S., Falkowski, M. J., Hudak, A.T., Morgan, P., Lewis, S.A., Gessler, P.E., Benson, N. C. (2006), Remote sensing techniques to assess active fire characteristics and post-fire effects, *International Journal of Wildland Fire*. 15: 319-345.

Miller, H.J. and Yool, S.R. (2002), Mapping forest post-fire canopy consumption in several overstory types using multi-temporal Landsat TM and ETM data, *Remote Sensing of Environment*. 82: 481–496.

Moreno, J.M. and Oechel, W.C. (1989), A Simple Method for estimating fire intensity after a burn in California Chaparral, *Acta Ecologica (Ecologia plantarum)*. 10(1): 57-68.

Moreno, J.M. and Oechel, W.C. (1991), Fire intensity effects on germination of shrubs and herbs in southern California chaparral, *Ecology*. 72(6): 1993-2004.

Navarro, R.M., Navarro, C., Salas, F.J., González, M.P. and Abellanas, B., (1996). Regeneración de la Vegetación después de un Incendio. Aplicación de Imágenes Landsat-TM a su caracterización y seguimiento: propuesta metodológica y desarrollo parcial, Seminario sobre Nuevas Tecnologías contra Incendios Forestales. ICONA, Madrid, pp. 1-13.

Parra, A. and Chuvieco, E. (2005), Assessing burn severity using Hyperion data. In: *Proceedings of the 5th International Workshop on Remote Sensing and GIS applications to Forest Fire Management: Fire Effects Assessment* (J. Riva, F. Pérez-Cabello and E. Chuvieco, Eds.), Universidad de Zaragoza, GOFC-GOLD, EARSeL, Paris, pp. 239-244.

Patterson, M.W. and Yool, S.R. (1998), Mapping Fire-Induced Vegetation Mortality Using Landsat Thematic Mapper Data: A Comparison of Linear Transformation Techniques, *Remote Sensing of Environment*. 65: 132-142.

Pereira, J.M.C., Mota, B., Privette, J.L., Caylor, K.K., Silva, J.M.N., Sa, A.C.L. and Ni-Meister, W. (2004), A simulation analysis of the detectability of understory burns in miombo woodlands, *Remote Sensing of Environment*. 93: 296-310.

Pérez, B. and Moreno, J.M. (1998), Methods for quantifying fire severity in shrubland-fires, *Plant Ecology*. 139: 91-101.

Roy, D., Lewis, P.E. and Justice, C.O. (2002), Burned area mapping using multi-temporal moderate spatial resolution data —a bi-directional reflectance model-based expectation approach, *Remote Sensing of Environment*. 83(1-2): 263-286.

van Wagtendonk, J.W., Root, R.R. and Key, C.H. (2004), Comparison of AVIRIS and Landsat ETM+ detection capabilities for burn severity, *Remote Sensing of Environment*. 92(3): 397-408.

White, J.D., Ryan, K.C., Key, C.C. and Running, S.W. (1996), Remote sensing of forest fire severity and vegetation recovery, *International Journal of Wildland Fire*. 6(3): 125-136.

I

Available online at www.sciencedirect.com
ScienceDirect
Remote Sensing of Environment 108 (2007) 422 - 435
Remote Sensing of Environment
www.elsevier.com/locate/rse

Burn severity estimation from remotely sensed data: Performance of simulation *versus* empirical models

Angela De Santis, Emilio Chuvieco

Department of Geography, University of Alcalá, Alcalá de Henares, Spain

Received 19 September 2006; received in revised form 22 November 2006; accepted 24 November 2006

Abstract

Burn severity is a key factor in post-fire assessment and its estimation is traditionally restricted to field work and empirical fitting from remotely sensed data. However, the first method is limited in terms of spatial coverage and cost effectiveness and the second is site and data specific. Since alternative approaches based on radiative transfer models (RTM) have been usefully applied in retrieving several biophysical plant parameters (leaf area index, water and dry matter content, chlorophyll), this paper has applied the inversion of a simulation model to estimate burn severity in terms of the Composite Burn Index (CBI). The performance of the model inversion method was compared to standard empirical techniques. The study area chosen was a large forest fire in central Spain which occurred in July 2005. The model inversion showed the most accurate estimation for high severity levels (for CBI> 2.7, RMSE=0.30) and for unburned areas (CBI< 0.5, RMSE=0). In both methodologies, the error associated to CBI from 0.5 to 2.7 was not acceptable (RMSE> 0.7), because it is higher than 25% of the total range of the index. Finally, burn severity maps from both methods were compared.

Keywords: Forest Fires; Burn Severity; Kuusk Model; RTM Inversion; Landsat TM; Spectral Indices; NBR; CBI

1. Introduction

Forest fires are a critical factor of disturbance in worldwide ecosystems. Their effects on soil and plants depend on frequency, fire intensity, and fire residence time, as well as on plant resilience and resistance (Pérez and Moreno, 1998). Moreover, the main consequences of fire on plants and atmospheric emissions depend largely on fire/burn severity. The term "fire severity", which has a long tradition within the forest fire research community, refers to the combination of soil and overstory effects caused by fire (Brewer *et al.*, 2005; Chappell and Agee, 1996; Doerr *et al.*, 2006; Ryan and Noste, 1985; Turner *et al.*, 1994; Wang, 2002; White *et al.*, 1996). More recently, other authors have used the term "burn severity" to address the same concept (Chuvieco *et al.*, 2005; Chuvieco *et al.*, 2006; Key, 2005; Key and Benson, 2004, 2005; Parra and Chuvieco, 2005; Patterson and Yool, 1998). This discrepancy of terminology makes comparing map products potentially ambiguous (Miller and Yool, 2002). To clarify these concepts, the analysis of fire effects can be better classified in the context of the fire disturbance continuum (Jain and Graham, 2004), which addresses three different temporal phases: before the fire, during the fire and after the fire. Within this framework, the term fire severity indicates the direct effects of the combustion process and refers to the active fire (direct effects of fire process). In contrast, burn severity identifies the impact of fire on soil and plants when the fire is extinguished, and it is related to the post-fire phase (what is left). The latter definition will be used in this paper.

Burn severity is generally estimated using post-fire field data (Moreno and Oechel, 1989; Pérez and Moreno, 1998), which consider several variables as: depth of char, percentage of tree basal area mortality (Chappell and Agee, 1996), decrease in plant cover (Jain and Graham, 2004; Rogan and Yool, 2001), volatilization or transformation of soil components to soluble mineral forms (Turner *et al.*, 1994; Wang, 2002; Wells and Campbell, 1979), proportion of fine branches remaining on the canopy (Moreno and Oechel, 1989), and degree of canopy consumption and mortality (Doerr *et al.*, 2006; Key and Benson, 2002; Patterson and Yool, 1998; Rogan and Franklin, 2001; Ryan and Noste, 1985; van Wagtendonk *et al.*, 2004). The poor spatial representation associated with field methods and the cost of these approaches make it advisable to use alternative methods.

Remote sensing can be potentially a sound choice to map burn severity, since vegetation removal, soil exposure, changes in soil and vegetation moisture content imply changes in reflectance (Jakubauskas *et al.*, 1990). Indeed, fire-related decreases in chlorophyll content and vegetation moisture lead to decreases in the visible and near-infrared (NIR) reflectance

and increases in the mid-infrared (SWIR) reflectance (White *et al.*, 1996). Since the amount of green biomass destroyed by fires depends upon the burn severity, several authors have found good correlations between vegetation indices, computed from post-fire remotely sensed data, and burn severity (Díaz-Delgado *et al.*, 2003; Doerr *et al.*, 2006; García-Haro *et al.*, 2001; Hammill and Bradstock, 2006; Ruiz-Gallardo *et al.*, 2004; Sunar and Özkan, 2001). The Normalized Difference Vegetation Index (NDVI) has been related to field measurements of burn severity (Chafer *et al.*, 2004; Hammill and Bradstock, 2006; Sunar and Özkan, 2001). NDVI is defined as:

$$NDVI = \frac{(\rho_{NIR} - \rho_{RED})}{(\rho_{NIR} + \rho_{RED})} \quad (1)$$

where ρ_{NIR} and ρ_{RED} are the reflectance of near infrared (NIR) and red bands respectively. However, according to White *et al.* (1996), a single post-fire band 7 (SWIR) of Landsat Thematic Mapper (TM) showed stronger correlations than NDVI. Likewise, Jakubauskas *et al.* (1990) used the 7/5 ratio of Landsat Multi Spectral Scanner (MSS) to map the burn area and extract degrees of burn severity. Other authors have found stronger correlations for spectral indices using the NIR and shortwave infrared (SWIR) bands rather than the NDVI. Although, these NIR-SWIR indices were originally designed to estimate plant water content (De Santis *et al.*, 2006; Fraser *et al.*, 2000; Gao, 1996; Hunt and Rock, 1989), they have also proved useful to map burnt areas (López García and Caselles, 1991) since burning implies a severe decrease in plant and soil moisture contents. The most effective NIR-SWIR index for burn severity available in the literature is the Normalized Burn Ratio (NBR) proposed by Key and Benson (2002):

$$NBR = \frac{(\rho 4 - \rho 7)}{(\rho 4 + \rho 7)} \quad (2)$$

where $\rho 4$ and $\rho 7$ are the reflectance of band 4 (NIR) and 7 (SWIR) of Landsat TM respectively. Since burn severity is dependent on the pre-fire vegetation conditions, these authors suggest the use of the temporal difference between pre- and post-fire NBR (ΔNBR) values (Key and Benson, 2002):

$$\Delta NBR = NBR_{PRE-FIRE} - NBR_{POST-FIRE} \quad (3)$$

This variable has been proposed as an operational index to estimate burn severity from satellite data.

The post-burn approach (simple NBR) is less expensive than the multi-temporal approach, and reduces the errors caused by differences in geometric correction, in sensor calibration, in sun-sensor geometry, in atmospheric effects and in plant phenology. However, the use of a single post-image, without the pre-burn reference image, leads to difficulties in mapping spectrally similar areas such water and recent burns, or senescent vegetation and older burns (Epting *et al.*, 2005; Garcia and Chuvieco, 2004; Pereira, 1999; Pereira and Setzer, 1993).

The ΔNBR index calculated from Landsat TM and ETM+ images have shown very strong correlation with burn severity values estimated in the field in several study cases (Cocke *et al.*, 2005; Epting *et al.*, 2005; Miller and Yool, 2002). A comparison between ΔNBR calculated from Landsat-TM and Airborne Visible and Infrared Imaging Spectrometer (AVIRIS) data, showed very similar results (van Wagtendonk *et al.*, 2004).

Other indices that include the mid-infrared spectral region have also shown high correlations, according to Rogan and Yool (2001) and van Wagtendonk *et al.* (2004), but generally did not perform as consistently as the NBR index. Similarly, the evaluation of six different approaches for classifying and mapping fire severity using multi-temporal Landsat TM data, performed by Brewer *et al.* (2005), confirms that the NBR provides a flexible, robust and analytically simple approach.

As well as spectral indices, linear transformation techniques have been used for the multi-temporal mapping of burn severity. Patterson and Yool (1998) compared two linear transformation techniques, the Kauth–Thomas (KT) and principal components (PC) transforms, for mapping fire severity. The KT or "Tasselled Cap" transform is sensitive to fire-induced changes in the moisture content of soil and vegetation and, in this study, produced betters result than the PC transform. Chuvieco (2002) and Caetano *et al.* (1994) concluded that spectral mixture analysis (SMA) proved to be efficient in detecting the charcoal signal even in lightly burnt areas that kept a strong vegetation signal, a situation that is typically considered to be problematic. SMA was considered advantageous over vegetation index-based methods, due to its improved capability to distinguish burns from other bare or sparsely vegetated areas (Caetano *et al.*, 1996; Díaz-Delgado *et al.*, 2001). This technique was also successful applied by Díaz-Delgado and Pons (1999) and Rogan and Franklin (2001) to carry out the burn severity classification.

The studies previously referred to are based on empirical approaches, which are relatively easy to compute, when a good set of field data is available. However, empirical approaches have also limitations due to the lack of physics introduced in the retrieval technique which

reduces their generalization power (Weiss *et al.*, 2000). Alternative approaches are based on radiative transfer model (RTM) techniques. In the forward mode, RTM help understand how the changes in plant biophysical parameters modify the spectral response at both leaf and canopy level, whereas inverse modelling uses spectral signatures as inputs to quantify plant parameters. The latter mode has been extensively used to estimate: leaf area index (LAI) (Fang and Liang, 2003; Koetz *et al.*, 2005), water and dry matter content (Riaño *et al.*, 2005; Zarco-Tejada *et al.*, 2003), and chlorophyll content (Zarco-Tejada *et al.*, 2001). The results of these studies are generally very precise, but the performance of RTM greatly depends on whether the assumptions of the model are properly met for a specific vegetation type and a specific biophysical parameter. There are few examples of the use of RTM in burned land mapping. Roy *et al.* (2005, 2002) have applied them indirectly for generating the standard burned land product of MODIS, which is based on multi-temporal analysis of BRDF (Bi-directional Reflectance Distribution Function) corrected images. Pereira *et al.* (2004) used these models to analyse the detectability of the burned signal in surface fires, which is a critical factor in tropical fires. In the specific field of burn severity, only a recent study by Chuvieco *et al.* (2006) explores the use of RTM (forward mode) to simulate different burn severities. The simulations were performed with a coupled leaf canopy model designed by Kuusk (2001). Several simulation scenarios were analysed, and different spectral indices proposed, underlying the importance of the red-edge (720–760 nm) and NIR-SWIR regions for discriminating burn severity values.

From an operative point of view, the final goal of RTM in remote sensing studies, is to be able to retrieve critical parameters by applying a model inversion technique. This has not yet been applied in burn severity studies and it is the main objective of this paper. The aim is therefore to determinate burn severity from the inversion of the simulation proposed by Chuvieco *et al.* (2006), in the context of an initial assessment, and to compare the performance of this technique with the empirical models.

2. Data and methods

2.1. Study area

The study area is located in the north-eastern part of the Province of Guadalajara (40–41°N and 1–2°W) in central Spain (figure 1). From a geological point of view, this site presents a

sequence of limestone and sandstone deposits and the dominant types of soil are Xerochrept, Plexeralf and Xerorthent. The topography is rugged and the altitudes range between 1100mand 1400 m. Rainfall in the region averages 600–800 mm per year. Maximum and minimum precipitations are recorded in November–December and in July–August, respectively. The average annual temperature is 12 °C. *Pinus pinaster* woodlands are the dominant vegetation community of this area, mixed with oak forest of *Quercus faginea* and *Quercus pyrenaica* (in the layer up to 5 m height). The shrub layer is dominated by *Cistus ladanifer*, *Cistus albidus*, *Rosmarinus officinalis*, *Juniperus oxycedrus*, *Rosa canina*, *Cytisus scoparius*, and *Lavanda pedunculata*. This area was affected by a very large forest fire in July, 16th 2005. The fire was caused by human carelessness, under very dry weather conditions: maximum temperature 35 °C; relative humidity 22%; 30 days since the last rainfall event; wind speed from 10 to 23 km/h (Meteológica S.A.). All these meteorological factors contributed to increase fire intensity and severity. The fire lasted four days and burned a total of 13,000 ha, mainly covered by pine trees mixed with semideciduous oaks and a marginal proportion of areas covered by Mediterranean shrubs. Eleven fire-fighters died while working in fire suppression, which caused a great impact in the national media.

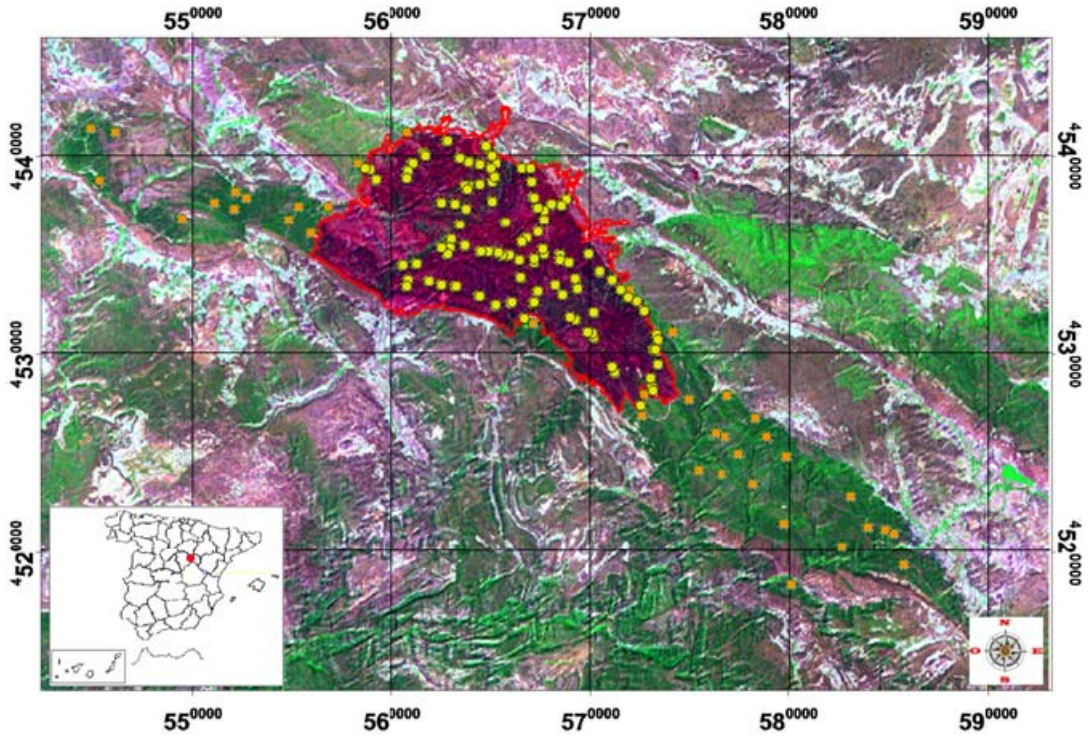

Figure 1. Study area location and field plot distribution (Landsat 5 TM image: R=TM7, G=TM4, B=TM1, Projection UTM 30T datum European 1950 mean).

2.2. Field data

The Composite Burn Index (CBI) is a field method to evaluate burn severity (Key and Benson, 2005). It was developed in the framework of the FIREMON Project (Fire Effects Monitoring and Inventory: http://fire.org/firemon/), by the U.S. Forest Service with contributions from U.S. Geological Survey. This index is designed to define burn severity from an ecological perspective, measuring ground fire effects that collectively provide a signal detected at moderate resolution by the Landsat Thematic Mapper (TM) (Key and Benson, 2004). Average conditions of the plant community are visually examined for 30-m diameter plots. The vegetation is considered to be composed of five strata, organized in a hierarchical structure (figure 2).

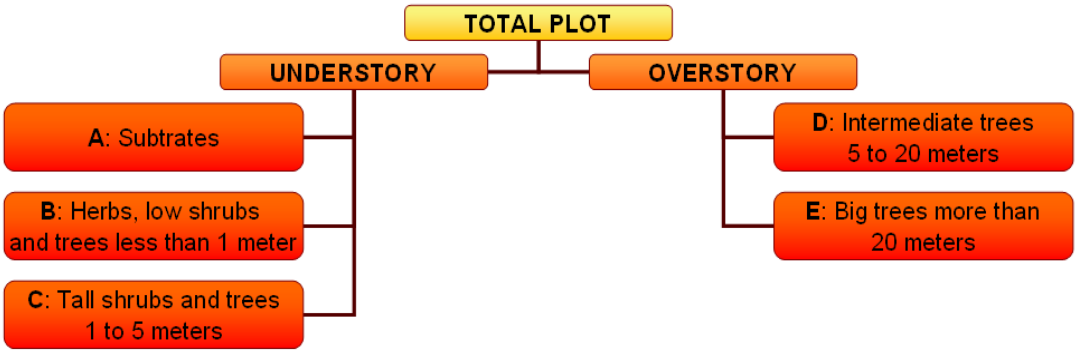

Figure 2. Strata considered in the CBI calculation.

Attributes are rated according to specific thresholds suggested by Key and Benson (2005). The scores are numerical, in a range of 0 to 3, implying a gradient from unburned to extremely burned conditions, respectively. The numerical rating derived for each attribute is obtained from a consensus of two field observers. Litter and fuel consumption, change in soil colour, foliage alteration, change in cover, canopy mortality and char height are the principal variables assessed. Therefore, although the CBI does not require quantitative measurements in the field, it provides a numerical estimation of burn severity for the site, which simplifies the statistical estimation derived from quantitative remotely sensed data. Different attributes are scored in each stratum and averaged into understory, overstory and overall composite ratings.

Since this index is focused on the percentage of change with respect to the pre-fire scenario, the CBI log sheet contains a few variables in each stratum for estimating pre-fire variables (such as cover, depth and density). Most rating factors are interpreted in relation to conditions

that existed before fire, and not in absolute quantities. This responds to the particular definition of severity as a magnitude of ecological change, such that the amount of change depends on the state of the community before fire. All factors are considered in terms of the area of the whole plot.

In this study, a modified version of the Composite Burn Index (CBI) was used to estimate burn severity in the field. Additional variables were introduced in the CBI field form:

1. the percentage of dead leaves on the soil;
2. the fraction of coverage (FCOV) of dominant vegetation type per stratum;
3. the percentage of changes in the leaf area index (LAI) of each stratum;
4. the amount of new sprouts after the fire.

These new variables improve the interpretation of the satellite images post-fire, because these factors can modify significantly the reflectance detected by the sensor. Moreover, the last factor listed provides information about the possibility of regeneration.

A total of 103 plots (30 m diameter) were sampled within the perimeter of the burnt area, between August and September 2005 (figure 1). The plots were selected within large areas with homogeneous burn severity levels and low slope gradients.

Each plot was identified with a code and its centre point coordinates, elevation, aspect, slope and type of soil were noted down before the CBI was evaluated. The coordinates of the plot centre were recorded with a GPS (GARMIN GPS 12). Three pictures per plot were taken (panoramic and close-ups) as reference for the post-processing phase. Figure 3 shows examples of field plots with diverse CBI values.

Since the field work started only 3 weeks after the fire and due to the risk of dead trees collapsing, it was difficult to gain access to some parts of the burnt area. Areas with maximum slopes were not covered, as recommended by Key and Benson (2004) in the specifications of CBI.

Finally, field spectroscopy was carried out in the study area 20 days after the fire using a CROPSCAN multi-spectral radiometer (CROPSCAN, Inc., 1932 Viola Heights Lane NE Rochester, MN 55906 USA, http://www.cropscan.com). This radiometer was selected for having the same spectral resolution as the satellite imagery used in this study (Landsat TM). Several types of burned and unburned vegetation were measured on different backgrounds (charcoal, litter and ash). The spectra were used as reference for satellite reflectance analysis.

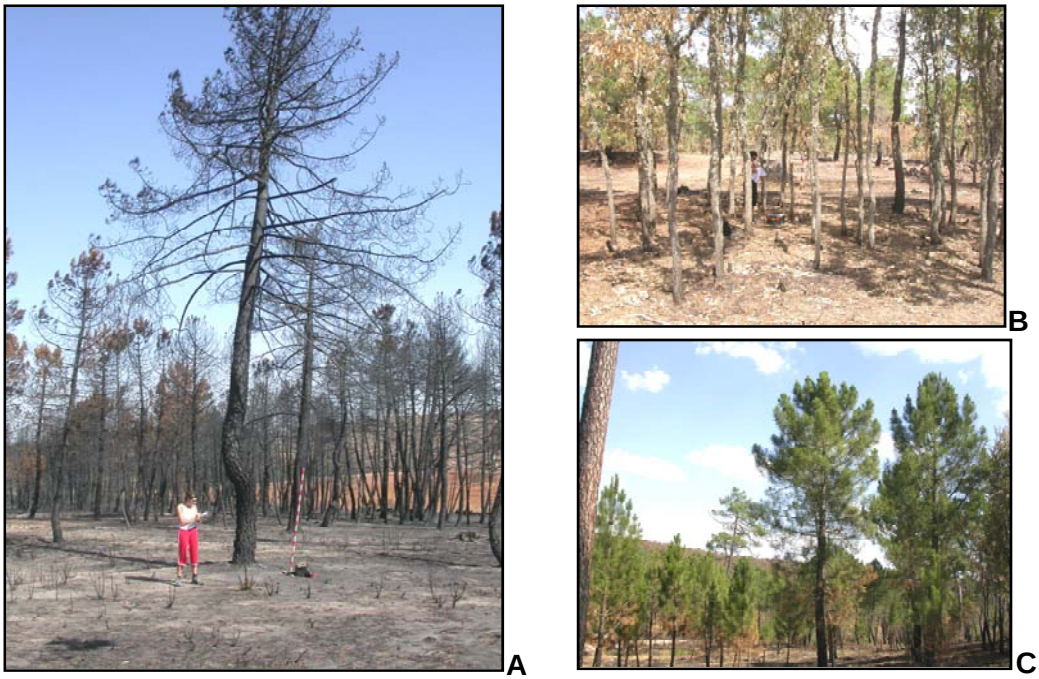

Figure 3. Examples of high (A, CBI=3), moderate (B, CBI=2.35) and low (C, CBI=0.9) burn severity.

2.3. Remotely sensed data

Two Landsat 5 Thematic Mapper (TM) images (path 200, row 32), corresponding to July 1st, 2004 (pre-fire) and August 5th, 2005 (post-fire) were selected. The original digital numbers of reflective TM bands were scaled to radiance values (L_λ) using the procedure proposed by Chander and Markham (2003) for TM images acquired after May 5th, 2003.

The radiance to reflectance (ρ) conversion (atmospheric correction) was performed using the dark object method proposed by Chavez (1996) with band-fixed transmissivity values.

A set of Ground Control Points (GCPs) was selected for the geometric correction using a Landsat ETM+ ortho-image (from the CORINE 2000 project, UTM 30 T European 1950 mean) as reference. The resulting Root Mean Square Error (RMSE) was under half a pixel (or 15 m). Moreover, pre- and post-fire images were co-registered (RMSE<15 m).

For the characteristics of the study area, an illumination correction was required. The correction was carried out using a digital terrain model (DTM, 10 m of resolution) and the method proposed by Civco (1989). The radiometric fitting between pre- and post-fire images was tested comparing spectral signatures of the pixels corresponding to areas with low seasonal changes (asphalt and rock). The comparison of reflectance values returned a RMSE=0.02.

Finally, to cover the entire range of CBI, 47 pixels were selected from the post-fire image, named PN from 1 to 47, which corresponded to unburned areas (CBI=0, orange points in figure 1), in addition to the 103 field plots.

2.4. Empirical fitting

For the empirical fitting, several spectral indices and transformations were tested. NBR (Key and Benson, 2002; Eq. (2)) was selected for being the only one index specifically developed for burn severity analysis. This index was calculated for the pre- and post-fire images, after which the ΔNBR (Eq. (3)) was computed. Likewise, NDVI from both pre- and post-fire images was obtained and consequently, ΔNDVI was generated. In addition to these indices, the Tasselled Cap (Kauth and Thomas, 1976) transformation and the Hue, Intensity, Saturation (HIS) transformation (Koutsias *et al.*, 2000) were computed from the TM7, TM4, TM1-RGB composition.

Single reflective bands of the TM post-fire image and the results of spectral indices and linear transformations were correlated against the CBI of all field plots.

Due to the spatial resolution of the TM sensor and to the size of field plots (30-m diameter), the data to be used in the empirical fittings were extracted using the pixel value corresponding to the coordinates of the centre of each field plot.

As suggested by Key and Benson (2005), a sub-sampling was carried out from the total 150 plots to obtain a similar representation of each severity group (CBI under 1.5, from 1.5 to 2.5, and over 2.5). A total of 46 plots were randomly selected and used for the calibration of the empirical model. In this sub-sample, the full range of severity variation is represented. The remaining 104 plots were used in the validation phase. The linear regression technique applied was the stepwise forward selection (SPSS 13), and the empirical fitting was evaluated using the RMSE between observed and predicted CBI.

2.5. Simulation models

The simulation model used in this paper was developed by Chuvieco *et al.* (2006). They used a leaf canopy model combination based on the PROSPECT and KUUSK RTM, respectively. The CBI was simulated by changing the substrate conditions (from soil to charcoal), the leaf properties (from green to brown leaves) and the leaf area index (from 2 to 3 maximum LAI to

0.01). Two vegetation strata, plus the substrate were included in the simulations. Two simulation scenarios were considered: a wide short-term and a post-fire high severity. For this paper, the wide short-term was selected since it considered general short-term effects of recent fires (within a few weeks after fire). To simulate this scenario, the authors assumed that the CBI of each stratum changed independently from the other two. However, within each stratum the increase in the percentage of altered foliage (PFA) and in the percentage of change in leaf cover (PCC) occur simultaneously. All the simulations were run for the solar spectrum (from 400 to 2500 nm) at 10-nm intervals (201 spectral bands). The number of the simulation cases was reduced by fixing the following variables throughout all the simulations: leaf angle distribution= plagiophile, leaf shape=ellipse form (eccentricity=0.95), sun zenith angle=30°, nadir angle=0°, azimuth angle=0°.

To avoid unrealistic combinations, three rules were applied:

1. CBI B+C > CBI A: since it is very unlikely that the CBI of a shrub stratum (b1mtall) can be greater than the CBI of the soil.
2. CBI B+C > CBI D+E: eliminates simulations when the CBI of a canopy is greater than the CBI of the understory, which was never observed in the field plots.
3. CBI B+C <4 *CBI A: eliminates simulations where the CBI of the understory is four times greater than the CBI of the background soil, in agreement with field observations.

Finally, from the original 1000 simulations, only 278 were considered significant and their corresponding CBI values ranged from 0.45 to 3. To fill the range gap existed between 0 and 0.45 (CBI nominally ranges from 0 to 3), additional simulations of unburned vegetation conditions were added to the original 278. These two spectral signatures were also derived from a simulation using the Kuusk model (David Riaño, personal communication).

2.6. Model inversion strategies

Inversion methods use different approaches to compare the simulated and observed spectra. A first distinction may be made on whether the process computes the simulated spectra before the actual inversion or does it iteratively during the inversion process. The former is more common, since the computation time is reduced (the iterative process requires running the model for each pixel) and the simulated spectra are better selected according to realistic assumptions (Gastellu-Etchegorry *et al.*, 2003; Kimes *et al.*, 2002; Liang, 2004). This method is commonly named look-up table (LUT) approach, and was selected for this study

since it provided a more operational approach to CBI retrieval. The LUT was generated from our forward simulations, considering the input scenarios previously commented.

The comparison between observed and simulated spectra can be based on several criteria, being the most common the minimum quadratic distance and neural networks (Kimes *et al.*, 2000). In this paper, the minimum angle between the simulated and observed spectra was used, since it provides a consistent measure of spectral similarity. For this study, all the spectra generated for the look-up table were used to build a spectral library (in ENVI 4.2™), which was adapted to simulate the response of TM sensor. Then, all the spectra in the resulting library were used as endmembers to perform a Spectral Angle Mapper (SAM) supervised classification of the post-fire TM image. SAM is a pixel-based supervised classification technique that measures the similarity between two spectra, in our case between each pixel in the TM image and the simulated spectra of CBI values included in the LUT. This similarity is computed from the spectral angle (in radians), when each spectrum is considered as an *m*-dimensional feature vector, with *m* being the number of spectral channels (Debba *et al.*, 2005; Kruse *et al.*, 1993). This angle is independent of the length of vectors (Bakker and Schmidt, 2002), so it is insensitive to illumination or albedo effects.

To be able to compare the results from the model inversion to the results from empirical estimation, the spectral angle threshold of SAM classification was left open. In this way, the not-classified category was not present.

After applying the SAM algorithm, a CBI value was assigned to each pixel in the image, the result of which can be directly considered as a burn severity map.

Finally, the verification was performed extracting the values of pixels corresponding to the same plots as in the empirical validation and by computing the RMSE between modelled and observed CBI.

3. Results

3.1. Results of the field work

Most of the burned area presented very high observed CBI values. Only 28 of 103 field plots have CBI values lower than 2.5, and 32 have CBI higher than 2.9. In all cases the burn severity is higher in the understory than the overstory.

3.2. Empirical fitting between spectral indices and CBI values

Table 1 shows the correlations between the CBI of the total plot and a number of variables: reflective bands of the post-fire TM image, spectral indices and results from linear transformation.

The CBI of the total plot correlated most strongly with Greenness (Tasselled Cap transformation result) and ΔNDVI (r=−0.76 and r=0.76, respectively), followed by TM band 4 and NDVI (r=−0.75). NBR and ΔNBR had a correlation coefficient slightly lower (r=−0.72 and r=0.73, respectively). These results suggest that the NIR is the most sensitive spectral region for burn severity estimation. In contrast, the SWIR has a low sensitivity to minor differences in high CBI values. This explains why TM band 7 (SWIR) had a low correlation (r=0.39), due to the fact that most observed CBI values were high.

Table 1. Correlation (*r* of Pearson) between the CBI of the total plot and the following variables: spectral bands (TM1 to TM7of post-fire image), spectral indices (NDVI, dNDVI, NBR and dNBR) and linear transformation results (Albedo, Greenness and Moisture= results from Tasselled Cap transformation; H, I and S= results from Hue, Intensity and Saturation transformation) of TM images. In bold are significant (p< 0.05) values.

***r* Pearson correlation coefficients**	
	CBI of the total plot
TM1 (0.45 -0.52 µm)	0.07
TM2 (0.52 -0.60 µm)	-0.19
TM3 (0.63 -0.69 µm)	-0.06
TM4 (0.76 -0.90 µm)	**-0.75**
TM5 (1.55 -1.75 µm)	0.05
TM7 (2.08 -2.35 µm)	**0.39**
NBR	**-0.72**
dNBR	**0.73**
NDVI	**-0.75**
dNDVI	**0.76**
I	**-0.30**
H	**0.33**
S	**-0.68**
Albedo	**-0.31**
Greenness	**-0.76**
Moisture	**-0.54**

A total of 46 randomly sub-sampled plots were used to perform the linear regression.

Although only small number of unburned plots were also included, their relative weight in the final linear fitting could be very significant. To avoid this, the coefficient D by CooK (SPSS) was computed to test the influence of each CBI value used in the calibration of regression model (Peña Sánchez de Rivera, 1989). This analysis confirmed that all selected values of CBI were acceptable ($p<0.05$).

The linear regression returned a model with the ΔNDVI and the S result of the HIS transformation:

$$CBI = 1.679 + 2.83\Delta NDVI - 9.574S \quad (4)$$

This model explained 67% of the total variance and its fitting showed an $R^2_{adjusted}$ =0.66 (Table 2).

Table 2. Empirical fitting and model inversion performances.

EMPIRICAL FITTING				MODEL INVERSION	
REGRESSION		VALIDATION		VALIDATION	
R^2	R^2adj.	R^2	RMSE	R^2	RMSE
0.82	0.66	0.85	0.64	0.84	0.48

In the verification phase, Eq. (4) was applied to the remaining 104 plots. The correlation obtained was r^2 =0.85 (figure 4) and the RMSE between estimated and observed CBI was 0.64 (Table 2). However, there is a marked offset from the 1:1 linear fitting, due to the overestimation of unburned plots.

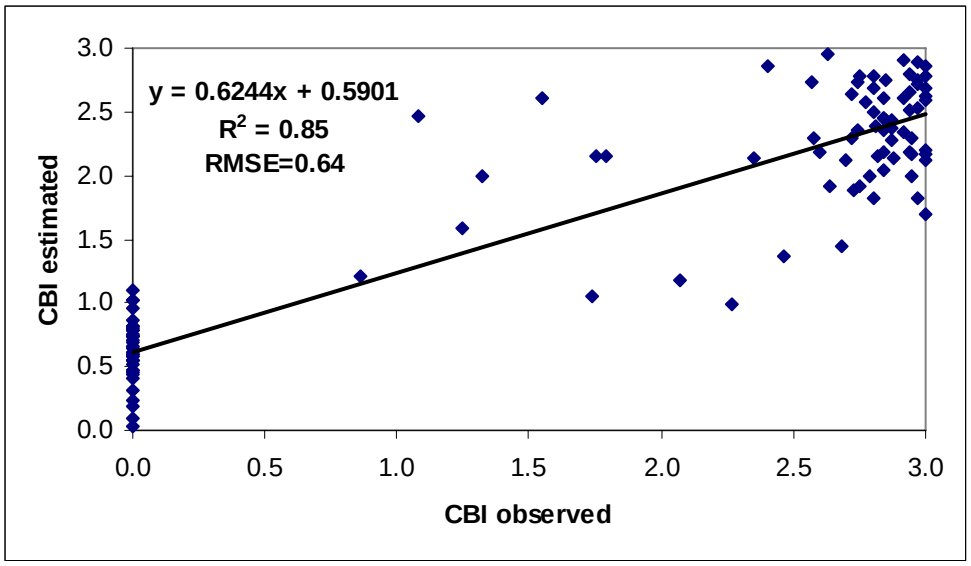

Figure 4. Scatter plot between estimated and observed CBI.

The unburned plots (CBI=0) were generally overestimated (figure 5), because this severity level did not clearly correspond to a single value of estimators (ΔNDVI and S). According to the composition of each plot, intermediate CBI values (0.9 < CBI <2.7) were either:

- ✓ underestimated when the fraction of cover (FCOV) of the tree strata was high, and over 50% of the scorched leaves remained on the tree crowns (plots 5, 11, 27, 58 and 62, figures 5 and 6A). In such cases the estimated CBI was more similar to the observed CBI of the overstory.
- ✓ Overestimated when the FCOV of the overstory was under 10% and the observed CBI of the understory was high (plots 44, 47 and 54, figures 5 and 6B).

High burn severity levels (CBI>2.7) were underestimated although there does not seem to be a clear relationship with the composition these plots.

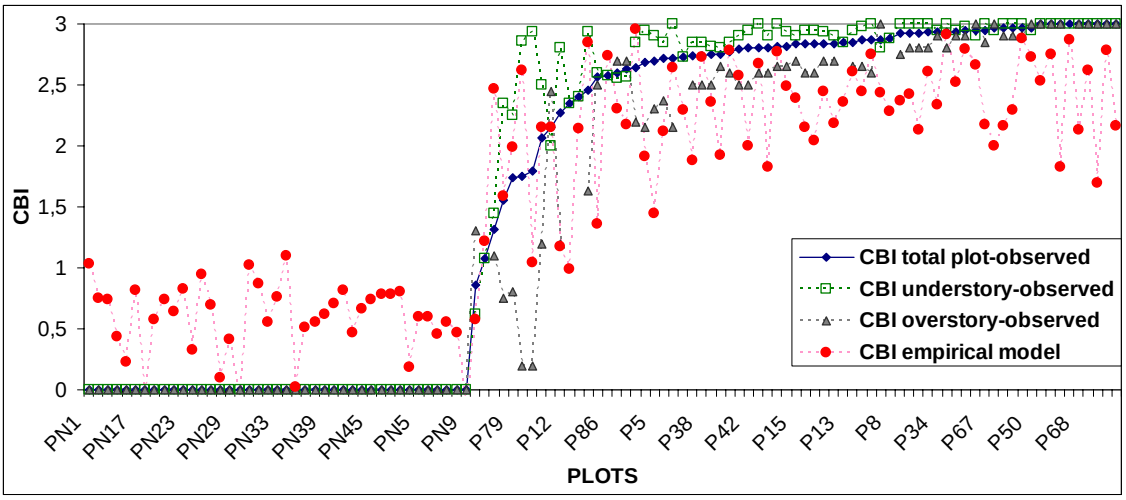

Figure 5. Comparison of observed (for the understory, the overstory and the total plot) and empirically modelled values of CBI. Plot numbers are ordered according to the observed CBI values (total plot) from 0 to 3.

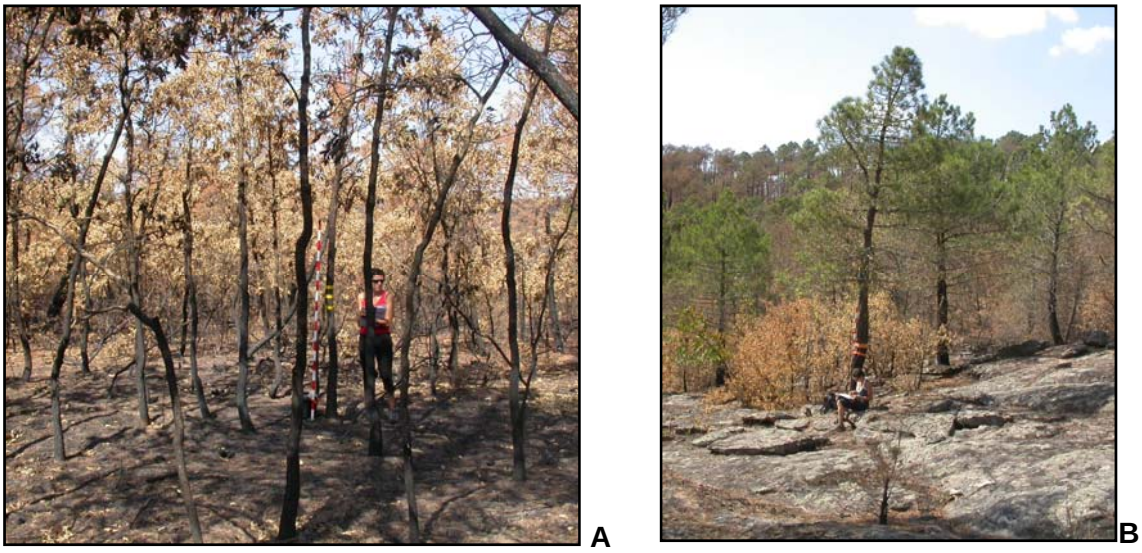

Figure 6. Examples of under- (plot 27, A) and over-estimated (plot 44, B) plots using the empirical method.

The severity map in figure 7 (top) was calculated using the empirical model. Since CBI is a continuous index, the value of each pixel was represented using a colour scale with six intervals that emphasize differences in high severity values. Unburned areas were masked using the fire perimeter. Intermediate values are predominant in this map, due to the overestimation of the lower CBI and to the underestimation of the higher CBI.

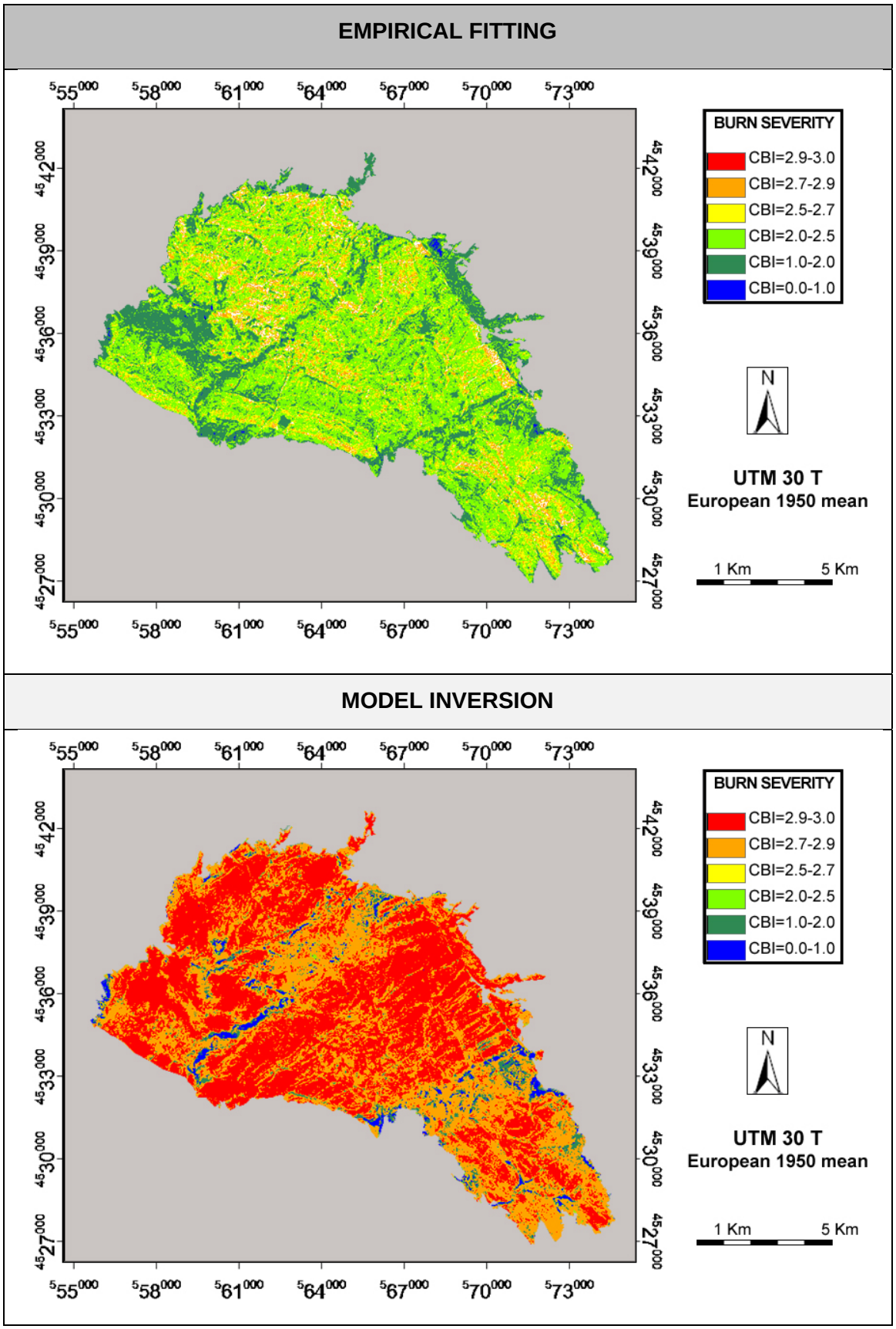

Figure 7. Empirical (top) and simulated (bottom) burn severity maps.

3.3. Model inversion results

The scatterplot between observed and simulated CBI values (figure 8) shows a high correlation coefficient (r^2 =0.84), which is very similar to that of the empirical estimation (r^2 =0.85). However, the RMSE was lower (RMSE=0.48, Table 2).

The verification results of model inversion showed a practically perfect estimation when CBI=0 and CBI>2.7 (figure 9).

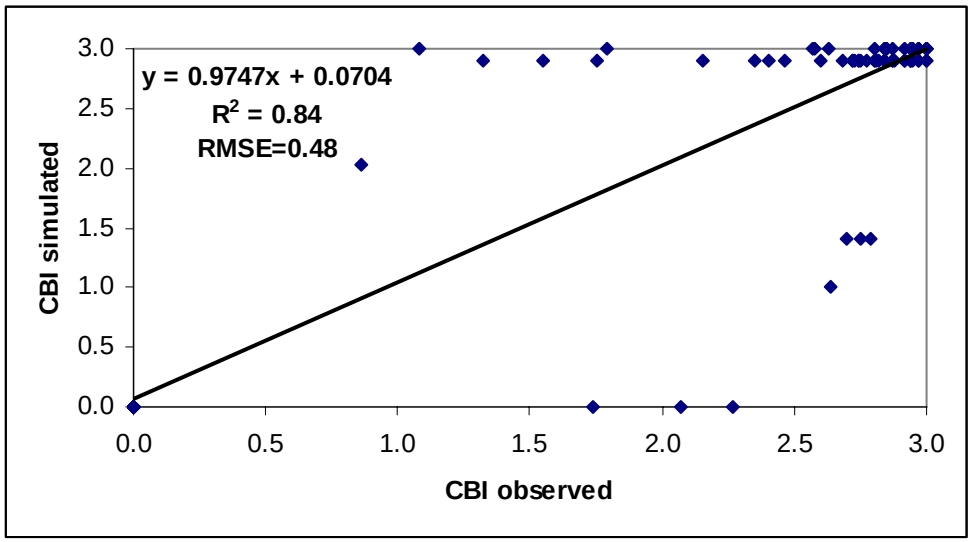

Figure 8. Scatterplot between observed and simulated CBI values (validation phase).

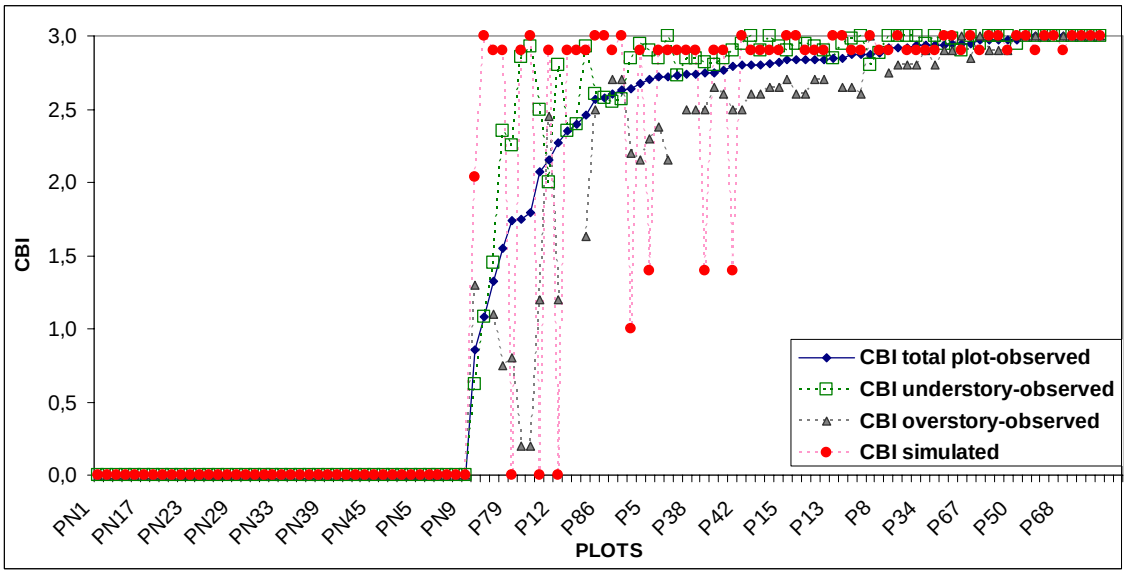

Figure 9. Comparison of observed (for the understory, the overstory and the total plot) and simulated values of CBI (plots numbers are ordered by observed CBI values from 0 to 3).

However, for CBI from 0 to 2.7 the model inversion overestimated 15 plots which can be divided into four case types:

- ✓ *Type A*: one plot (99, figure 9) was probably badly located in the image. Since it was placed between two firebreaks, it is possible that part of it was included in the selected pixel (geometric correction errors).
- ✓ *Type B*: four plots (3, 61, 75 and 80, figure 9) had a very low FCOV (b10%) of tree strata. In this case the CBI values simulated were very similar to the CBI of the understory.
- ✓ *Type C*: six plots (10, 28, 46, 58, 64 and 94, figure 9) had low FCOV and low CBI values in the tree strata and high FCOV and high CBI values for the understory.
- ✓ *Type D*: three plots (85, 77 and 86, figure 9) had a high FOCV in the tree strata. Most scorched leaves remained on the tree crowns.

The estimation error in types C and D was due to the presence of two conditions which were not considered in the simulation model (figure 10):

1. low LAI (or FCOV) and green leaves,
2. high LAI (or FCOV) and scorched leaves.

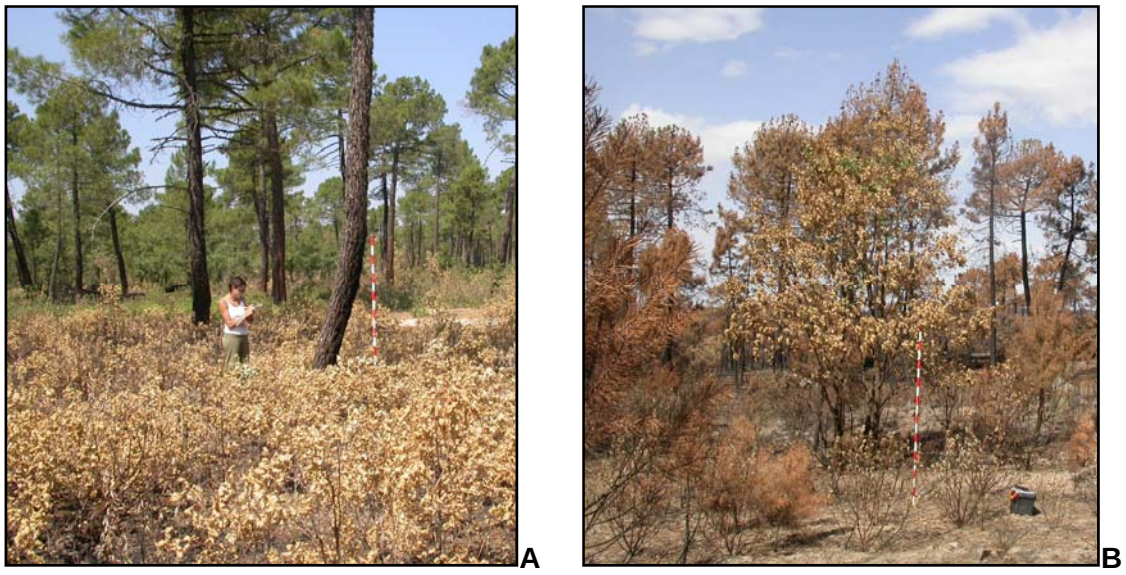

Figure 10. Examples of: A) low LAI and green leaves (P10); B) high LAI and scorched leaves (P62) in the tree strata.

Spectral signatures which fulfilled these two conditions were not included in the spectral library used in the SAM classification, hence the error in these plots. If the SAM spectral angle threshold had been constrained, these pixels would have probably been assigned as not classified. However, in order to be able to compare these results with the empirical method all pixels had to be classified.

Seven plots (2, 4, 5, 6, 12, 33 and 79, figure 9), which had an observed CBI between 1.7 and 2.7, were underestimated. These plots had a very high FCOV (>70%) of overstory and green canopies which masked the signal of the understory.

A severity map was also generated for the model inversion method (figure 7). The map shows three zones or belts in a NE–SW direction. The two outer belts show a great contrast between very high and very low CBI values. The central belt is more homogeneous (very high CBI), but since the colour scale emphasizes the small differences between CBI=2.7–2.9 and CBI=2.9–3, which are due to the presence/absence of tree crowns, it is possible to identify narrow stripes with high and very high CBI, parallel to the maximum slope line (figure 11). The red plotted areas correspond to the zones which had a direct contact with the flames, whereas the yellow–orange areas represent the areas where the crown was scorched by the high temperatures from the surrounding the fire (figure 11). In the eastern sector and the northern border, the linear elements plotted as CBI=0 correspond to fire breaks.

Figure 11. Photograph taken from a helicopter showing the NE-SW direction of stripes corresponding to CBI values between 2.8 and 3 (courtesy of Dr. Domingos Viegas).

4. Discussion

4.1. Critical factors in burn severity estimation from remotely sensed data

The original CBI field form proposed by Key and Benson (2004) did not consider the percentage of dead leaves litter nor the FCOV of each stratum, but the results from the model inversion suggest that both variables and their mixing effects are key factors of burn severity estimation from remotely sensed data.

The first one can lead to an underestimation of the severity level of burned plots where high canopy consumption took place. The reason for this is that the spectral signature of dead leaf litter is very similar to the spectrum of a scorched tree canopy that has a medium–high LAI and a charcoal soil background (figure 12).

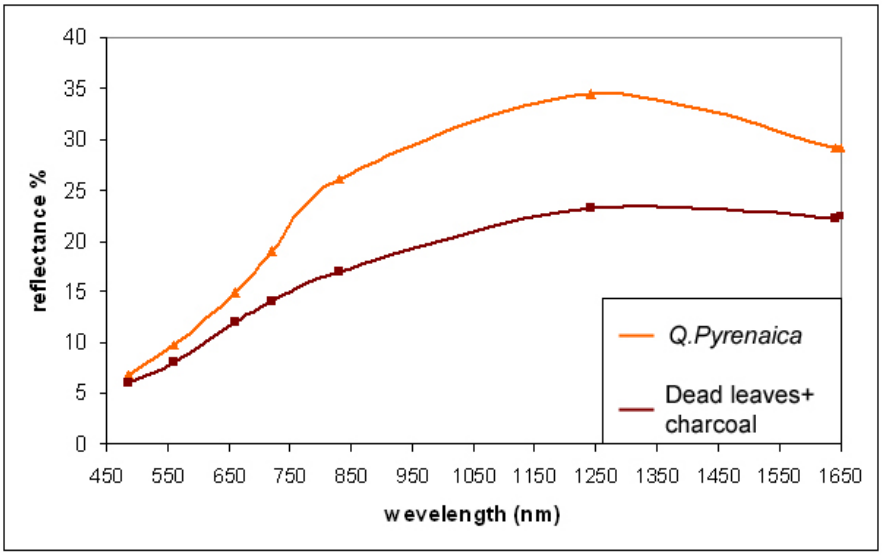

Figure 12. Spectral signatures of a scorched *Quercus pyrenaica* with charcoal background and a charcoal soil covered by dead leaf litter, measured with a CROPSCAN multi-spectral radiometer.

Similarly, the second factor (FCOV of tree strata) can modify CBI estimation because it can mask the signal of the understory. In such cases, the errors in severity determination depend on the similarity between the CBI of the overstory and the CBI of the total plot. In the study area the CBI of the understory showed almost a one to one relation with the CBI of total plot, which was always higher than the CBI of overstory (figure 13). Therefore, CBI is underestimated in the pixels which correspond to the field plots with a high FCOV in the tree strata.

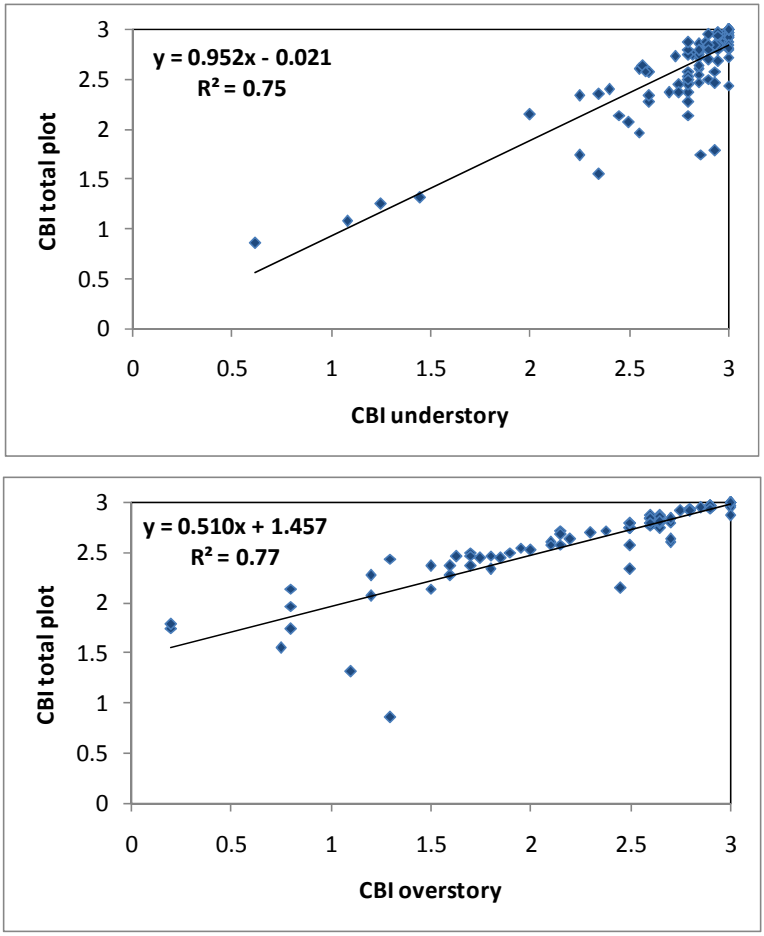

Figure 13. Scatterplot between the CBI of the total plot and the CBI of the understory (top) and the overstory (bottom).

4.2. Comparison between the empirical fitting and the model inversion method

The CBI values estimated by empirical and model inversion methods coincided only in seven of the 104 plots used in the verification (P5, P48, P54, P64, PN3, PN18 and PN35, figure 14). In the rest of plots, CBI values obtained from both methods were quite different.

Therefore, to better understand estimation dynamics of both empirical and model inversion techniques, the RMSE between estimated and observed CBI was classified into three groups: CBI under 0.5, 0.5 to 2.7 and over 2.7 (Table 3).

Since the unburned level corresponds to several types and biophysical conditions in the vegetation, the model inversion, which uses all spectral information available, had a RMSE=0 (Table 3). However, the empirical fitting, which uses only ΔNDVI and S, had a RSME=0.65 (Table 3).

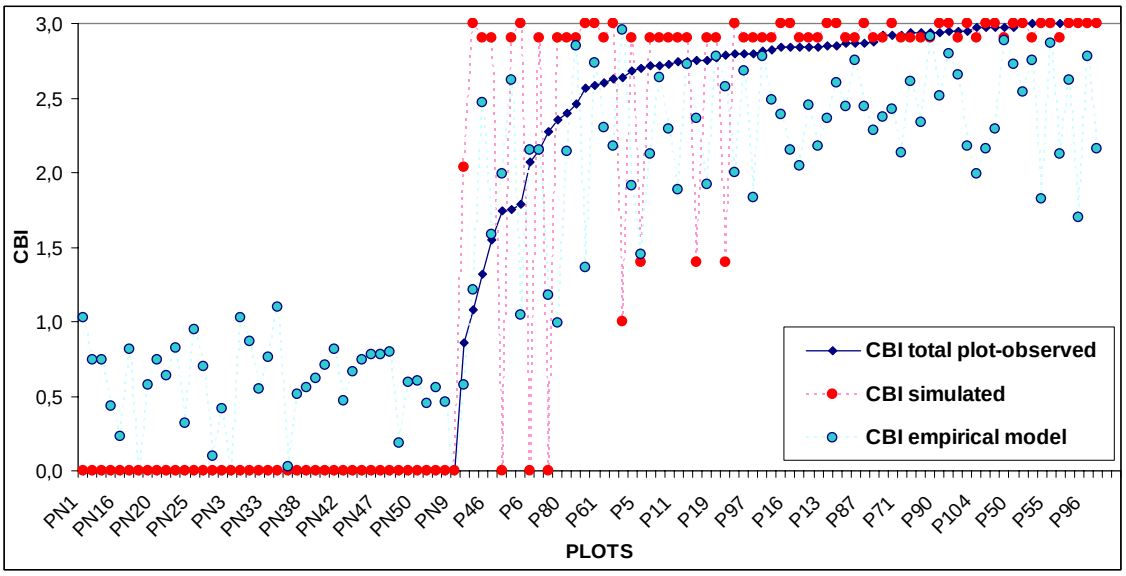

Figure 14. Comparison of observed, simulated and empirically modelled values of CBI (plots numbers are ordered by observed CBI values from 0 to 3).

The performance of the empirical fitting was better (Table 3) than the model inversion, for the second range of burn severity considered (CBI=0.5 to 2.7). However, the mean residual in either methodologies was not acceptable (RMSE>25% of the total range of the CBI). Intermediate severity levels were the result of a high CBI contrast between the understory (very high CBI values) and the overstory (low values). Thus, the FCOV of tree strata was the key parameter that determined the estimation accuracy. The simulation showed best results for high CBI (RMSE=0.30, Table 3), which is the most critical range for the post-fire assessment.

The empirical estimation showed similar mean residuals throughout the CBI ranges. In addition, CBI variability observed was reduced since the empirical estimation overestimated low CBI values and underestimated high CBI values. This can be seen in the final maps, where intermediate CBI values are predominant.

Table 3. RMSE distribution of both empirical and inversion methods.

	EMPIRICAL FITTING			MODEL INVERSION		
CBI	**< 0.5**	**0.5-2.7**	**>2.7**	**< 0.5**	**0.5-2.7**	**>2.7**
RMSE	0.65	0.70	0.58	0	1.1	0.30

Finally, observed high CBI values, as well as being the most important in terms of post-fire assessment, are the most abundant in the study area. In contrast, the intermediate values, which were poorly estimated by both models, were scarce. Therefore, for this study case the model inversion method performed better than the empirical model. Future studies should explore whether this conclusion is applicable to other sites with different ecosystems and different ranges of CBI values.

5. Conclusions

Burn severity is a key factor in post-fire assessment, but has normally been estimated from field observations and empirical fittings using remotely sensed data.

The first method is costly in terms of time and both human and economic resources, and has a limited spatial coverage, although is critical in the verification phase of remote sensing methods. Empirical fittings between remotely sensed data and field sampling measurements of burn severity provide easy and generally accurate estimations of burn severity. However the results are site-specific and difficult to apply in other areas. RTMs offer an alternative approach to represent the variability of burn severity. Simulation results are independent of local conditions and are therefore applicable to all site and sample conditions (Privette *et al.*, 1996). The accuracy of biophysical variable estimations from inversion techniques mainly depends on the quality of the radiative transfer model and the type of inversion technique used, as well as the a priori knowledge of the distribution of input variables (Gastellu-Etchegorry *et al.*, 2003; Weiss *et al.*, 2000).

This study is a first approach to estimate burn severity using a model inversion method that is independent of site conditions and adaptable to different sensor capabilities. Moreover, this technique uses the total amount of spectral information available and not just single spectral indices.

In this paper, the model inversion and the empirical fitting methods were compared, using Landsat TM imagery. In order to identify the differences in the performance of both methods, their RMSE were split into three ranges of CBI (under 0.5, 0.5 to 2.7 and over 2.7). The model inversion method was more accurate than the empirical approach when CBI >2.7 (RMSE=0.30, Table 3), which tended to smooth contrast in the lower and upper part of CBI scale. This is very important for burn severity determination, since the higher burn severities are the most critical for the post-fire assessment. In contrast, the simulation model was less accurate when

CBI ranges from 0.5 to 2.7 (RMSE=1.1, Table 3), due to the noise effects caused by overstory FCOV and dead leaf litter, which agrees with the conclusions of several authors (Cocke *et al.*, 2005; Chuvieco *et al.*, 2006; Rogan and Franklin, 2001). In this range of CBI, the mean residuals (Table 3) of the two techniques were not acceptable (RMSE>25% of the total range of the CBI). High burn severity levels represent the majority of CBI values sampled in this study and are best estimated from model inversion. The information derived from these burn severity maps can be used to identify areas with different levels of burn severity, and thereby assist forest managers in allocating resources for restoration efforts (Patterson and Yool, 1998).

In future work, simulation results are expected to be improved by introducing in the model the spectral signatures of dead leaf litter, ash background and random combinations of LAI and leaf colour parameters. The model will be applicable to other study sites and in different ecosystems.

Acknowledgements

Special thanks to the Spanish Forest Service staff of the Province of Guadalajara who have been extremely helpful during the fieldwork campaign. The Spanish Ministry of Science and Technology supports Angela De Santis within the FPU Programme framework. Funding for this project was obtained through the Preview European Project (www.preview-risk.com, EA21.CR/AC/03.064).

References

Bakker, W. H., and Schmidt, K. S. (2002). Hyperspectral edge filtering for measuring homogeneity of surface cover types. *ISPRS Journal of Photogrammetry and Remote Sensing*, 56, 246−256.

Brewer, C. K., Winne, J. C., Redmond, R. L., Opitz, D. W., and Mangrich, M. V. (2005). Classifying and mapping wildfire severity: A comparison of methods. *Photogrammetric Engineering and Remote Sensing,* 71, 1311−1320.

Caetano, M. S., Mertes, L., Cadete, L., and Pereira, J. M. C. (1996). Assessment of AVHRR data for characterising burned areas and post-fire vegetation recovery. *EARSeL Advances in Remote Sensing*, 4, 124−134.

Caetano, M. S., Mertes, L. A. K., and Pereira, J. M. C. (1994). Using spectral mixture analysis for fire severity mapping. *Proceedings of 2nd international conference on forest fire research* (667−677). Coimbra.

Civco, D. L. (1989). Topographic normalization of Landsat thematic mapper digital imagery. *Photogrammetric Engineering and Remote Sensing*, 55, 1303−1309.

Chafer, C. J., Noonan, M., and Macnaught, E. (2004). The post-fire measurement of fire severity and intensity in the Christmas 2001 SydneyWildfires. *International Journal of Wildland Fire*, 13, 227−240.

Chander, G., and Markham, B. (2003). Revised Landsat-5 TM radiometric calibration procedures and postcalibration dynamic ranges. *IEEE Transactions on Geoscience and Remote Sensing*, 41, 2674−2677.

Chappell, C. B., and Agee, J. K. (1996). Fire severity and tree seedling establishment in Abies magnifica forests, Southern Cascades, Oregon. *Ecological Applications*, 6, 628−640.

Chavez, P. S. (1996). Image-based atmospheric corrections. Revisited and improved. *Photogrammetric Engineering and Remote Sensing*, 62, 1025−1036.

Chuvieco, E. (2002). *Teledetección Ambiental: La observación de la Tierra desde el Espacio*. Barcelona: Ariel Ciencia.

Chuvieco, E., Riaño, D., Danson, F. M., Bowyer, P., and Martín, M. P. (2005). Use of canopy reflectance models to simulate burn severity levels. In J. Riva, F. Pérez-Cabello, and E. Chuvieco (Eds.), *Proceedings of the 5th international workshop on remote sensing and GIS applications to forest fire management: Fire effects assessment* (pp. 233−238). EARSeL, Paris: Universidad de Zaragoza, GOFC-GOLD.

Chuvieco, E., Riaño, D., Danson, F. M., and Martín, M. P. (2006). Use of a radiative transfer model to simulate the post-fire spectral response to burn severity. *Journal of Geophysical Research-Biosciences*, 111, doi:10.1029/ 2005JG000143.

Cocke, A. E., Fule, P. Z., and Crouse, J. E. (2005). Comparison of burn severity assessments using Differenced Normalized Burn Ratio and ground data. *International Journal of Wildland Fire*, 14, 189−198.

Debba, P., van Ruitenbeek, F. J. A., van der Meer, F. D., Carranza, J. M., and Stein, A. (2005). Optimal field sampling for targeting minerals using hyperspectral data. *Remote Sensing of Environment*, 99, 373−386.

De Santis, A., Vaughan, P., and Chuvieco, E. (2006). Foliage moisture content estimation from 1-D and 2-D spectroradiometry for fire danger assessment. *Journal of Geophysical Research- Biosciences*, 111, G04S03, doi: 10.1029/2..5JG000149.

Díaz-Delgado, R., Lloret, F., and Pons, X. (2003). Influence of fire severity on plant regeneration by means of remote sensing imagery. *International Journal of Remote Sensing*, 24, 1751−1763.

Díaz-Delgado, R., and Pons, X. (1999). Empleo de imágenes de teledetección para el análisis de los niveles de severidad causados por el fuego. *Revista Española de Teledetección*, 12, 63−68.

Díaz-Delgado, R., Pons, X., and Lloret, F. (2001). Fire severity effects on vegetation recovery after fire. The Bigues i Riells wildfire case study. In E. Chuvieco and M. P. Martín (Eds.), 3rd *International Workshop on Remote sensing and GIS applications to Forest Fire Management*. *New methods and sensors* (pp. 152−155). Paris: EARSeL.

Doerr, S. H., Shakesby, R. A., Blake, W. H., Chafer, C. J., Humphreys, G. S., and Wallbrink, P. J. (2006). Effects of differing wildfire severities on soil wettability and implications for hydrological response. *Journal of Hydrology*, 319, 295−311.

Epting, J., Verbyla, D. L., and Sorbel, B. (2005). Evaluation of remotely senses indices for assessing burn severity in interior Alaska using Landsat TM and ETM+. *Remote Sensing of Environment*, 96, 328−339.

Fang, H., and Liang, S. (2003). Retrieving leaf area index with a neural network method: Simulation and validation. *IEEE Transactions on Geoscience and Remote Sensing*, 41, 2052−2062.

Fraser, R. H., Li, Z., and Landry, R. (2000). SPOT vegetation for characterizing boreal forest fires. *International Journal of Remote Sensing*, 21, 3525−3532.

Gao, B. C. (1996). NDWI. A normalized difference water index for remote sensing of vegetation liquid water from space. *Remote Sensing of Environment*, 58, 257−266.

García-Haro, F. J., Gilabert, M. A., and Meliá, J. (2001). Monitoring fire-affected areas using thematic mapper data. *International Journal of Remote Sensing*, 22, 533−549.

Garcia, M., and Chuvieco, E. (2004). Assessment of the potential of SAC-C/ MMRS imagery for mapping burned areas in Spain. *Remote Sensing of Environment*, 92, 414−423.

Gastellu-Etchegorry, J. P., Gascon, F., and Estève, P. (2003). An interpolation procedure for generalizing a look-up table inversion method. *Remote Sensing of Environment*, 87, 55−71.

Hammill, K. A., and Bradstock, R. A. (2006). Remote sensing of fire severity in the Blue Mountains: Influence of vegetation type and inferring fire intensity. *International Journal of Wildland Fire*, 15, 213−226.

Hunt, E. R., and Rock, B. N. (1989). Detection of changes in leaf water content using near and middle-infrared reflectances. *Remote Sensing of Environment*, 30, 43−54.

Jain, T. B., and Graham, R. T. (2004). Is forest structure related to fire severity? Yes, no, and maybe: Methods and insights in quantifying the answer. *USDA Forest Service Proceedings RMRS-P 34* (pp. 217234).

Jakubauskas, M. E., Lulla, K. P., and Mausel, P. W. (1990). Assessment of vegetation change in a fire-altered forest landscape. *Photogrammetric Engineering and Remote Sensing*, 56, 371−377.

Kauth, R. J.,andThomas, G. S. (1976). The Tasseled Cap. A graphic description of the spectral-temporal development of agricultural crops as seen by Landsat. *Symp. on Machine Processing of Remotely Sensed Data* (pp. 41−51). Purdue.

Key, C. (2005). Remote sensing sensitivity of fire severity and fire recovery. In J. Riva, F. Pérez-Cabello, and E. Chuvieco (Eds.), *Proceedings of the 5th international workshop on remote sensing and GIS applications to forest fire management: Fire effects assessment* (pp. 29−39). Zaragoza: Universidad de Zaragoza, GOFC-GOLD, EARSeL.

Key, C., and Benson, N. (2002). Landscape assessment, in fire effects monitoring (FireMon) and inventory protocol: Integration of standardized field data collection techniques and sampling design with remote sensing to assess fire effects. *NPS-USGS National Burn Severity Mapping Project.*

Key, C.H., and Benson, N. (2004). Ground measure of severity: The Composite Burn Index. *FIREMON Landscape Assessment V4. In.*

Key, C.H., and Benson, N. (2005). Landscape assessment: Ground measure of severity, the Composite Burn Index; and remote sensing of severity, the Normalized Burn Ratio. In D.C. Lutes, R.E. Keane, J.F. Caratti, C.H. Key, N.C. Benson and L.J. Gangi (Eds.), *FIREMON: Fire Effects Monitoring and Inventory System* (pp. CD:LA1-LA51). Ogden, UT: USDA Forest Service, Rocky Mountain Research Station, Gen. Tech. Rep. RMRS-GTR-164.

Kimes, D., Gastellu-Etchegorry, J., and Estève, P. (2002). Recovering forest canopy characteristics through inversion of a complex 3D model. *Remote Sensing of Environment*, 79, 320−328.

Kimes, D., Knyazikhin, Y., Privette, J. L., Abuelagasim, A. A., and Gao, F. (2000). Inversion methods for physically based models. *Remote Sensing Reviews*, 18, 381−439.

Koetz, B., Baret, F., Poilvé, H., and Hill, J. (2005). Use of coupled canopy structure dynamic and radiative transfer models to estimate biophysical canopy characteristics. *Remote Sensing of Environment*, 95, 115−124.

Koutsias, N., Karteris, M., and Chuvieco, E. (2000). The use of intensity–hue–saturation transformation of Landsat-5 thematic mapper data for burned land mapping. *Photogrammetric Engineering and Remote Sensing*, 66, 829−839.

Kruse, F. A., Lefkoff, A. B., Boardman, J. B., Heidebrecht, K. B., Shapiro, A. T., Barloon, P. J., and Goetz, A. F. H. (1993). The spectral image processing (SIPS)—interactive visualization and analysis of imaging spectrometer data. *Remote Sensing of Environment*, 44, 145−163.

Kuusk, A. (2001). A two-layer canopy reflectance model. *Journal of Quantitative Spectroscopy and Radiative Transfer*, 71, 1−9.

Liang, S. (2004). *Quantitative remote sensing for land surface characterization*. Hoboken, NJ: Wiley.

López García, M. J., and Caselles, V. (1991). Mapping burns and natural reforestation using thematic mapper data. *Geocarto International*, 1, 31−37.

Miller, H. J., and Yool, S. R. (2002). Mapping forest post-fire canopy consumption in several overstory types using multi-temporal Landsat TM and ETM data. *Remote Sensing of Environment,* 82, 481−496.

Moreno, J.M.,andOechel,W.C. (1989).A Simple Method for estimating fire intensity after a burn in California Chaparral*. Acta Ecologica (Ecologia plantarum)*, 10, 57−68.

Parra, A., and Chuvieco, E. (2005). Assessing burn severity using Hyperion data. In J. Riva, F. Pérez-Cabello, and E. Chuvieco (Eds.), *Proceedings of the 5th international workshop on remote sensing and GIS applications to forest fire management: Fire effects assessment* (pp. 239−244). Paris: Universidad de Zaragoza, GOFC-GOLD, EARSeL.

II

Simulation approaches for burn severity estimation using remotely sensed images

Emilio Chuvieco [1,3], Angela De Santis [1], David Riaño [1,2] and Kerry Halligan[3]

[1]*Department of Geography, University of Alcalá*
Calle Colegios 2, Alcalá de Henares, Madrid 28801, Spain

[2]*Center for Spatial Technologies and Remote Sensing, University of California, Davis*
One Shields Avenue, Davis, CA 95616 (USA)

[3]*Department of Geography, University of California, Santa Barbara*
3611 Ellison Hall, Santa Barbara, CA 93106 (USA)

Abstract

Traditional field-based methods for estimating burn severity are time-consuming, labour intensive and normally limited in spatial extent. Remotely sensed data provide a means to estimate severity levels across large areas, but it is critical to understand the causes of variability in spectral response with variations in burn severity. Since experimental measurements over a range of burn severities are difficult to obtain, the simulation tools provided by radiative transfer models (RTM) offer a promising alternative to better understand factors affecting burn severity reflectances. Two-layer RTM, such as the combined leaf (PROSPECT) and canopy (Kuusk) model can be used to simulate a wide range of burn severity conditions. Specifically, the effects of changes in soil background, leaf colour and leaf area index as a result of different burn severities can be simulated with two-layer RTM models in the forward mode. This approach can provide a deeper understanding of the effects of each factor in satellite-sensed reflectance, as well as their relative importance. Additionally, RTMs can also be used in an inverse mode, and therefore burn severities can be retrieved from remotely sensed data by comparing measured and simulated reflectance.

Examples of these two-way modes of RTMs are presented in this paper. Burn severity was measured using the Composite Burn Index (CBI). The Kuusk model was used to simulate scenarios of different combinations of changes in the substrate, upper vegetation, and lower vegetation strata. This paper shows some results of inverting the simulated reflectances to estimate CBI from calibrated reflectance derived from different satellite sensors. The case study is based on a large forest fire that affected central Spain in July, 2005. Landsat-TM, SPOT-HRG, IRS-AWIFS, Envisat-MERIS and Terra-MODIS data were used for this retrieval. Determination coefficients (r^2) values range between 0.436 (MODIS) to 0.629 (Landsat-TM), with lower precision for the intermediate range of CBI values.

Keywords: burn severity, fire effects, forest fires, radiative transfer models, reflectance.

1. Introduction

Discrimination of different degrees in post-fire effect assessment is critical to improve management of fire-affected areas, either to help natural regrowth, reduce soil erosion and degradation, or improve landscape diversity (Key, 2005; Lachowski *et al.,* 1997: Lentile *et al.*, 2006; Turner *et al.*, 1994). Additionally, the degree of biomass consumed by the fire is one of the key factors to estimate gas emissions derived from wildland fires (Chuvieco *et al.*, 2004; Epting *et al.*, 2005; Michalek *et al.*, 2000).

In recent years, several papers have tried to clarify the terminology of post-fire effects assessment (Jain and Graham, 2004; Lentile *et al.*, 2006). Following these papers, the term burn severity will be used throughout this paper to refer to the analysis of post-fire characteristics of vegetation and substrate after the fire is fully extinguished. When referring to other papers, we will try to convert their terminology to this one, based on this "what is left after the fire" concept.

Several authors have proposed field methods to discriminate burn severity based on quantitative or qualitative criteria (Key and Benson, 2005; Lentile *et al.*, 2006; Miller and Yool, 2002; Moreno and Oechel, 1989; Pérez and Moreno, 1998). These methods are laborious and costly and present severe obstacles to be spatially representative.

Remotely sensed images have been used as an alternative because they provide a spatial comprehensive view, are cost-efficient, and provide up to date information on landscape conditions. In the last years, a large number of papers have explored the use of remote sensing in burn severity assessment (Brewer *et al.*, 2005; Cocke *et al.,* 2005; Díaz-Delgado *et al.,* 2003; Díaz-Delgado *et al.,* 2001; Epting *et al.,* 2005; Kachmar and Sanchez-Azofeifa, 2006; Key, 2005; Michalek *et al.,* 2000; Miller and Yool, 2002; Parra and Chuvieco, 2005; Rogan and Franklin, 2001; Rogan and Yool, 2001; Roy and Landmann, 2005; Roy *et al.,* 2006; Ruiz-Gallardo, 2004; Sa *et al.,* 2005; van Wagtendonk *et al.,* 2004; White *et al.,* 1996). These papers covered a range of different techniques: spectral indices, principal components, classification, multitemporal change detection, etc. Although most rely on Landsat-TM/ETM+ data, there are also some examples of hyperspectral data (Parra and Chuvieco, 2005; van Wagtendonk *et al.,* 2004).

One of the main difficulties of using these studies for global assessment of burn severity from remotely sensed data is the empirical approach that has guided most studies published so far. Empirical models are simple to calibrate and provide a quantitative estimation of burn severity, but they provide little confidence on whether they are applicable or not to other ecosystems or fuel characteristics.

For this reason, the use of alternative tools for interpreting remotely sensed data is desirable. In recent years, physical models have been proposed as a viable alternative to derive quantitative information from reflectance calibrated images. Successful application of these models has been reported in the estimation of chlorophyll (Zarco-Tejada *et al.,* 2001), moisture content (Danson and Bowyer, 2004), and dry matter (Riaño *et al.,* 2005). Simulation models attempt to account for the effects of different factors that modify plant reflectance and transmittance: chemical composition, geometrical configuration, illumination and observation angles, etc. The large number of proposed models can be classified into general groups depending on their main assumptions: turbid medium models, geometrical models, stochastic models and ray-tracing models (Liang, 2004). Most common models are based on the radiative transfer equation and therefore are named radiative transfer models (RTM) since they account for the multiple scattering of radiation as it interacts with the vegetation canopy and soil background. Such interaction can be modelled assuming that the vegetation represents one or more homogenous layers. Other possibilities include the consideration of discontinuous canopies, such as row structure in crops or grid structure in tree plantations, and higher levels of complexity such as the consideration of three-dimensional vegetation structure models (Pinty *et al.,* 2004). Although more complex models are closer to reality than those based on homogeneous canopies, they require a large number of input variables, making them harder to parameterize with real data.

Models can be used in forward and backward approaches (Liang, 2004). The former implies changing the input parameters to simulate the effects of those changes in the final reflectance. The latter inverts the given model, such that the input parameters that generated an observed reflectance spectrum may be estimated. Burn severity studies have made very little use of simulation models so far. Roy *et al.* (2005, 2002) used a RTM to simulate reflectance from burned and unburned areas for different view and illumination angles of MODIS data. Their goal was to obtain an automatic algorithm for mapping burned areas from multitemporal acquisitions of MODIS data. Pereira *et al.* (2004) used a mixed geometrical-turbid medium model to simulate whether understory fires could be detectable in the Miombo woodlands at different tree densities. A forward RTM simulation for burn severity was recently proposed by Chuvieco *et al.* (2006) to identify the most sensitive wavelength regions for burn severity retrieval from remote sensing imagery. De Santis and Chuvieco (2007) compared the results of inverting this simulation model with those obtained from an empirical model in the retrieval of burn severity values from Landsat-TM images. Results from this inversion showed a good agreement in the upper and lower part of the severity range, while more error occurred in the central values.

The objectives of this paper are twofold. First we tried to extend the RTM simulations previously published (Chuvieco *et al.,* 2006) by including a wider range of scenarios and input conditions, with the goal of improving the middle range of the severity scale. The second objective was to extend the estimations provided by model inversion (De Santis and Chuvieco, 2007) to other sensors, including both higher spatial resolution data: Landsat-TM, SPOT-HRG and IRS-AWIFS; and lower: Envisat-MERIS and Terra-MODIS.

2. Methods

2.1 Reference Burn Severity Measure

Among the different procedures to measure burn severity, we selected the Composite Burn Index (CBI) as the target estimation variable. CBI was originally proposed by Key and Benson in 1999 (Key and Benson, 2005) and was intended to provide a quantitative estimation of burn severity that could be derived from satellite data. The index was developed within the FIREMON project and has been widely used by researchers using satellite data for mapping burn severity (Cocke *et al.,* 2005; De Santis and Chuvieco, 2007; Epting *et al.,* 2005; Key, 2005; Lentile *et al.,* 2006; Parra and Chuvieco, 2005).

CBI provides a semi-quantitative index of severity instead of using qualitative ranges (high, medium, low) commonly adopted by other authors. This numerical rating facilitates the statistical validation of the estimates derived from quantitative remotely sensed data. The CBI is based on evaluating different variables associated with fire effects in different strata of a field plot. The observations can be performed quickly and easily in the field, therefore maximizing the number of plots that can be sampled with a fixed field effort. Five strata are evaluated in the CBI: A: substrate (material lying on the floor); B: herbs, short shrubs and small trees (<1 m tall); C: tall shrub and sapling trees (<5 m tall); D: intermediate trees (5 m to 20 m tall); and E: large trees (>20 m tall). The first three are used to compute the CBI value of the understory of the plot (A+B+C), while the last two forms the overstory (D+E). The final CBI for each plot is the average of all strata, if they are present in that plot (A+B+C+D+E), or otherwise the average of the strata present.

CBI score of each stratum is estimated after visual inspection of the plot, considering several variables, including: % litter consumed, % foliage consumed, % living or re-sprouting species, % green or brown leaves, height of charring, % canopy mortality (Key and Benson, 2005). A burn

severity scale, adapted to each sampled variable, is used to quantify the impact from 0 (no effect) to 3 (highest effect).

2.2 RTM Model Selection

The selection of the RTM for our study was based on the input requirements of the burn severity estimation. The model should be sensitive to burn severity variations in different vegetation layers, since CBI scores take into account five strata. From the available RTM in the literature, the Kuusk Markov Chain Canopy Reflectance Model (MCRM) was selected (Kuusk, 2001) because it allows consideration of two vegetation canopies. It could therefore be used to model any scenario with variations of soil substrate and two vegetation layers. This would be the case when a tree canopy (with different levels of fire effects) has shrubs below (also with various levels of fire effects), as well as a mixture of soil and charcoal in the background.
The Kuusk model considers that the vegetation is homogeneously distributed for each layer and uses leaf optical properties derived from the PROSPECT model (Jacquemoud, 1990). The canopy directional reflectance is generated based on the single scattering and diffuse fluxes from each layer, using direct and diffuse solar irradiance.

One alternative to the Kuusk model would have been to use an RTM that considers the three-dimensional structure of the vegetation such as Forest Light Interaction model (FLIGHT) (North 1996), Discrete Anisotropic Radiative Transfer model (DART) (Gastellu-Etchegorry *et al.,* 1996; Gastellu-Etchegorry *et al.,* 2004) or Geometric Optical Radiative Transfer model (GORT) (Li *et al.,* 1995; Ni *et al.,* 1999). Although these models can provide a more realistic characterization of heterogeneous vegetation canopies with individuals of various sizes and fire severity levels, they are also much more complex to parameterize. The more simplistic Kuusk model, on the other hand, is more easily parameterized due to its assumptions of homogenous canopies, while still providing sufficient complexity through its inclusion of two vegetation layers with independent input conditions. This model, therefore, it is well suited to the vertical stratification of observed burn severity levels.

2.3 Input Conditions to Simulate CBI Values

To simulate CBI values with the Kuusk model, the four vegetation strata of the CBI approach were reduced to two (Figure 1): the B and C strata of the CBI were identified with low vegetation (lower canopy of the Kuusk model) and D and E strata were assumed to be the

upper canopy in the Kuusk model. The CBI A (substrate) was considered as the soil background of the Kuusk model. Each simulation had a corresponding CBI value, following the original FIREMON criterion where the CBI of the plot is a simple average of the CBI for the five strata (three in our case).

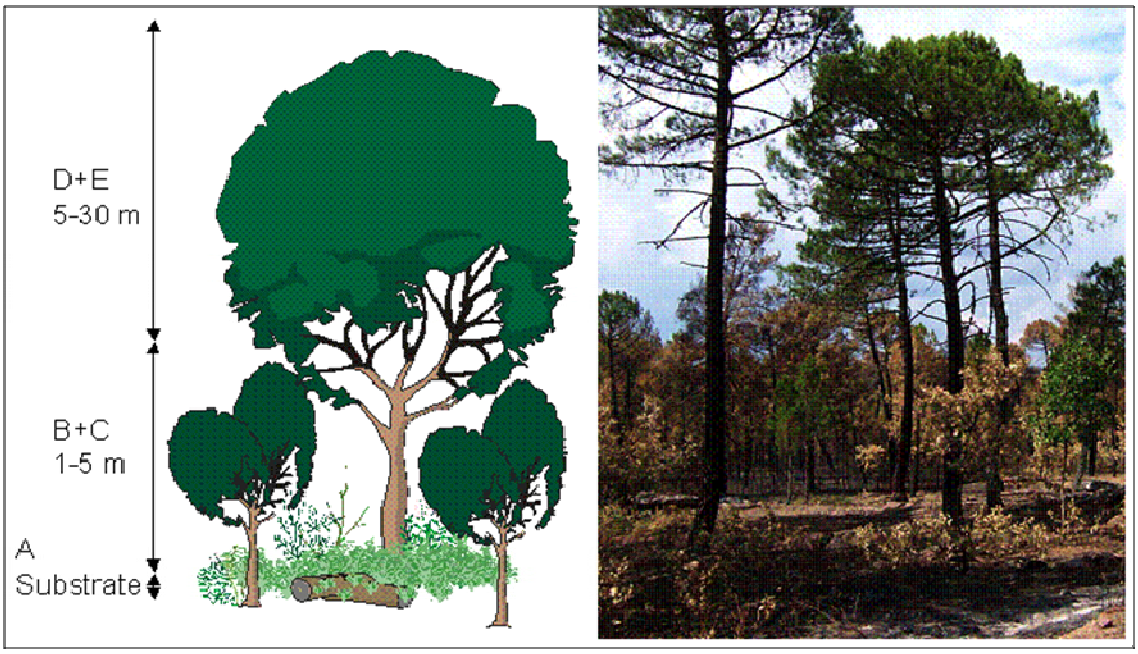

Figure 1. Vegetation strata of CBI (left) and photograph of an area recently burned (right) in the fire used as study case.

CBI is designed to measure burn severity from a set of variables that are critical in assessing fire effects. However, not all of them can be simulated with reflectance models, and therefore a further simplification of the CBI components was required for this study. The variables that were taken into account for the simulations were: change in soil substrate, percentage of foliage altered, and percentage change in vegetative cover. These variables were included in the Kuusk model as described by Chuvieco *et al.* (2006). The input spectra for the simulations were either measured using a GER-2600 spectroradiometer (Geophysical & Environmental Research Corporation, Millbrook, NY) or taken from LOPEX database (Hosgood *et al.,* 1994). The former was the case for soil, ash, and charcoal spectra, while the latter was the case for the green and brown leaf spectra (Figure 2). Variations in leaf colour (PFA) and canopy cover (PCC) were simulated from the Kuusk model by assuming different proportions of green versus brown leaves and changing the Leaf Area Index (LAI), respectively (Chuvieco *et al.,* 2006). LAI thresholds for full cover of vegetation were fixed at 2 for the lower stratum and 3 for the

upper one. These values were based on LAI values for typical Mediterranean shrubs derived from the literature (Scurlock *et al.,* 2001) and from our own field data. CBI values for each stratum were computed using the thresholds defined in the FIREMON protocol, while intermediate values were obtained using linear interpolation.

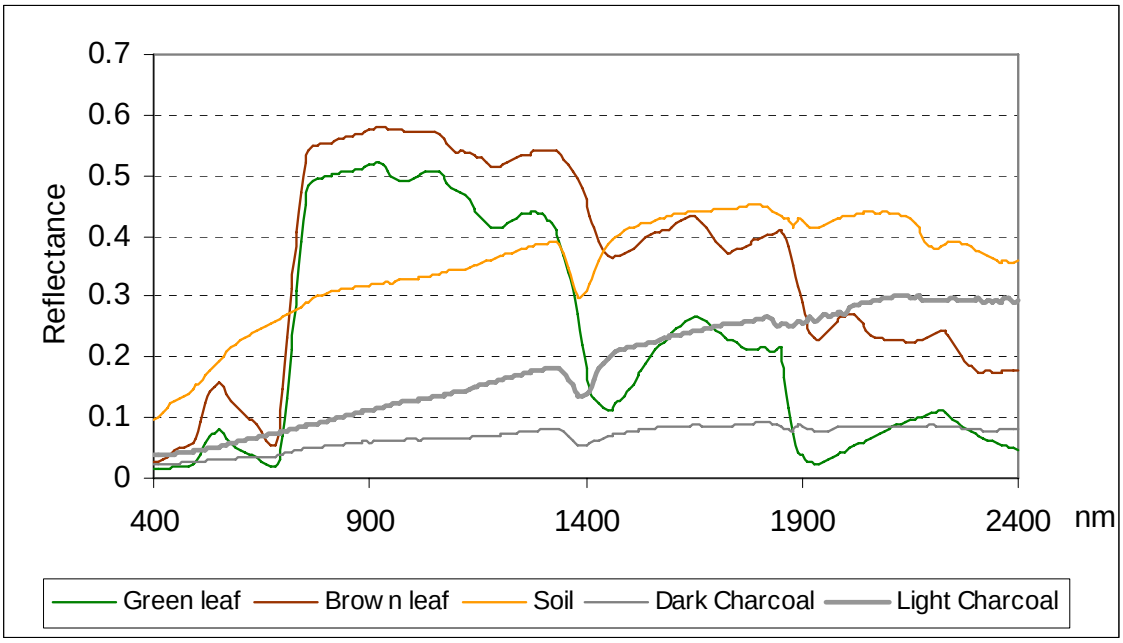

Figure 2. Input spectra used in the simulations.

2.4 Simulation Scenarios

Several simulation scenarios were considered to account for the diversity of post-fire severity conditions and the complexity of potential pre- and post-fire changes. Four scenarios were considered:

1. *Single post-fire*, assuming that fire causes simultaneous leaf consumption and leaf browning.
2. *Extended post-fire*, supposing that fire may either consume the leaves or brown them or both.
3. *Multitemporal*, by modelling changes in leaf colour and cover from fixed pre-fire conditions.
4. *Supervised approach*, by selecting the most commonly found combinations of input parameters from field experience.

The first scenario was the simplest, assuming that changes in leaf colour and leaf cover occurred in parallel. In other words, the larger the fire effect, the browner the leaves and the lower the leaf area index were (Figure 3).

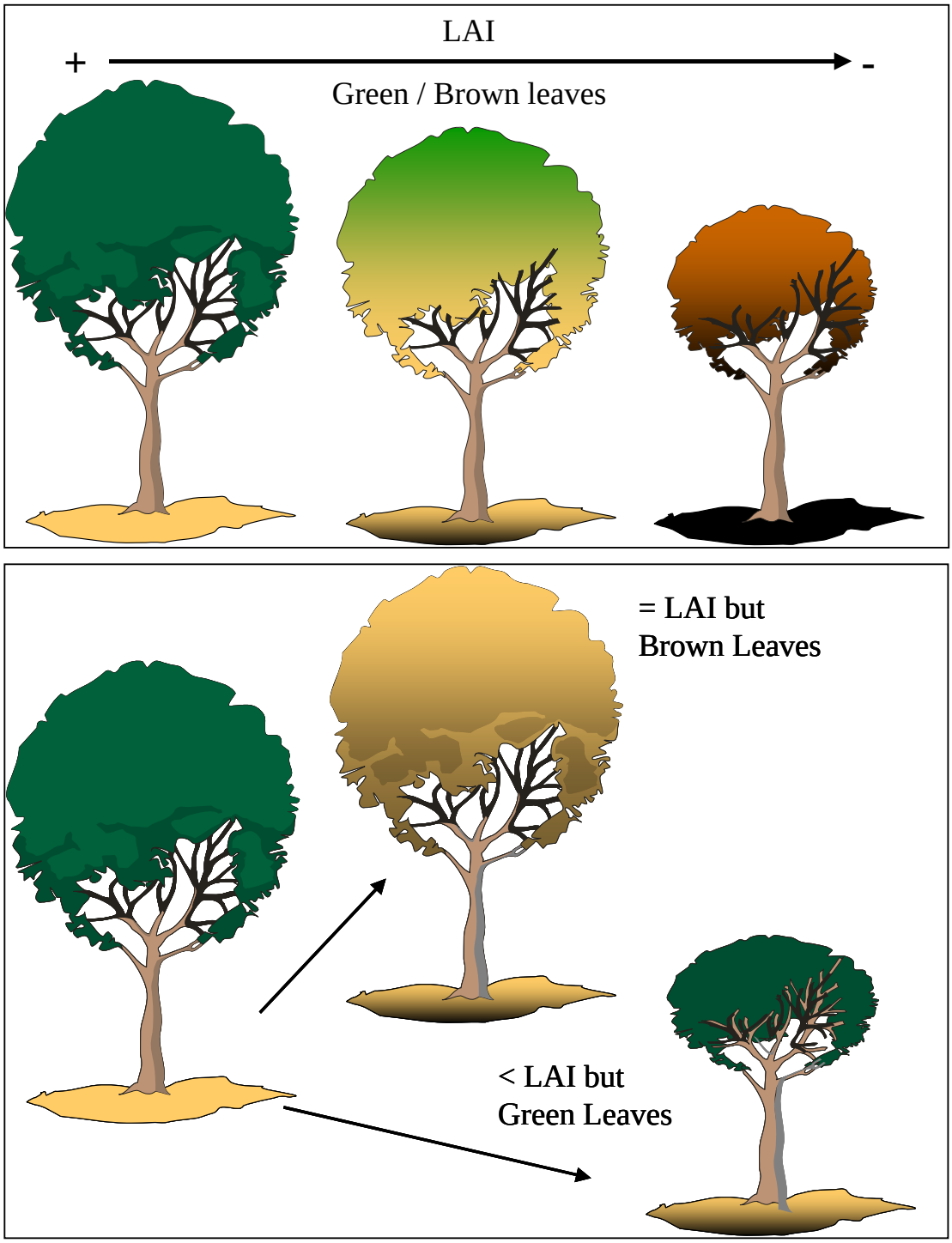

Figure 3. Simulation strategies: top) PFA and PCC change simultaneously; bottom) PFA and PCC change independently.

To simulate this scenario, ten different cases for each stratum were considered, as indicated in Table 1. From the 1,000 output cases, several filters were applied to avoid unrealistic combinations of CBI values for the different strata (high crown CBI and very low CBI underneath, for instance) following our field observations (Chuvieco *et al.,* 2006; De Santis and Chuvieco, 2007).

Table 1. Input parameters for the first simulation scenario (Chuvieco *et al.*, 2006). A, B+C, and D+E are the CBI strata, CBI refers to the Composite Burn Index, LAI is the Leaf Area Index.

A		B+C			D+E		
CBI	**% BURNED SOIL**	**CBI**	**% DRY LEAVES**	**LAI VALUE**	**CBI**	**% DRY LEAVES**	**LAI VALUE**
0.00	0.0	0.00	0.0	2.00	0.00	0.0	3.00
0.33	3.3	0.50	5.0	1.85	0.50	5.0	2.78
0.67	6.7	1.00	10.0	1.70	1.00	10.0	2.55
1.00	10.0	1.33	24.9	1.34	1.33	24.9	2.01
1.33	19.9	1.67	40.2	0.96	1.67	40.2	1.44
1.67	30.1	2.00	55.0	0.60	2.00	55.0	0.9
2.00	40.0	2.25	72.5	0.40	2.25	72.5	0.60
2.33	53.2	2.50	90.0	0.20	2.50	90.0	0.30
2.67	66.8	2.75	95.0	0.11	2.75	95.0	0.16
3.00	80.0	3.00	100.0	0.01	3.00	100.0	0.01

The second scenario assumed an independent variation of PFA and PCC, which implied that leaves could become brown and still remain on the tree, or that the LAI could be reduced while the remaining leaves maintained their green colour (Figure 3). Unlike in the first scenario, the soil substrate in the second scenario included not only charcoal and soil, but ash as well. Ash, which is the result of a full combustion process, is very important in the initial post-fire spectral response, as several authors have pointed out (Pereira *et al.,* 1999; Trigg and Flasse, 2000). However, the ash signal is very ephemeral, because ash is commonly blown away by the wind within a few days following a fire. For the second scenario, 19 combinations of soil, ash and carbon were selected (Table 2). For the PFA and PCC, seven combinations of each were chosen for each stratum. Therefore, a total of 49 cases were considered in the two vegetation strata. The result of varying the substrate conditions plus the two vegetation strata created a total of 45,619 output cases. The same filters as in the first scenario were applied, including an extra

one to remove unrealistic combinations of PFA and PCC. Cases with a high consumption of leaves (high PCC) are very unlikely to occur without any change in leaf colour (low PFA).

Table 2. Variations of background for the second simulation scenario.

CASE	% CHARCOAL	% ASH	% SOIL
1	0.00	0.00	100.00
2	5.00	0.00	95.00
3	3.75	1.25	95.00
4	2.50	2.50	95.00
5	10.00	0.00	90.00
6	7.50	2.50	90.00
7	5.00	5.00	90.00
8	25.00	0.00	75.00
9	18.75	6.25	75.00
10	12.50	12.50	75.00
11	40.00	0.00	60.00
12	30.00	10.00	60.00
13	20.00	20.00	60.00
14	70.00	0.00	30.00
15	52.50	17.50	30.00
16	35.00	35.00	30.00
17	100.00	0.00	0.00
18	75.00	25.00	0.00
19	50.00	50.00	0.00

Linear regressions between PCCe and PFA in each stratum were derived from our field data. These linear models were then applied to the simulation cases, and cases with high residuals eliminated. These linear models were as follows:

$PCC_e = PFA*0.9188 + 0.2858$ for the lower vegetation, and

$PCC_e = PFA*0.8912 – 0.0008$ for the upper vegetation layer.

Cases with higher or lower PCC than ± PCC_e were eliminated. A total of 4,100 cases remained after applying all these filters.

In both of the two first scenarios, it was assumed that before the fire the understory and the overstory had the maximum LAI values (2 and 3, respectively). In other words, we modelled the fire effects in a high-density forest area. Therefore, lower LAI values were assumed to be caused by higher burn severity (leaf losses as a result of the fire) and not by lower leaf density before the fire. This may not be realistic in those forested areas where recent fires or forestry clearing have occurred.

A third simulation scenario considered the changes in spectral reflectance from before to after the fire. While the same number of simulation cases was used for the post-fire condition as in the second scenario, only four pre-fire cases with medium to high LAI values and full green leaves were considered in both the lower and upper vegetation strata. This was done to avoid a large number of combinations derived from very different pre-fire conditions. Changes in PFA and PCC from those four pre-fire conditions were modelled by subtracting simulated post-fire reflectances of the second scenario from the four pre-fire simulated reflectance spectra (Tables 3a, 3b and 3c). Likewise, the image that was inverted was a pre-fire minus post-fire image. In this scenario, any changes in LAI are more soundly related to changes in canopy cover as a result of fire consumption than when using a single post-fire scenario.

Table 3a. Pre- and post-fire conditions for 18 combinations of charcoal, ash and soil substrates used to simulate multitemporal changes of burn severity. Simulations were conducted by subtracting each post-fire condition from the corresponding pre-fire condition.

%CHARCOAL	%ASH	%SOIL
PRE-FIRE CONDITIONS (%)		
0.00	0.00	100.00
POST-FIRE CONDITIONS (%)		
5.00	0.00	95.00
3.75	1.25	95.00
2.50	2.50	95.00
10.00	0.00	90.00
7.50	2.50	90.00
5.00	5.00	90.00
25.00	0.00	75.00
18.75	6.25	75.00
12.50	12.50	75.00
40.00	0.00	60.00
30.00	10.00	60.00
20.00	20.00	60.00
70.00	0.00	30.00
52.50	17.50	30.00
35.00	35.00	30.00
100.00	0.00	0.00
75.00	25.00	0.00
50.00	50.00	0.00

Table 3b. Pre- and post-fire conditions for six combinations of LAI values (PCC) for lower and upper vegetation layers. Pre-fire condition ranged form medium to low for each layer. Simulations were conducted by subtracting each post-fire condition from the corresponding pre-fire condition.

LOWER VEGETATION				UPPER VEGETATION			
PRE-FIRE CONDITIONS (LAI)				**PRE-FIRE CONDITIONS (LAI)**			
2.00	1.85	1.70	1.15	3.00	2.78	2.55	1.73
POST-FIRE CONDITIONS (LAI)				**POST-FIRE CONDITIONS (LAI)**			
1.85	1.71	1.57	1.06	2.775	2.57	2.36	1.60
1.70	1.57	1.45	0.98	2.55	2.36	2.17	1.47
1.15	1.06	0.98	0.66	1.725	1.60	1.47	0.99
0.60	0.56	0.51	0.35	0.9	0.83	0.77	0.52
0.20	0.19	0.17	0.12	0.3	0.28	0.26	0.17
0.01	0.01	0.01	0.01	0.01	0.01	0.01	0.01

Table 3c. Pre- and post-fire conditions for six combinations of leaf colour (PFA) for percentage of dry/green leaves, optical thickness (N) , chlorophyll content (Ca+b), brown pigment content (Cb), water content (Cw) and dry matter content (Cm). Simulations were conducted by subtracting each post-fire condition from the corresponding pre-fire condition.

% DRY / GREEN LEAVES	N	Ca+b	Cb	Cw	Cm
PRE-FIRE CONDITIONS					
0	1.4	42	30	0.0075	0.006
POST-FIRE CONDITIONS					
12.5	1.6	39	34	0.0056	0.006
25	1.8	39	42	0.0050	0.006
43.2	1.9	34	60	0.0031	0.006
80	2.5	28	91	0.0013	0.006
95	2.9	28	102	0.0006	0.006
100	3	28	106	0.0006	0.006

All simulations consider a wide range of combinations of the input parameters, which could cause confusion in the model inversion, because similar reflectance properties could be derived from different combinations of input parameters. As a result, similar reflectance patterns would correspond to different CBI values. This situation has been observed in other applications of RTM inversion (Combal *et al.,* 2002). For this reason, we considered a fourth simulation scenario, that was named post-fire "supervised approach," in which we selected only those input conditions that are the most common in Mediterranean fires, according to our field experience. In other words, instead of using the full range of variation for the input variables, only a limited number of cases were selected. This small set of spectra was extracted from the modelled spectra obtained in the second simulation scenario. It should be stressed that these spectra are derived from the simulations and not from the image, so they are independent of image conditions. Table 4 includes the simulation cases that were selected for this supervised model.

Table 4. Input conditions for the supervised simulation scenario. The CBI value of each stratum may be different regarding leaf conditions (PFA) and canopy cover (PCC) as in the second simulation.

AVERAGE	LOWER VEGETATION		UPPER VEGETATION		SUBSTRATE	
CBI	%Dry leaves	LAI	%Dry leaves	LAI	CBI A	TYPE
0.00	0	0	0	0	0	Soil
0.00	0	0	0	0	0	Soil
0.00	25	0	25	0	0	Soil
0.40	25	1.2	0	0	0	Charcoal 10%
0.50	25	1.2	25	0	0	Charcoal 10%
0.70	43	0.6	25	2.78	1	Soil
1.00	25	0.01	25	1.8	1.5	Charcoal 100%
1.50	43	1.2	43	1.8	1	Charcoal 10%
1.50	100	1.7	100	2.55	1.5	Charcoal 100%
1.60	95	0.01	25	0.5	0	Charcoal 12.5%+Ash 12.5%
1.70	80	0.2	25	2.55	3	Charcoal 25%
1.90	80	0.6	80	0.9	3	Charcoal 100%
1.90	2.5	0.6	25	1.8	1.5	Charcoal 25%
2.00	100	0	0	0.9	3	Charcoal 100%
2.00	100	1.2	100	2.55	1.5	Charcoal 25%
2.00	95	0.6	43	1.8	3	Charcoal 100%
2.10	80	0.2	95	1.8	3	Charcoal 100%
2.30	95	0.6	80	0.9	3	Charcoal 100%
2.30	100	0	80	0.01	3	Charcoal 100%
2.50	95	0.01	95	0.3	1.5	Charcoal 25%
2.70	100	0.2	100	0.3	3	Charcoal 100%
2.80	100	0.01	100	0.01	3	Charcoal 100%
3.00	100	0.01	100	0.01	3	Charcoal 100%
3.00	100	0.01	100	0.01	3	Charcoal 100%
3.00	0	0	0	0	3	Charcoal 75% + Ash25%

2.5 Forward and Backward Simulation

Forward simulation was based on the input parameters described above. All simulations were performed for the spectral range of 400 nm to 2,400 nm, at 10 nm-intervals giving a total of 201 spectral bands per modelled spectrum. To reduce model complexity, some variables were kept fixed through all simulations: leaf angle distribution = plagiophile, leaf shape = ellipse form (eccentricity = 0.95), sun zenith angle = 30^{o}, nadir angle = 0^{o}, azimuth angle = 0^{o}.

Forward simulations are useful to analyze the effect of input parameters in the simulated reflectance to better understand their importance in the final output, as well as to identify which bands are more sensitive to each input parameter. In our case, we were interested in determining which bands or band combinations were more sensitive to variations in soil substrate, leaf colour or leaf cover, as they are combined in the CBI computation.

The simulations generated in the different scenarios can then be related to reflectance values as extracted from satellite data. The most similar spectra between each observed spectrum and the whole range of simulated spectra should provide an estimation of the input parameters that generated that particular spectrum. This is the basis for the inversion of RTM, which is based on minimizing the merit function:

$$\chi^2 = \sum_{i=1}^{n} \left[\rho_i - \mathrm{M}(\Theta, X_i)\right]^2 \quad (1)$$

where χ is the difference between the observed reflectance (ρ) and the modelled reflectance M(Θ, X), for a certain set of input parameters (Θ, X), with X being the value to be estimated, and n the spectral wavelengths of the input image.

There are several alternatives for model inversion in the literature: iterative processes, neural networks, statistical fitting and previous generation of a look up table (LUT) (Liang, 2004). The look up table is used in this paper because it is quicker and provides a control scenario for searching for the input parameters. The LUT includes the output from running the RTM for the different simulation scenarios (M(Θ, X) as stated in equation 1), so the inversion process does not need to run the model again, but rather it focuses on finding which observed reflectance spectrum is the most similar to the modelled one.

For the merit function of "similarity," several strategies are used, the most common of which was the minimum quadratic distance (as formulated in equation 1). In this paper, several methods were explored based on hyperspectral methods of classification. The most robust for our purposes was the Spectral Angle Mapper (SAM; Kruse *et al.,* 1993), which calculates the angle between two spectral vectors with the same origin and selects, for each pixel in the image, the reference spectrum with the lowest spectral angle. In this case, the reference spectra were produced by the simulations and stored in the LUT along with their CBI value. Once the reference spectrum with the minimum spectral angle was selected, the image pixel was labelled with the CBI value of the reference spectrum.

2.6 Study Site

The efficiency of model inversion from the different simulation scenarios was tested using a large forest fire that recently occurred in central Spain (Figure 4). The fire occurred in the middle of July 2005 and was caused by human carelessness under very dry weather conditions: maximum temperature 35 ^{o} C; relative humidity 22%; 30 days since the last rainfall event; wind speed 10-23 Km/h. The fire lasted four days and burned approximately 13,000 ha in an area dominated by pine trees (*Pinus pinaster* L.) mixed with semi-deciduous oaks (*Quercus faginea* Lam. and *Quercus pyrenaica* Willd.) and a marginal sector covered mostly by Mediterranean shrubs (*Cistus ladanifer* L., *Cistus albidus* L., *Rosmarinus officinalis* L., *Juniperus oxycedrus* L., *Rosa canina* L., *Cytisus scoparius* L., and *Lavandula pedunculata* L.).

Eleven fire-fighters died while suppressing the fire, which caused a great impact in the national media.

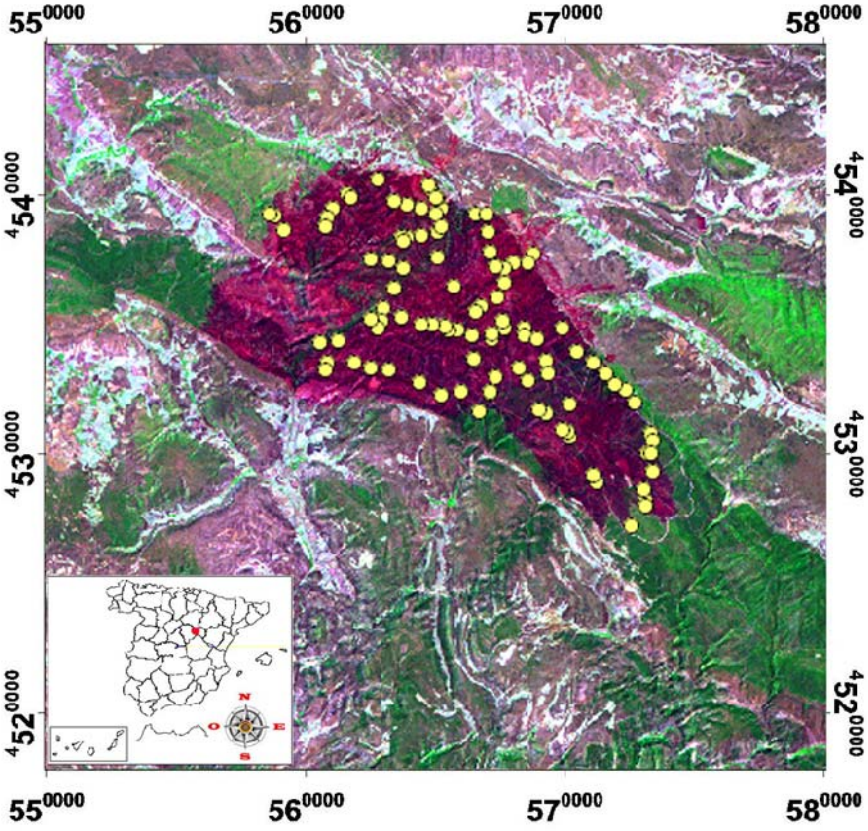

Figure 4. Location of the study case.

The topography of the area is rugged and the altitudes range from 1,100 m to 1,400 m. Rainfall in the region averages 600 mm to 800 mm per year. Maximum and minimum precipitations are recorded in November to December, and in July to August, respectively.

The average annual temperature is 12 ^{o}C.

A field campaign to obtain CBI values for the burn area was undertaken between August and September, a few weeks after the fire. Therefore, the measured CBI values reflect the short-term burn severity, using Key's terminology (Key, 2005). A total of 103 plots were sampled in the field using the CBI protocol. Plot coordinates were registered with a Garmin GPS system (GARMIN GPS 12, http://www.garmin.com), with an average precision of ± 10 m. Most of the burn area presented high CBI values. Only 18 out of 103 plots had CBI values lower than 2, and 31 had CBI higher than 2.9. In spite of being a large fire, the severity values did not cover the whole spectrum of possible CBI values, and intermediate levels (CBI between 1 and 2) were uncommon. This imposed a challenge for verifying the performance of the inversion results, as will be discussed later.

2.7 Image Processing

Sensors with different spectral and spatial resolution were used for testing the robustness of the model inversion results. Table 5 shows the spatial and spectral characteristics of the images used. In spite of the large differences in spectral and spatial resolution, all images showed a clear and similar pattern in their portrayal of the burn area (Figure 5). They were acquired between 15 to 30 days post-fire, except for SPOT-HRG that was collected 60 days post-fire.

The images were geometrically corrected using reference data extracted from a previously ortho-rectified Landsat image. The SPOT-HRG, Landsat-TM and AWIFS images were converted to radiance using calibration coefficients included in the image header. Atmospheric correction was based on the dark-object method proposed by Chavez (1996). They were also corrected for topographic shade using a variation of the Teillet's C correction method (Riaño *et al.,* 2003). MERIS and MODIS images were obtained from the FR2P-level 02 product and the standard MOD09 reflectance product respectively, which include radiometric calibration and atmospheric correction.

Table 5. Spatial resolution (m) and center wavelength (µm) of the sensors used for this study.

	SENSOR				
	SPOT-HRG	LANDSAT-TM[2]	IRS-AWIFS	ENVISAT-MERIS	TERRA-MODIS
	SPATIAL RESOLUTION (m)				
	10 / 20	30	60	300	500
BAND	CENTER WAVELENGHTS (µm)				
1	0.545	0.487	0.555	0.413	0.469
2	0.645	0.571	0.650	0.442	0.555
3	0.835	0.661	0.815	0.490	0.645
4	1.675[1]	0.837	1.625	0.510	0.857
5		1.677		0.560	1.240
6		Thermal [2]		0.620	1.640
7		2.215		0.665	2.130
8				0.681	
9				0.709	
10				0.754	
11				0.778	
12				0.865	
13				0.885	

[1]HRG 1.675 µm has 20 m resolution. [2]Landsat-TM thermal band was not considered.

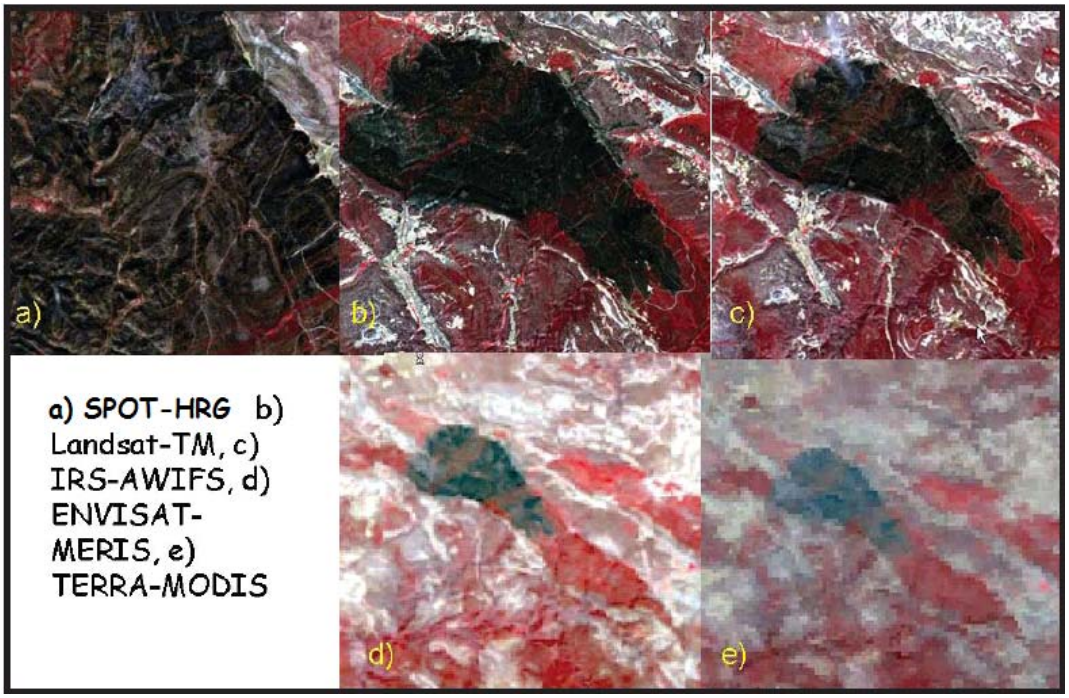

Figure 5. Images used for the model inversion: a) SPOT-HRG, b) Landsat-TM, c) IRS-AWIFS, d) ENVISAT-MERIS, e) TERRA-MODIS.

3. Results

3.1 Comparison of simulated and actual reflectances

To simplify the comments, the comparison of simulated and observed reflectances will be based on Landsat-TM images because it provides the best compromise between spatial and spectral resolution from our image dataset.

Figure 6 shows the spectral reflectance of simulated and actual spectra for a set of sample ranges of CBI values from the supervised post-fire simulation. The image spectra were extracted from the post-fire Landsat-TM image. It is noticeable that the observed reflectance for the lower values of CBI is significantly lower than the simulated reflectance, which may be caused by our RTM assumptions, as will be discussed later on. This discrepancy in absolute reflectance values between the modelled and the observed reflectance supports the use of the SAM as the most appropriate strategy for model inversion because SAM relies on directions of spectral vectors and not on absolute values. The higher CBI values show a closer fit between observed and simulated reflectance.

3.2 Performance of Simulation Models for Retrieval of CBI

Table 6 presents the results for the estimation of CBI using the inversion of simulated values for the Landsat-TM images. All Pearson r values are highly significant and provide coherent trends. Slope is close to 1 for the post-fire scenarios (single, extended, and supervised), while it is lower for the multitemporal simulation. The multi-temporal scenario also has the lowest r value, which is mainly caused by the small sensitivity of the model to low CBI values. The slope values of less than 1 indicate that underestimations occurred frequently for all scenarios. The standard errors of the estimation are in the range of 0.47 to 0.68. This is about one sixth of the total CBI range, which implies that CBI values can be estimated with fairly good accuracy. The best results were obtained in the fourth (supervised) scenario, where only a selected set of substrate, PFA and PCC combinations, were extracted. This scenario is by far the simplest one because it only requires 25 reference spectra and performs better than others, especially when considering the total correlation, standard error, and average extreme residuals. Figure 7 shows a map of the study case with the spatial variation of CBI values for this fourth simulation scenario. The spatial patterns show a good agreement with field-observed severities, especially for the upper part of the CBI scale.

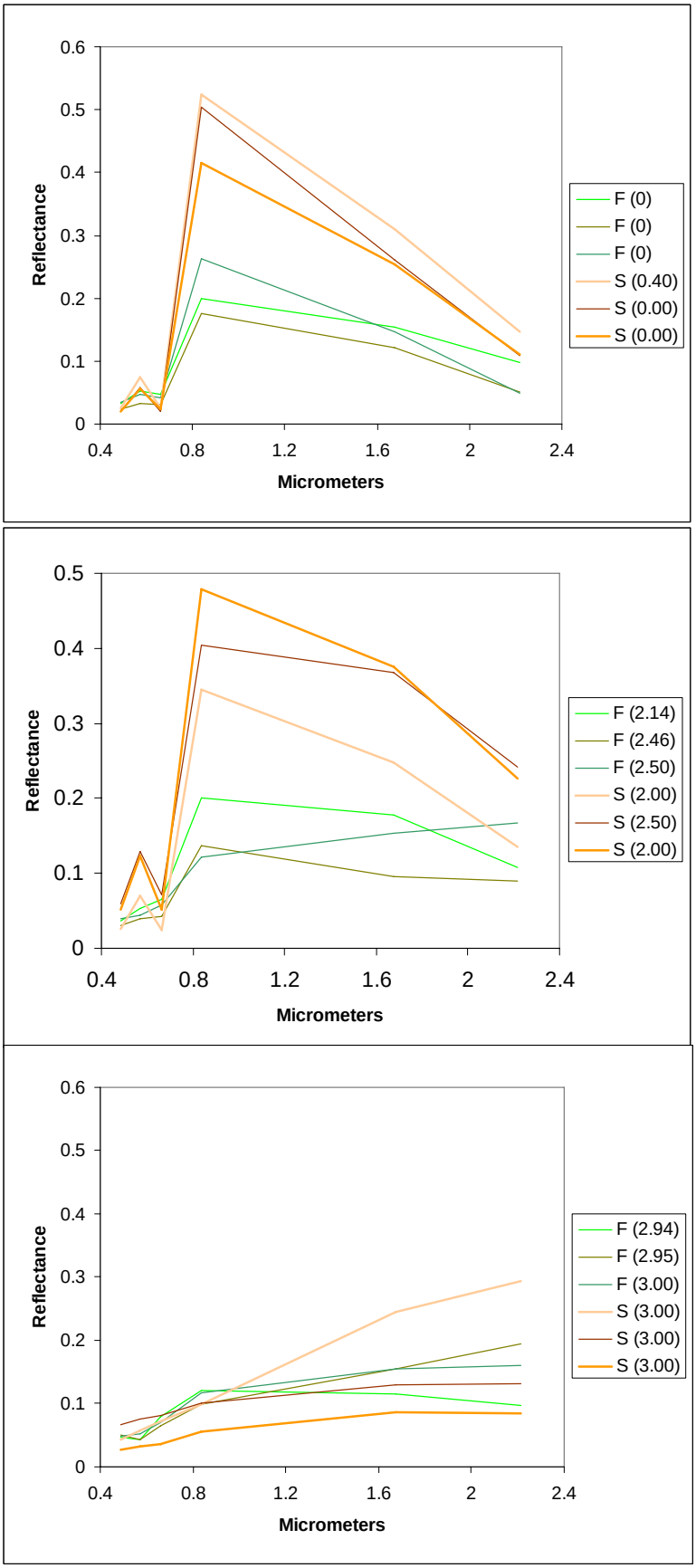

Figure 6. Comparison of simulated (S) spectra and actual TM data (F) for several ranges of CBI values.

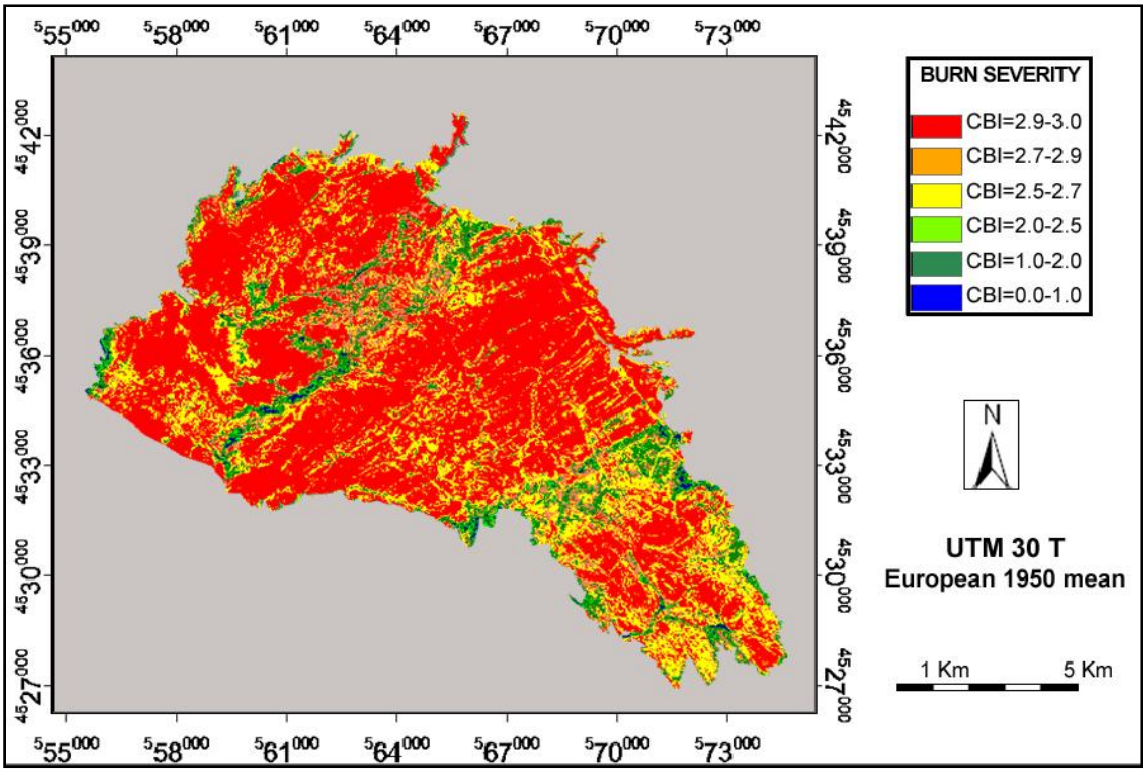

Figure 7. Estimation of CBI values for the study area from the inversion of the fourth simulation scenario (supervised) with Landsat-TM images.

3.3 Comparison of sensors

Using the LUT generated for the supervised simulation scenario, inversion techniques were applied to the other images of our study case. The spectral library created for the LUT was convolved to the center wavelengths of the SPOT-HRG, IRS-AWIFS, ENVISAT-MERIS and TERRA-MODIS sensors. The results are included in Figure 8, which shows the scattergraph between observed and predicted CBI values for the different sensors. The higher accuracy was obtained by the Landsat- TM reflectance data, which has the best compromise between spectral and spatial resolution of all images used. The second best result was obtained from AWIFS data, instead of the SPOT-HRG, as we had hypothesized. In spite of having the same spectral resolution, the finer pixel size of SPOT-HRG apparently tends to create more spatial variability, which confounds estimation problems.

The coarser resolution data perform generally well, with r^2 values in the range of 0.5. MERIS offers a greater sensitivity than MODIS, which is likely caused by both greater spectral and spatial resolution. In general, all sensors analyzed tend to underestimate the CBI value, with regression intercepts between 0.7 and 2.2.

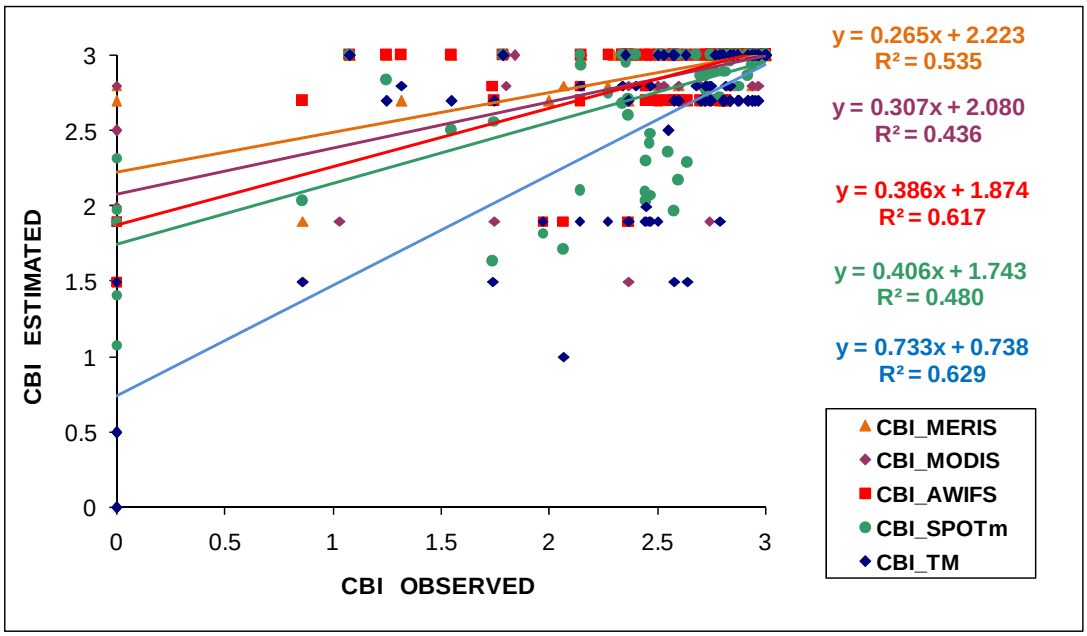

Figure 8. Comparison of simulation results for different sensors using the same LUT.

4. Discussion

This paper has presented several approaches to the use of RTM simulation for burn severity estimation using different satellite images. The study has shown the common advantages and disadvantages of simulation models in the interpretation of remotely sensed images.

The most important disadvantages refer to the complexity of selecting and parameterizing the RTM so it can provide a similar pattern to observed reflectance. As it was shown in Figure 6, the actual reflectance values clearly differ from modelled values in the lower part of the CBI scale, which is when vegetation is greener and more dense. This problem may be associated to the Kuusk model assumptions. Kuusk's is a canopy model, and therefore, when simulated and pixel reflectances are compared, it is assumed that each pixel is fully covered by a canopy. In the case of forested areas, this assumption implies that shade and soil are only affecting the canopy but not the areas outside the canopy. Typically, a Landsat-TM pixel would be a combination of vegetation canopies (one or several, depending on vertical structure, but this is taken into account in the Kuusk model), soil background, and shadows. When the canopy cover is close to 100%, this assumption may be valid. However, in other cases where the canopy is sparse such as in our area, the assumption is not as valid. Consequently, the use of landscape scale or geometric models (such as Geosail, GORT, DART) that account for discontinuous canopies would be more desirable. However, these models do not provide

simulation for vertical stratification, which is very important in burn severity determination, and was one of the reasons for our selection of the Kuusk model.

In any case, regardless of the canopy versus landscape approach, our simulations perform well in modelling spectral shape across all the bands. In this respect, tendencies between simulated and observed spectral shape are more similar than absolute reflectance values, which supports the use of the Kuusk model as a first approximation to burn severity simulation.

As far as parameterization is concerned, this paper has explored the use of four simulation scenarios, testing a wide range of assumptions regarding burn conditions. It has been shown that extending the range of input conditions does not necessarily improve the results of inversion, but rather it decreases them. The ill-posed problem (Combal *et al.,* 2002) of model inversion may be behind this lack of improvement because very similar reflectance patterns can be derived from different CBI values and that introduces noise into the inversion process. Therefore, additional efforts are required to obtain models and simulation scenarios that can be more confident in providing consistent reflectance signatures for specific burn severities.

As far as multitemporal change is concerned, the reduction of accuracy with respect to the supervised post-fire simulation scenario is probably caused by the multiplying effect of potential noises introduced by radiometric correction in pre-fire and post-fire images.

In spite of all these difficulties, it has been demonstrated that model inversion is a quick and universal mechanism to estimate CBI values because it is sensor and site independent. The same simulation scenario was applied with consistent results with different sensors. Only one study case has been presented here, but the physical basis of our simulation should be applicable to other fires with similar ecosystem characteristics: ie., Mediterranean fires. In any case, it is important to emphasize that model inversion does not require any field data, assuming of course that the model is properly parameterized and validated. In other words, the relations are not dependent on the specific burn conditions, but are associated to ecophysiological changes caused by fire (changes in soil background, leaf colour or leaf cover proportion).

As far as accuracy concerns, the supervised scenario provided similar results to other study cases based on empirical equations with an r^2 close to 0.65. For instance, Cocke *et al.* (2005) obtained 73% to 75% agreement to estimates CBI from Landsat multitemporal images using an empirical model with the Normalized Burn Ratio (NBR) in Arizona. Similarly, Epting *et al.* (2005) found r^2 correlations between 0.63 and 0.9 again using the CBI and the NBR in Alaska boreal forest, while van Wagtendonk *et al.* (2004) found r^2 values of 0.83 in the Yosemite National Park, although they used a polynomial model to relate CBI and changes in NBR. In this context,

the simulation scenarios provide a good alternative to derive CBI estimations from empirical models as the field measurements can be focused on validating the results.

Future improvements of this simulation approach should include new models that take into better account the shade and soil variation to be expected in forested areas within a pixel. Geometrical and hybrid models should be tested in this regard. Additional effort is also needed to parameterize the input variables to reduce factors of noise that have been observed in our full range simulations.

In summary, this paper has shown that simulation models have a great potential in burn severity estimation. First, because they provide a physical explanation for relations observed empirically, they make it possible to generalize local findings. Secondly, they reduce the amount of field work required to extract severity information from remote sensing images because the interpretation is not based on statistical fitting. Finally, they provide a much wider range of conditions than those that are commonly observed in a single fire, regardless of fire behaviour patterns, since the output conditions can be simulated for a wide range of scenarios. The main drawbacks of simulation models are the complexity of their formulation and calibration.

Acknowledgements

This paper was originally presented at the 2006 Fire Ecology and Management Congress, San Diego. The main author received financial support from the organization, as well as from the sabbatical program of the University of Alcalá. This research is also part of the Preview European Project (www.preview-risk.com, EA21.CR/AC/03.064).

References

Brewer, C.K., J.C. Winne, R.L. Redmond, D.W. Opitz, and M.V. Mangrich (2005). Classifying and mapping wildfire severity: a comparison of methds. *Photogrammetric Engineering and Remote Sensing.* 71: 1311-1320.

Chavez, P.S. (1996). Image-based atmospheric corrections: revisited and improved. *Photogrammetric Engineering and Remote Sensing.* 62: 1025-1036.

Chuvieco, E., D. Cocero, I. Aguado, A. Palacios-Orueta, and E. Prado (2004). Improving burning efficiency estimates through satellite assessment of fuel moisture content. *Journal of Geophysical Research – Atmospheres*.109: 1-8.

Chuvieco, E., D. Riaño, F.M. Danson, and M.P. Martín (2006). Use of a radiative transfer model to simulate the post-fire spectral response to burn severity. *Journal of Geophysical Research – Biosciences.* 111: 1-15.

Cocke, A.E., P.Z. Fule, and J.E. Crouse (2005). Comparison of burn severity assessments using Differenced Normalized Burn Ratio and ground data. *International Journal of Wildland Fire* 14: 189-198.

Combal, B., F. Baret, M. Weiss, A. Trubuil, D. Mace, A. Pragnere, R. Myneni, Y. Knyazikhin, and L. Wang (2002). Retrieval of canopy biophysical variables from bidirectional reflectance using prior information to solve the ill-posed inverse problem. *Remote Sensing of Environment*. 84: 1-15.

Danson, F.M., and P. Bowyer (2004). Estimating live fuel moisture content from remotely sensed reflectance. *Remote Sensing of Environment*. 92: 309-321.

De Santis, A., and E. Chuvieco (2007). Burn severity estimation from remotely sensed data: performance of simulation versus empirical models. *Remote Sensing of Environment*. 108: 422-435.

Díaz-Delgado, R., F. Lloret, and X. Pons (2003). Influence of fire severity on plant regeneration by means of remote sensing imagery. *International Journal of Remote Sensing.* 24: 1751-1763.

Díaz-Delgado, R., X. Pons, and F. Lloret (2001). Fire severity effects on vegetation recovery after fire. The Bigues i Riells wildfi re case study. Pages 152-155 in: E. Chuvieco and M.P. Martín, editors. *3rd International Workshop on Remote sensing and GIS applications to Forest Fire Management. New methods and sensors*. EARSeL, Paris, France.

Epting, J., D.L. Verbyla, and B. Sorbel (2005). Evaluation of remotely sensed indices for assessing burn severity in interior Alaska using Landsat TM and ETM+. *Remote Sensing of Environment*. 96: 328-339.

Gastellu-Etchegorry, J.P., V. Demarez, V. Pinel, and F. Zagolski (1996). Modelling radiative transfer in heterogeneous 3-D vegetation canopies. *Remote Sensing of Environment.* 58: 131-156.

Gastellu-Etchegorry, J.P., E. Martin, and F. Gascon (2004). DART: a 3D model for simulating satellite images and studying surface radiation budget. *Remote Sensing of Environment*. 25: 73-96.

Hosgood, B., S. Jacquemoud, G. Andreoli, J. Verdebout, G. Pedrini, and G. Schmuck (1994). Leaf Optical Properties EXperiment 93 (LOPEX93). Page 21 in: *European Commission, Joint Research Centre, Institute for Remote Sensing Applications.*

Jacquemoud, S. (1990). PROSPECT: a model to leaf optical properties spectra. *Remote Sensing of Environment.* 34: 74-91.

Jain, T.B., and R.T. Graham (2004). Is forest structure related to fi re severity? Yes, no, and maybe: methods and insights in quantifying the answer. Pages 217-234 in: *USDA Forest Service Proceedings RMRS-P 34.*

Kachmar, M., and G.A. Sanchez-Azofeifa (2006). Detection of post-fire residuals using high- and medium-resolution satellite imagery. *Forestry Chronicle*. 82: 177-186.

Key, C. (2005). Remote Sensing sensitivity of fire severity and fire recovery. Pages 29-39 in: J. Riva, F. Pérez-Cabello and E. Chuvieco, editors. *Proceedings of the 5th International Workshop on Remote Sensing and GIS applications to Forest Fire Management: Fire Effects Assessment*. Universidad de Zaragoza, Spain, and GOFC-GOLD, EARSeL, Paris, France.

Key, C.H., and N. Benson (2005). Landscape Assessment: Ground measure of severity, the Composite Burn Index; and remote sensing of severity, the Normalized Burn Ratio. Pages CD: LA1-LA51 in D.C. Lutes, R.E. Keane, J.F. Caratti, C.H. Key, N.C. Benson and L.J. Gangi, editors. *FIREMON: Fire effects monitoring and inventory system. USDA Forest Service, General Technical Report RMRS-GTR-164.*

Kruse, F.A., A.B. Lefkoff, J.B. Boardman, K.B. Heidebrecht, A.T. Shapiro, P.J. Barloon, and A.F.H. Goetz (1993). The spectral image processing (SIPS) - interactive visualization and analysis of imaging spectrometer data. *Remote Sensing of Environment*. 44: 145-163.

Kuusk, A. (2001). A two-layer canopy reflectance model. *Journal of Quantitative Spectroscopy and Radiative Transfer*. 71: 1-9.

Lachowski, H.M., P. Hardwick, R. Griffith, A. Parsons, and R. Warbington (1997). Faster, better data for burned watersheds needing emergency rehab. *Journal of Forestry*. 95: 4-8.

Lentile, L.B., Z.A. Holden, A.M.S. Smith, M.J. Falkowski, A.T. Hudak, P. Morgan, S.A. Lewis, P.E. Gessler, and N.C. Benson (2006). Remote sensing techniques to assess active fire characteristics and post-fire effects. *International Journal of Wildland Fire.* 15: 319-345.

Li, X., A.H. Strahler, and C.E. Woodcock (1995). A hybrid geometric optical-radiative transfer approach for modelling albedo and directional reflectance of discontinuous canopies. *IEEE Transactions on Geoscience and Remote Sensing*. 33: 466-480.

Liang, S. (2004). *Quantitative remote sensing for land surface characterization*. Wiley and Sons, Hoboken, New Jersey, USA.

Michalek, J.L., N.H.F. French, E.S. Kasischke, R.D. Johnson, and J.E. Colwell (2000). Using Landsat TM data to estimate carbon release from burned biomass in an Alaskan spruce forest complex. *International Journal of Remote Sensing*. 21: 323-338.

Miller, J.D., and S.R. Yool (2002). Mapping forest post-fire canopy consumption in several overstory types using multi-temporal Landsat TM and ETM data. *Remote Sensing of Environment*. 82:481–496.

Moreno, J.M., and W.C. Oechel (1989). A simple method for estimating fire intensity after a burn in California chaparral. *Oecologia Plantarum.* 10: 57-68.

Ni, W.G., X.W. Li, C.E. Woodcock, M.R. Caetano, and A.H. Strahler (1999). An analytical hybrid GORT model for bidirectional reflectance over discontinuous plant canopies. *IEEE Transactions On Geoscience And Remote Sensing. IEEE Transactions on Geoscience and Remote Sensing*. 37: 987-999.

North, P.R.J. (1996). Three-dimensional forest light interaction model using a MonteCarlo method. *IEEE Transactions on Geoscience and Remote Sensing.* 34: 946-956.

Parra, A., and E. Chuvieco (2005). Assessing burn severity using Hyperion data. Pages 239-244 in: J. Riva, F. Pérez-Cabello and E. Chuvieco, editors. *Proceedings of the 5th International Workshop on Remote Sensing and GIS applications to Forest Fire Management: Fire Effects Assessment.* Universidad de Zaragoza, Spain and GOFC-GOLD, EARSeL, Paris, France.

Pereira, J.M.C., B. Mota, J.L. Privette, K.K. Caylor, J.M.N. Silva, A.C.L. Sa, and W. Ni-Meister (2004). A simulation analysis of the detectability of understory burns in miombo woodlands. *Remote Sensing of Environment*. 93: 296-310.

Pereira, J.M.C., A.C.L. Sa, A.M.O. Sousa, J.M.N. Silva, T.N. Santos, and J.M.B. Carreiras (1999). Spectral characterisation and discrimination of burnt areas. Pages 123-138 in E. Chuvieco editor. *Remote Sensing of Large Wildfires in the European Mediterranean Basin*. Springer-Verlag, Berlin, Germany.

Pérez, B., and J. Moreno (1998). Methods for quantifying fire severity in shrubland-fires. *Plant Ecology*. 139: 91-101.

Pinty, B., J.L. Widlowski, M. Taberner, N. Gobron, M.M. Verstraete, M. Disney, F. Gascon, J.P. Gastellu, L. Jiang, and A. Kuusk (2004). Radiation Transfer Model Intercomparison (RAMI) exercise: results from the second phase, 109, D06210, doi:06210.01029/02003JD004252.

Riaño, D., E. Chuvieco, F.J. Salas, and I. Aguado (2003). Assessment of Different Topographic Corrections in Landsat-TM Data for Mapping Vegetation Types. *IEEE Transactions on Geoscience and Remote Sensing*. 41: 1056-1061.

Riaño, D., P. Vaughan, E. Chuvieco, P. Zarco-Tejada, and S.L. Ustin (2005). Estimation of fuel moisture content by inversion of radiative transfer models to simulate equivalent water thickness and dry matter content: analysis at leaf and canopy level. *IEEE Transactions on Geoscience and Remote Sensing*. 43: 819-826.

Rogan, J., and J. Franklin (2001). Mapping wildfire burn severity in southern California forests and shrublands using enhanced Thematic Mapper imagery. *Geocarto International*. 16: 89-99.

Rogan, J., and S.R. Yool (2001). Mapping fi re-induced vegetation depletion in the Peloncillo Mountains, Arizona and New Mexico. *International Journal of Remote Sensing.* 22: 3101-3121.

Roy, D., Y. Jin, P. Lewis, and C. Justice (2005). Prototyping a global algorithm for systematic fire affected area mapping using MODIS time series data. *Remote Sensing of Environment.* 97: 137-162.

Roy, D., and T. Landmann (2005). Characterizing the surface heterogeneity of fire effects using multi-temporal reflective wavelength data. *International Journal of Remote Sensing*. 26: 4197- 4218.

Roy, D., P.E. Lewis, and C.O. Justice (2002). Burned area mapping using multi-temporal moderate spatial resolution data—a bi-directional reflectance model-based expectation approach. *Remote Sensing of Environment.* 83: 263-286.

Roy, D.P., L. Boschetti, and S.N. Trigg (2006). Remote sensing of fire severity: assessing the performance of the Normalized Burn Ratio*. IEEE Geoscience and Remote Sensing Letters.* 3: 112-116.

Ruiz-Gallardo, J.R., S. Castaño, and A. Calera (2004). Application of remote sensing and GIS to locate priority intervention areas after wildland fires in Mediterranean system: a case study from south-eastern Spain. *International Journal of Wildland Fire*. 13: 241-252.

Sa, A.C.L., J.M.C. Pereira, and J. Silva (2005). Estimation of combustion completeness based on fire-induced spectral reflectance changes in a dambo grassland (Western Province, Zambia). *International Journal of Remote Sensing.* 26: 4185-4195.

Scurlock, J.M.O., G.P. Asner, and S.T. Gower (2001). Worldwide historical estimates of leaf area index, 1932–2000. *Oak Ridge National Laboratory Technical Report* ORNL/TM-2001/268.

Trigg, S., and S. Flasse (2000). Characterizing the spectral-temporal response of burned savannah using in situ spectroradiometry and infrared thermometry. *International Journal of Remote Sensing.* 21: 3161-3168.

Turner, M.G., W.W. Hargrove, R.H. Gardner, and W.H. Romme (1994). Effects of fire on landscape heterogeneity in Yellowstone National Park, Wyoming. *Journal of Vegetation Science.* 5: 731- 742.

van Wagtendonk, J.W., R.R. Root, and C.H. Key (2004). Comparison of AVIRIS and Landsat ETM+ detection capabilities for burn severity. *Remote Sensing of Environment* . 92: 397-408.

White, J.D., K.C. Ryan, C.C. Key, and S.W. Running (1996). Remote sensing of forest fire severity and vegetation recovery. *International Journal of Wildland Fire*. 6: 125-136.

Zarco-Tejada, P.J., J.R. Miller, T.L. Noland, G.H. Mohammed, and P.H. Sampson (2001). Scaling-up and model inversion methods with narrowband optical indices for chlorophyll content estimation in closed forest canopies with hyperspectral data. *IEEE Transactions on Geoscience and Remote Sensing.* 39: 1491-1507.

III

Available online at www.sciencedirect.com
ScienceDirect
Remote Sensing of Environment
Remote Sensing of Environment
www.elsevier.com/locate/rse

GeoCBI: a modified version of the Composite Burn Index to estimate burn severity for remote sensing applications

Angela De Santis, Emilio Chuvieco

Department of Geography, University of Alcalá, Alcalá de Henares, Spain

Received 11 April 2008; under review

Abstract

Burn severity estimation is a key factor in the post-fire management. Remote sensing studies of burn severity have generally focused on the performance of specifically designed spectral indices when correlated against field estimation and, overall, results have been inconsistent. Therefore, this paper has studied the relationship between the widely used Composite Burn Index (CBI) and spectral data, using a simulation analysis. Subsequently, a modified version of this index, called GeoCBI, is proposed. The new index takes into account two critical parameters: fraction of cover (FCOV) per vegetation stratum and changes in the leaf area index (LAI). Compared to CBI, field results show that GeoCBI is more related to spectral signatures of burned field plots. In addition, GeoCBI maintains the ecological meaning of CBI and the changes in the field protocol do not increase the difficulty of field work.

Keywords: Forest fire; burn severity; CBI; GeoCBI; simulation analysis; PROSPECT; GeoSail; spectral indices.

1. Introduction

Forest fires can be a major ecological disturbance agent that modifies landscapes, especially when normal fire frequencies and/or intensities are modified. The main negative fire effects are: vegetation biomass loss, soil degradation (Doerr *et al.*, 2006; García-Haro *et al.*, 2001; Salgado *et al.*, 2004, Lewis *et al.*, 2006) and greenhouse gas emissions (Andreae and Merlet, 2001; Nagahamaa and Suzuki, 2007; Narayan *et al.*, 2007). Due to the wide range of spatial and temporal scales, the interpretation of causal factors, fire effects and ecosystem responses are a growing challenge for both researchers and managers (Lentile *et al.*, 2006).

To clarify the complex interaction between fires and ecosystems, two different orders of fire effects have been proposed (Key, 2006). The *first-order effects,* which are associated to the short-term response immediately after the fire and correspond to the ecological consequences on the biophysical pre-fire components (Key and Benson, 2005). The *second-order effects* (long-term response) describe the recovery of the ecosystem from the impacts of the fire (Kasischke *et al.*, 2007). Both short and long-term post-fire effects on vegetation and soil, as well as other subsequent processes, can be estimated in terms of "burn severity" (Chuvieco *et al.*, 2006; De Santis and Chuvieco, 2007; Jain, 2004a; Key and Benson, 2005; Lentile *et al.*, 2006; van Wagtendonk *et al.*, 2004; White *et al.*, 1996), which can be defined as the amount of damage or change of a burned area respect to the pre-fire scenario (Key and Benson, 2005).

A detailed and rapid knowledge of the level of damage and its spatial distribution (burn severity map) is essential to quantify the impact of fires on landscapes (van Wagtendonk *et al.*, 2004), select and prioritize treatments applied on site (Bobbe *et al.*, 2001; Patterson and Yool, 1998), plan and monitor restoration and recovery activities and, finally, to provide baseline information for future monitoring (Brewer *et al.*, 2005).

Several methods have been proposed to estimate burn severity on site, using a post-fire field evaluation of soil and vegetation conditions (table 1).

Table 1. Field variables assessed to estimate burn severity.

VARIABLES ASSESSED IN THE FIELD	REFERENCE
Percentage of tree basal area mortality	(Chappell and Agee, 1996)
Decrease in plant cover	(Jain and Graham, 2004b; Rogan and Yool, 2001)
Volatilization or transformation of soil components to soluble mineral forms	(Turner *et al.*, 1994; Wang, 2002; Wells and Campbell, 1979)
Proportion of fine branches remaining on the canopy	(Moreno and Oechel, 1989)
Degree of canopy consumption and mortality	(Doerr *et al.*, 2006; Kokaly *et al.*, 2007; Kushla and Ripple, 1998; Patterson and Yool, 1998; Rogan and Franklin, 2001; Ryan and Noste, 1985)
Char and ash cover	(Smith *et al.*, 2005b)
Composite Burn Index (CBI, Key and Benson, 2005) and its modifications	(Chuvieco *et al.*, 2007; Cocke *et al.*, 2005; De Santis and Chuvieco, 2007; Epting *et al.*, 2005; Key and Benson, 2005; Miller and Yool, 2002; Miller and Thode, 2007; Sorbel and Allen, 2005; van Wagtendonk *et al.*, 2004; Wimberly and Reilly, 2006).

However, the definition of a common field index to quantify fire effects would ensure consistent and comparable results (Key, 2006). An example of this attempt is the Composite Burn Index (CBI, Key and Benson, 2005), which was developed as an operational methodology for burnt severity assessment on a national scale in the U.S, in the framework of the FIREMON (Fire Effects Monitoring and Inventory Protocol) project. CBI discriminates burn severity variations in forests better than in shrublands and grassland (Kasischke *et al.*, 2007; Key and Benson, 2005). According to Key and Benson (2005), CBI was also focused on estimating the main field variables which determine the reflectance of pixels of medium resolution satellite imagery, namely Landsat TM. Thus, the CBI field form includes the average conditions of soil and plant communities in 30m-diameter plots. Fire effects are assessed at five vertical strata, organized in a hierarchical structure (table 2). The principal field variables estimated are litter and fuel consumption, changes in soil colour, foliage alteration, canopy mortality and char height. These attributes are rated in numerical scores ranging from 0 (unburned) to 3 (completely burned), by at least two field observers. Different attributes per stratum are scored and averaged into understory, overstory and overall composite rating.

Table 2. Hierarchical structure of the CBI.

CBI of TOTAL PLOT	**UNDERSTORY**	**A**: Substratum
		B: Herbs, low shrubs and tree < 1m
		C: Tall shrubs and trees = 1 to 5 m
	OVERSTORY	**D**: Intermediate trees = 5 to 20 m
		E: Large trees > 20 m

Although field estimations are not operative for mapping burn severity systematically in large areas, they are still necessary to calibrate and validate remote sensing methods. In fact, a number of empirical remote sensing studies have attempted to estimate burn severity, even though results have been generally inconsistent.

The traditional approach has been to correlate field CBI with spectral indices, such as the Normalized Burn Ratio (NBR, Key and Benson, 1999), the difference between pre- and post-fire NBR (dNBR, Key and Benson, 1999) and, more recently, the relative delta Normalized Burn Ratio (RdNBR, Miller and Thode, 2007):

$$NBR = \frac{\rho 4 - \rho 7}{\rho 4 + \rho 7} \quad (1)$$

$$dNBR = NBR_{PRE-FIRE} - NBR_{POST-FIRE} \quad (2)$$

$$RdNBR = \frac{NBR_{PRE-FIRE} - NBR_{POST-FIRE}}{\sqrt{ABS(NBR_{PRE-FIRE}/1000)}} \quad (3)$$

where ρ_4 and ρ_7 are the reflectance of band 4 (near infrared, NIR) and band 7 (short wave infrared, SWIR) of Landsat TM, respectively.

Having analyzed the results of 10 different studies that correlated dNBR and/or RdNBR with the CBI, Kasischke *et al.* (2007) found that:

- in Western U.S. coniferous forests, r^2 ranged from 0.49 to 0.89;
- in North American boreal forests, r^2 ranged from 0.11 to 0.88;
- in Alaskan boreal forests, r^2 ranged from 0.01 to 0.81.

The lowest correlations were generally explained by the non-linear relationship between CBI and dNBR, together with a signal saturation when CBI >2.3 (van Wagtendonk *et al.*, 2004). Moreover, the estimation accuracies were only quantified using the correlation coefficient r^2, without considering other statistical ways of quantifying estimation errors, such as the Root

Mean Square Error (RMSE) between observed and estimated values or the dispersion of the point distribution with respect to the 1:1 linear correlation. Table 3 lists cases in which, despite the high r^2 coefficients, estimation accuracies were rather low (high omission/commission errors).

Table 3. Examples of low accuracy in burn severity estimation.

REFERENCE	SEVERITY CLASSES	INDEX USED	R^2	KAPPA	CLASS WITH LOWER ACCURACY	OMISSION ERROR	COMMISSION ERROR
Epting *et al.*, 2005	4 (unburned, low, moderate, high)	dNBR	0.7	0.525	Low	0.75	0.5
					Moderate	0.45	0.57
Miller and Thode, 2007	4 (unchanged, low, moderate, high)	dNBR	0.49	0.411	Low	0.40	0.43
		RdNBR	0.61	0.421	Unchanged	0.25	0.58
					Low	0.45	0.45

Therefore, due to the heterogeneity of the results obtained combining CBI with either NBR, dNBR or RdNBR, it may be necessary to re-evaluate the utility of both the (1) remote sensing methods and (2) the field index used for assessing fire impacts (Kasischke *et al.*, 2007). Regarding the first aspect, the studies carried out by Roy *et al.* (2006) in different environments did not find evidence that the NBR is an optimal spectral index for short-term burn severity estimations. However, whether these inconsistent relations are caused by the NBR (or dNBR) or by the CBI has not been clearly demonstrated.

Therefore, the main purpose of this paper is first, to analyze the relationship between CBI and reflectance and, second, to adapt CBI to remote sensing estimation of burn severity. The modifications on CBI intend to preserve both its ecological meaning and its straightforward approach. Finally, the validation is carried out in Mediterranean areas considering only first-order (short-term) effects.

2. Data and methods

2.1. Suitability of CBI

Although CBI was originally designed for remote sensing applications and it is the most widely used burn severity field index (table 1), its correlation with the spectral response of burned areas is subject to improvement. In the computation of the average CBI of the total plot, all vegetation strata are assigned the same weight, regardless of their degree of coverage within the field plot. However, from a remote sensing point of view, the spectral response of the total plot is strongly related to the vegetation coverage per stratum, which CBI does not record. Therefore, the same CBI value could be assigned to plots with different spectral responses. In such cases, burn severity estimation from remotely sensed data will inevitably produce errors, regardless the specific spectral technique applied (spectral indices, classification methods, etc.). The following section explains this point in detail.

2.2. The effect of vegetation coverage on the spectral response: a simulation analysis

The quantity of vegetation per stratum within a given plot can be described using two variables:

- Leaf Area Index (LAI): the area of leaf surface per unit of soil surface (Ceccato *et al.*, 2002a).
- Fraction of Cover (FCOV): percentage of coverage in respect to the total plot area.

For burn severity estimation, the change in LAI due to the fire is a key factor to assess the level of damage within each vegetation stratum. In addition, FCOV is a means of quantifying the contribution of each vegetation stratum (with a given LAI) to the total plot reflectance.

In order to quantify the effect of FCOV on plot-level reflectance, a simulation analysis was carried out for forested areas. Two widely used radiative transfer models were combined: PROSPECT (at leaf level, Jacquemoud, 1990) and GeoSail (at canopy level, Huemmrich, 2001).

At leaf level, the CBI field form records the percentage of two types of leaves which are present on the canopy: green (undamaged) and brown (damaged) leaves. PROSPECT was then run in forward mode to simulate only one representative spectrum for each of these two reference leaf types (green and brown). The model input values (table 4) were fixed using both

literature and field data (De Santis and Chuvieco, 2008). Finally, the outputs of the PROSPECT model (i.e. the two simulated leaf spectra) were then used as inputs for the GeoSail model (figure 1, a).

Table 4. Input values of simulation at leaf level.

INPUTS	GREEN LEAF	BROWN LEAF
Leaf structural parameter: **N**	2.5	2.5
Chlorophyll a+b content: **Ca+b (µg/cm^2)**	70	20
Equivalent water thickness: **Cw (g/cm^2)**	0.048	0.0008
Dry matter content: **Cm (g/cm^2)**	0.035	0.035
Brown pigments content: **Cs (%SLW)**	0.2	1.5

At canopy level (table 5), five burn severity scenarios were simulated (from high severity to unburnt), which are based on field experience and correspond to representative CBI values. For each severity scenario, 10 spectra were generated, keeping fixed all inputs and varying only the FCOV from 0.1 to 1. Both the understory and the overstory are assigned the same FCOV value, which increase also at the same time in every simulation step.

Table 5. Parameterization of the model at canopy level (DCH= dark charcoal, strata B+C= understory, strata D+E= overstory, LAD= Leaf angle distribution; Rv to Rh= Crown height to width ratio).

SIMULATION AT CANOPY LEVEL						
BURN SEVERITY SCENARIO		**HIGH**	**MODERATE-HIGH**	**MODERATE**	**LOW**	**UNBURNT**
CBI		**3**	**2.85**	**2.45**	**0.9**	**0**
EXAMPLE						
strata B+C	**LEAF TYPE**	----	----	BROWN	BROWN	GREEN
	LAI	----	----	1.7	0.5	1
strata D+E	**LEAF TYPE**	BROWN	BROWN	GREEN	GREEN	GREEN
	LAI	0.01	0.1	0.7	1.8	2.5
SUB-STRATUM TYPE		DCH	DCH	DCH	50% SOIL 50% DCH	SOIL
OTHER INPUTS (fixed)		LAD= spherical; Rv to Rh= 2.36; Sun zenith angle = 30º; Crown shape= cone; *NOTE*: all simulations were performed from 400 to 2400 nm, at 10 nm-intervals.				

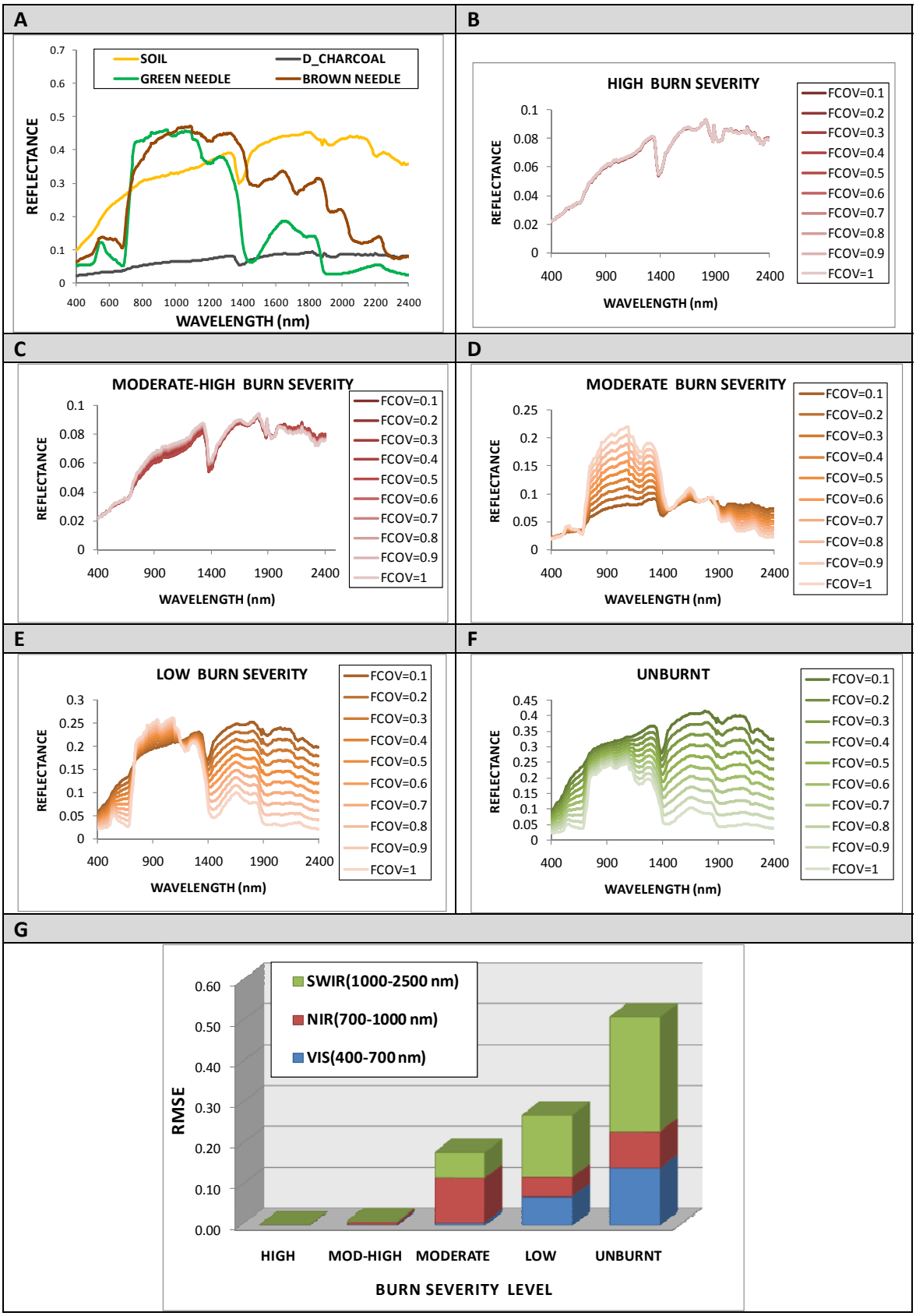

Figure 1. (a) Input spectra of Geosail and (b-g) simulation results for each burn severity scenario.

Simulation results (figure 1, b- f) show that changes in FCOV have a higher effect as the burn severity level decreases, since the contribution of green vegetation is also higher. The RMSE computed between the cases with FCOV=0.1 (minimum) and FCOV=1 (maximum) (figure 1, g) shows that:

- ✓ in *high* and *moderate-high severity* scenarios, FCOV does not cause considerable changes in reflectance. Since LAI in vegetation strata are very low, it is the substratum which mostly contributes to the total reflectance.
- ✓ in the *moderate severity* scenario, FCOV affects principally the NIR and the SWIR, where changes in reflectance are in the range of 6% to 11%. The presence of green leaves on the top of the tree crowns modifies the total plot spectral response as FCOV increases.
- ✓ in *moderate* and *low* burn severity scenarios, relatively small variations in FCOV have significant effects on NIR and SWIR reflectances (changes from 5% to 28%). Therefore, NBR is unlikely to produce accurate results unless the FCOV is taken into account. In these cases, the effect of FCOV is most evident, due to the higher LAI of the vegetation strata and the different substratum types.

2.3. New field index definition

Taking into account the simulation analysis results and field experience, a series of modifications in the original CBI are proposed to improve its performance in satellite imagery analysis, maintaining a similar ecological meaning. The original version of the CBI estimates the percentage of change with respect to the pre-fire scenario, but does not include information about its spatial extent. Therefore, two new variables per stratum were added to the original field form (in grey boxes in the figure 2):

1. the percentage of changes in the LAI;
2. the fraction of coverage (FCOV) of the vegetation, respect to the total plot.

In accordance with the original CBI variables, the percentage of changes in LAI was scored from 0 to 3 and was estimated for strata C, D and E (table 1). However, FCOV was scored from 0 to 1 for strata B, C, D and E (table 1) since it was used as a weighting factor: strata with higher FCOV have a greater weight in the computation of the CBI of the total plot.

Consequently, the new version of CBI proposed, called GeoCBI (which is short for *Geometrically structured* Composite Burn Index), was computed as follows:

$$GeoCBI = \frac{\sum_{m_1}^{m_n} (CBI_m * FCOV_m)}{\sum_{m_1}^{m_n} FCOV_m} \quad (4)$$

where *m* is the identification of each stratum and *n* is the number of strata.

Finally, the amount of new sprouts was added to the original CBI variables (figure 2), because it can modify significantly background reflectance. In short term assessment (under a month), sprout sizes normally fall into stratum B (herbs, shrubs and trees less than 1 meter).

These changes in the field protocol are quite straightforward and should hardly increase the time spent on field work.

STRATA	BURN SEVERITY SCALE							FACTOR SCORES
	No Effect	Low		Moderate		High		
	0	0.5	1.0	1.5	2.0	2.5	3.0	
A. SUBSTRATES								
%DEAD LEAVES ON THE SOIL=						SOIL DEPTH (cm)=		
Litter/Light Fuel Consumed	Unchanged	--	50% litter	--	100% litter	>80% light fuel	98% light fuel	
Duff	Unchanged	--	light char	--	50% loss deep char	--	Consumed	
Medium /heavy Fuel	Unchanged	--	20% consumed	--	40% consumed	--	>60% loss, deep char	
Soil & Rock Cover/Color	Unchanged	--	10% change	--	40% change	--	>80% change	
			A. ∑ =		*N*=	$\overline{X}$ =		
B. HERBS, LOW SHRUBS AND TREES LESS THAN 1 METER								
DOMINANT VEGETATION TYPE =					FCOV=			
%Foliage altered (blk- brn)	Unchanged	--	30%	--	80%	95%	100%+branch loss	
Frequency % Living	100%	--	90%	--	50%	<20%	0%	
New sprouts	Abundant	--	moderate-high	--	moderate	--	low-none	
			B. ∑ =		*N*=	$\overline{X}$ =		
C. TALL SHRUBS AND TREES 1 TO 5 METERS								
DOMINANT VEGETATION TYPE =					FCOV=			
%Foliage altered (blk- brn)	0%	--	20%	--	60-90%	>95%	significant branch loss	
Frequency % Living	100%	--	90%	--	30%	<15%	<1%	
LAI change %	Unchanged	--	15%	--	70%	90%	100%	
			C. ∑ =		*N*=	$\overline{X}$ =		
D. INTERMEDIATE TREES 5 TO 20 METERS								
DOMINANT VEGETATION TYPE =					FCOV=			
% Green (unalterad)	100%	--	80%	--	40%	<10%	none	
%Black/ Brown	0%	--	20%	--	60-90%	>95%	significant branch loss	
Frequency % Living	100%	--	90%	--	30%	<15%	<1%	
LAI change %	Unchanged	--	15%	--	70%	90%	100%	
Char Height	none	--	1,5 m	--	2,8 m	--	>5 m	
			D. ∑ =		*N*=	$\overline{X}$ =		
E. BIG TREES >20 METERS								
DOMINANT VEGETATION TYPE =					FCOV=			
% Green (unalterad)	100%	--	95%	--	50%	<10%	none	
%Black/ Brown	0%	--	20%	--	60-90%	>95%	significant branch loss	
Frequency % Living	100%	--	90%	--	30%	<15%	<1%	
LAI change %	Unchanged	--	15%	--	70%	90%	100%	
Char Height	none	--	1,8 m	--	4 m	--	>7 m	
			E. ∑ =		*N*=	$\overline{X}$ =		

Figure 2. The new version of the field form proposed for estimating burn severity as GeoCBI. New variables are in grey boxes.

2.4. Validation method

The performance of both indices was tested comparing (1) their burn severity estimation for a Mediterranean area and (2) their values with the spectral signature of the field plots.

The validation area, which is located in central Spain (40-41º N and 1-2º W, figure 3), was affected by a large forest fire on July 16th 2005 (De Santis and Chuvieco, 2007). After four days, the fire had burnt a total of 13,000 ha which were mainly composed by pine trees (*Pinus pinaster*) mixed with semi-deciduous oaks (*Quercus pyrenaica* and *Quercus faginea*).

Burn severity was assessed in the field three weeks after the fire, in terms of both CBI and GeoCBI. A total of 104 field plots (figure 3) were selected within areas with homogeneous burn severity levels and gentle slopes, as recommended by Key and Benson (2005). In each field plot the new field form was filled in, digital photographs were taken and its centre coordinates were recorded using a GARMIN 12 GPS (5-10 m of error in x and y).

Spectral signatures corresponding to the field plots were extracted from a post-fire Landsat 5 Thematic Mapper (TM) (acquired on August 5th, 2005; figure 3). Radiometric, geometric and illumination corrections were applied as in De Santis and Chuvieco (2007).

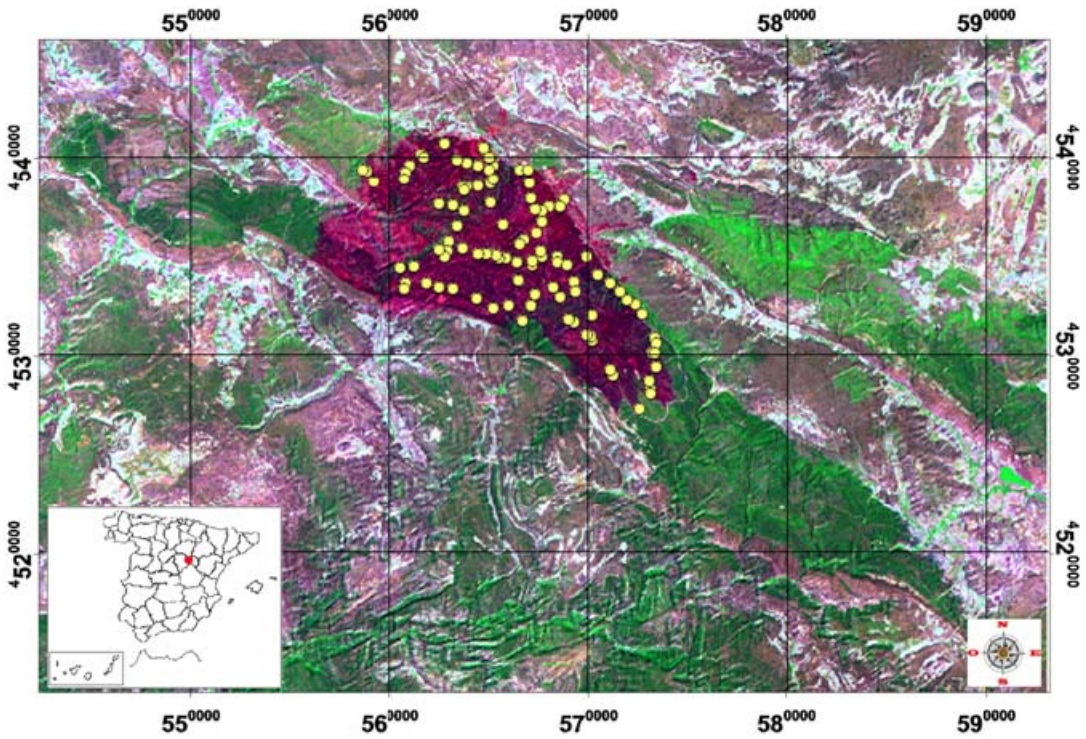

Figure 3. Study area location and field plots distribution (Landsat 5 TM image: R= band 7, G= band 4, B= band 1, Projection UTM 30 T datum European 1950 mean).

3. Results

3.1 Performance of GeoCBI versus CBI

Figure 4 shows a comparison between both CBI and GeoCBI field values. The highest differences between both indices are observed in intermediate-low severity values (~1.5 to ~2.6). In this range, CBI values generally tend to be lower than GeoCBI, especially when the FCOV of the tree stratum is under 50%, as in plot C (figure 4). In this plot (see also case C, figure 5) the understory is highly affected, whereas the tree stratum still maintains green canopies despite its very low (10%) FCOV.

Exceptionally, in two of the plots CBI values are higher than GeoCBI (cases A and B, figure 4). In these two plots, which are shown in figure 5 (cases A and B), the understory has a very high burn severity whereas its FCOV is very low (5-15%).

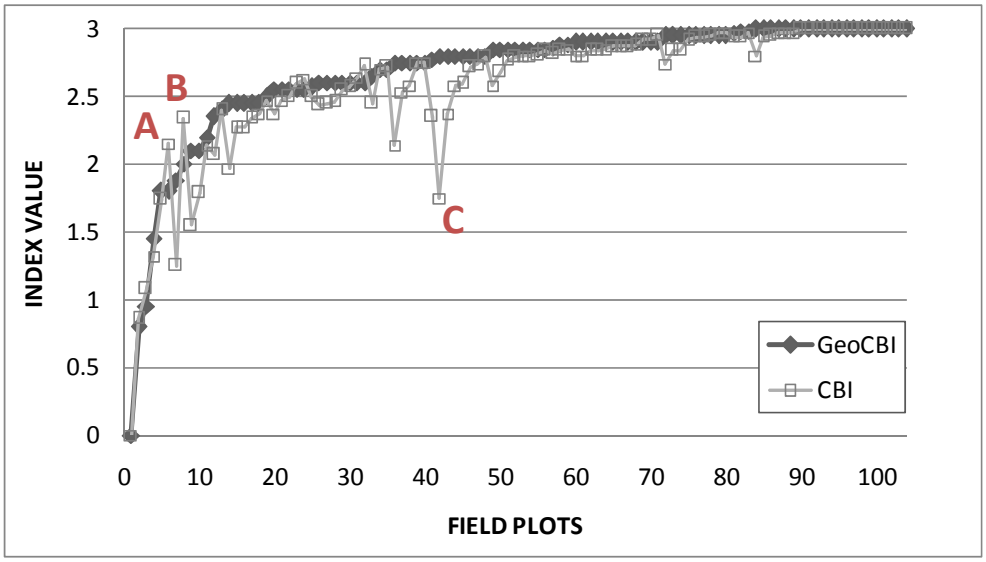

Figure 4. Comparison between CBI and GeoCBI (field plots are ordered in terms of GeoCBI, from 0 to 3).

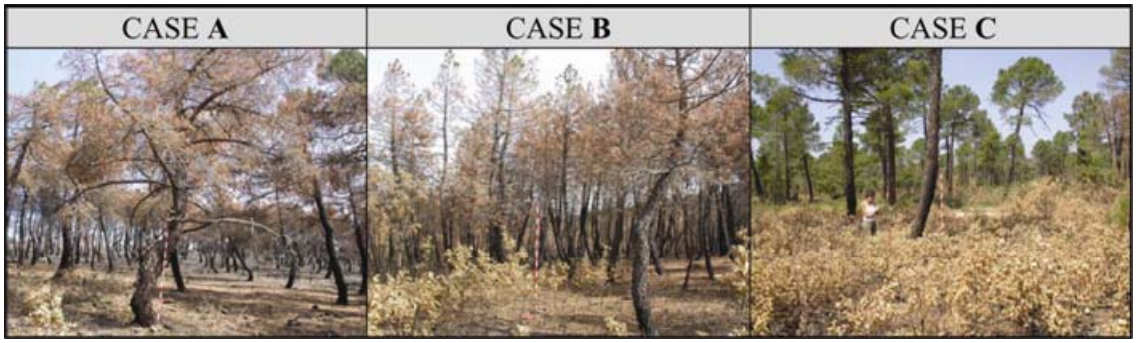

Figure 5. Field plots which have the higher overestimation (Case A and B) and underestimation (Case C) of burn severity using the original CBI respect to GeoCBI.

4. Discussion

4.1 Improvement of the GeoCBI respect to the original CBI

GeoCBI improves the general performance of the traditional CBI. In particular, GeoCBI corrects over-estimation errors in cases where the plot is composed by a tree stratum with a green canopy and a very low FCOV, under which both substratum and understory have a high burn severity (figure 6 a).

By introducing the FCOV as a weighting factor, the spectral mixture of the different plot components/variables are better represented, without adding a significant effort to the field work. For post-fire management purposes, the correction the of burn severity overestimation in the cases described, can help to maximize resources by skipping burnt areas that are less critical.

However, the estimation of CBI values of the understory and substratum when the overstory has a high FCOV value (figure 6 b and c) remains an open problem. In these cases, the model moderately underestimates the burn severity level. This appears to be a limitation for optical remote sensing techniques, since background reflectance can hardly penetrate denser canopy covers. However, from the point of view of short-term post-fire management, such cases normally do not require a rapid intervention, since they have mainly intermediate to low values of GeoCBI.

Figure 6. Examples tree stratum compositions: a) overstory with green canopies, a low FCOV and a dark charcoal substratum; b) overstory with green canopies, a high FCOV and a dark charcoal substratum; c) overstory with green canopies, a high FCOV and an unburnt soil substratum.

A correct definition of both vegetation structure and composition within the plot are critical, especially in the case of intermediate values of burn severity. Table 6 shows two opposite examples of such situation. In the first example, the first three field plots listed have the same CBI value (P95, P86, P23) in spite of having very different structures, compositions and burn severity, which is clearly seen in the photographs and in the spectral signatures extracted from the Landsat TM image. In these cases, GeoCBI is more accurate than CBI, because the FCOV of the tree stratum is the most relevant factor that modifies the spectral signature.

In contrast, the second example shows how the last three field plots listed in table 6 (P7, P102, P21), have different CBI values despite having the same structure and quite similar spectral signatures. CBI variations are influenced by the absence/presence of highly affected shrubs that have a very low FCOV, whereas GeoCBI takes into account this factor and thus correctly assigns the same value.

Table 6. Comparisons between CBI, GeoCBI and spectral signatures of the same plots.

FIELD PLOTS		CBI	GeoCBI	SPECTRAL SIGNATURES
P95		2.58	2.7	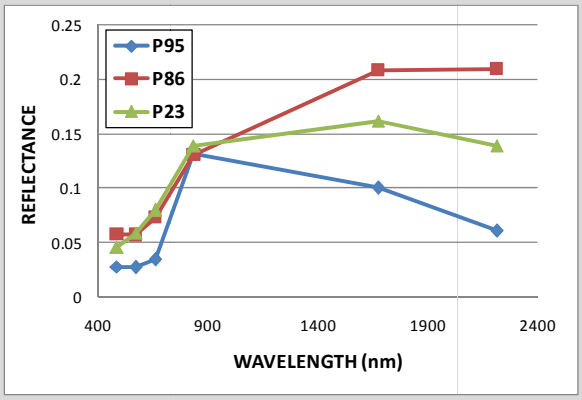
P86			2.85	
P23			2.8	
P7		1.97	2.45	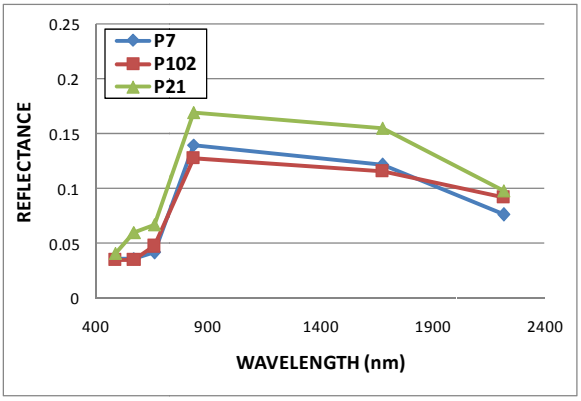
P102		2.27		
P21		2.37		

5. Conclusions

Burn severity is a key factor in post-fire management in order to quantify and map fire impacts and, consequently, to plan the mitigation and rehabilitation treatments in the burned areas. Post-fire field assessment of burn severity is costly in terms of time and economic resources and does not provide a good spatial coverage. However, this field work is a source of ground truth which is important to understand the critical variables that determinate burn severity and, subsequently, calibrate and validate remote sensing methods.

Although CBI is the most widely used field index, results have been inconsistent up to now when correlated with remotely sensed data. This paper has shown that minor modifications can significantly improve its performance. Therefore, a new version of this index, called GeoCBI, is proposed after (1) having assessed in the field the most relevant variables that affect the spectral response of the burned area, and (2) having verified the effect of these variables using a simulation analysis.

GeoCBI provides a better characterization of the field plots than the original CBI, and a higher correlation with the spectral signatures extracted from Landsat TM data. In addition, GeoCBI maintains the ecological meaning of CBI and the changes in the field protocol do not increase the difficulty nor the time spent on field work.

Therefore, in future work, GeoCBI field estimation will be used to validate a simulation model, for the short-term assessment of burn severity.

Acknowledgements

Special thanks to the Spanish Forest Service staff of Guadalajara and all team of the Geography Department of the University of Alcalá, who have been extremely helpful during the long fieldwork campaigns. The Spanish Ministry of Science and Technology supports Angela De Santis within the FPU Programme framework. This project was founded by the EU Preview Project (www.preview-risk.com, EA21.CR/AC/03.064).

References

Andreae, M.O. and Merlet, P. (2001), Emission of trace gases and aerosols from biomass burning, *Global Biogeochemical Cycles*. 15(4): 955-966.

Bobbe, T., Finco, M.V., Quayle, B., Lannom, K., Sohlberg, R., Parsons, A. (2001). Field Measurements for the Training and Validation of Burn Severity Maps from Spaceborne, Remotely Sensed Imagery, USDA Forest Service, Remote Sensing Applications Center, Salt Lake City, Utah.

Brewer, C.K., Winne, J.C., Redmond, R.L., Opitz, D. W., Mangrich, M.V. (2005), Classifying and Mapping Wildfire Severity: A Comparison of Methods, *Photogrammetric Engineering and Remote Sensing*. 71(11): 1311-1320.

Ceccato, P., Gobron, N., Flasse, S., Pinty, B, Tarantola, S. (2002a), Designing a spectral index to estimate vegetation water content from remote sensing data: Part 1 Theoretical approach, *Remote Sensing of Environment*. 82: 188–197.

Chappell, C.B. and Agee, J.K. (1996), Fire severity and tree seedling establishment in Abies Magnifica forests, Southern Cascades, Oregon., *Ecological Applications*. 6(2): 628-640.

Chuvieco, E., De Santis, A., Riaño, D., Halligan, K. (2007), Simulation approaches for burn severity estimation using remotely sensed images, *Fire ecology*. 3 (1): 129-150.

Chuvieco, E., Riaño, D., Danson, F.M., Martín, P. (2006), Use of a radiative transfer model to simulate the postfire spectral response to burn severity, *Journal of Geophysical Research*. 111(G04S09): doi: 10.1029/2005JG000143.

Cocke, A.E., Fule, P.Z. and Crouse, J.E. (2005), Comparison of burn severity assessments using Differenced Normalized Burn Ratio and ground data, *International Journal of Wildland Fire*. 14: 189-198.

De Santis, A. and Chuvieco, E. (2007), Burn severity estimation from remotely sensed data: performance of simulation versus empirical models, *Remote Sensing of Environment*. 108(4): 422-435.

De Santis, A., Chuvieco, E., Vaughan, P.J. (2008), Short-term assessment of burn severity using the inversion of the GeoSail model, *Remote Sensing of Environment,* under review.

Doerr, S.H., Shakesby, R.A., Blake, W.H., Chafer, C.J., Humphreys, G.S., Wallbrink, P.J. (2006), Effects of differing wildfire severities on soil wettability and implications for hydrological response., *Journal of Hydrology*. 319: 295-311.

Epting, J., Verbyla, D.L. and Sorbel, B. (2005), Evalation of remotely senses indices for assessing burn severity in interior Alaska using Landsat TM and ETM+, *Remote Sensing of Environment*. 96: 328-339.

García-Haro, F.J., Gilabert, M.A. and Meliá, J. (2001), Monitoring fire-affected areas using Thematic Mapper data, *International Journal of Remote Sensing*. 22(4): 533-549.

Huemmrich, K.F. (2001), The GeoSail model: a simple addition to the SAIL model to describe discontinuous canopy reflectance, *Remote Sensing of Environment*. 75: 423-431.

Jacquemoud, S. (1990), PROSPECT: a model to leaf optical properties spectra, *Remote Sensing of Environment*. 34: 74-91.

Jain, T.B. (2004a), Confused meanings for common fire terminology can lead to fuels mismanagement. A new framework is needed to clarify and communicate the concepts, *Wildfire*. july-aug: 22-26.

Jain, T.B. and Graham, R.T., (2004b). Is forest structure related to fire severity? Yes, no, and maybe: methods and Insights in quantifying the answer., USDA Forest Service.

Kasischke, E., Hoy, E.E., French, N.H.F., Turetsky, M.R., (2007). Post-fire evaluation of the effects of fire on the environment using remotely-sensed data. In: C.C.-M. Ioannis Z. Gitas (Editor), 6th International Workshop of the EARSel Special Interest Group on Forest Fires: Advances in Remote Sensing and GIS applications in forest fire managment. Torwards an operational use of Remote Sensing in Forest Fire Managment. European Communities, Thessaloniki, Greece, pp. 34-52.

Key, C. and Benson, N., (1999). The Normalized Burned Ratio, a Landsat TM radiometric index of burn severity incorporating multi-temporal differencing. U.S. Geological Survey.

Key, C.H. (2006), Ecological and sampling constraints on defininf landscape fire severity, *Fire Ecology*. 2(2): 34-59.

Key, C.H. and Benson, N. (2005), Landscape Assessment: Ground measure of severity, the Composite Burn Index; and Remote sensing of severity, the Normalized Burn Ratio. In: *FIREMON: Fire Effects Monitoring and Inventory System* (D.C. Lutes, R.E. Keane, J.F. Caratti, C.H. Key, N.C. Benson and L.J. Gangi, Eds.), USDA Forest Service, Rocky Mountain Research Station, Gen. Tech. Rep. RMRS-GTR-164, Ogden, UT, pp. CD:LA1-LA51.

Kokaly, R.F., Rockwell, B.W., Haire, S.L., King, T.V.V. (2007), Characterization of post-fire surface cover, soils, and burn severity at the Cerro Grande Fire, New Mexico, using hyperspectral and multispectral remote sensing, *Remote Sensing of Environment*. 106 (3): 305-325.

Kushla, J.D. and Ripple, W.J. (1998), Assessing wildfire effects with Landsat thematic mapper data, *International Journal of Remote Sensing*. 19(13): 2493-2507.

Lentile, L.B., Holden, Z. A., Smith, A.M.S., Falkowski, M. J., Hudak, A.T., Morgan, P., Lewis, S.A., Gessler, P.E., Benson, N. C. (2006), Remote sensing techniques to assess active fire characteristics and post-fire effects, *International Journal of Wildland Fire*. 15: 319-345.

Lewis, S.A., Wu, J.Q., Robichaud, P.R. (2006), Assessing burn severity and comparing soil water repellency, Hayman fire, Colorado. *Hydrological Processes*. 20: 1-16.

Miller, H.J. and Yool, S.R. (2002), Mapping forest post-fire canopy consumption in several overstory types using multi-temporal Landsat TM and ETM data, *Remote Sensing of Environment*. 82: 481–496.

Miller, J.D. and Thode, A.E. (2007), Quantifying burn severity in a heterogeneous landscape with a relative version of the delta Normalized Burn Ratio (dNBR), *Remote Sensing of Environment*. 109 (1): 66-80.

Moreno, J.M. and Oechel, W.C. (1989), A Simple Method for estimating fire intensity after a burn in California Chaparral, *Acta Ecologica (Ecologia plantarum)*. 10(1): 57-68.

Nagahamaa, Y. and Suzuki, K. (2007), The influence of forest fires on CO, HCN, C2H6, and C2H2 over northern Japan measured by infrared solar spectroscopy, *Atmospheric Environment*. 41: 9570-9579.

Narayan, C., Fernandes, P.M., van Brusselen, J., Schuck, A. (2007), Potential for CO2 emissions mitigation in Europe through prescribed burning in the context of the Kyoto Protocol, *Forest Ecology and Management*. 251: 164-173.

Patterson, M.W. and Yool, S.R. (1998), Mapping Fire-Induced Vegetation Mortality Using Landsat Thematic Mapper Data: A Comparison of Linear Transformation Techniques, *Remote Sensing of Environment*. 65: 132-142.

Rogan, J. and Franklin, J. (2001), Mapping wildfire burn severity in Southern California Forests and shrublands using enhanced Thematic Mapper imagery, *Geocarto International*. 16(4): 89-99.

Rogan, J. and Yool, S.R. (2001), Mapping fire-induced vegetation depletion in the Peloncillo Mountains, Arizona and New Mexico, *International Journal of Remote Sensing*. 22(16): 3101-3121.

Roy, D.P., Boschetti, L., Trigg, S.N. (2006), Remote sensing of fire severity: assessing the performance of the normalized burn ratio, *IEEE Geoscience and Remote Sensing Letters*. 3(1): 112-116.

Ryan, K.C. and Noste, N.V., (1985). Evaluating prescribed fires. In: USDA (Editor), Workshop on Wildness Fires, pp. 230-238.

Salgado, J., Mato, M.M., Vásquez-Galiñanes, Paz-Andrade, M.I., Carballas, T. (2004), Comparison of two calorimetric methods to determine the loss of organic matter in Galician soils (NW Spain) due to forest wildfires, *Thermochimica Acta*. 410: 141-148.

Smith, A.M.S., Wooster, M. J., Drake, N.A., Dipotso, F.M., Falkowski, M.J., Hudak, A.T. (2005b), Testing potential of multi-spectral remote sensing for retrospectively estimating fire severity in African savannah environments, *Remote Sensing of Environment*. 97: 92-115.

Sorbel, B. and Allen, J. (2005), Space-based burn severity mapping in Alaska's Nat. Parks., *Alaska Park Science*. 4-11.

Turner, M.G., Hargrove, W.W., Gardner, R.H. and Romme, W.H. (1994), Effects of fire on landscape heterogeneity in Yellowstone National Park, Wyoming, *Journal of Vegetation Science*. 5: 731-742.

van Wagtendonk, J.W., Root, R.R. and Key, C.H. (2004), Comparison of AVIRIS and Landsat ETM+ detection capabilities for burn severity, *Remote Sensing of Environment*. 92(3): 397-408.

Wang, G.G. (2002), Fire severity in relation to canopy composition within burned boreal mixewood stands, *Forest Ecology and Management*. 163: 85-92.

Wells, C.G. and Campbell R.E., (1979). Effects of fire on soil : A state-of-knowledge review., Forest service national fire effects workshop. US Department of Agriculture, Forest service, Denver, CO.

White, J.D., Ryan, K.C., Key, C.C. and Running, S.W. (1996), Remote sensing of forest fire severity and vegetation recovery, *International Journal of Wildland Fire*. 6(3): 125-136.

Wimberly, M.C. and Reilly, M.J. (2006), Assessment of fire severity and species diversity in the southern Appalachians using Landsat TM and ETM+ imagery, *Remote Sensing of Environment*.108 (2):189-197.

IV

Available online at www.sciencedirect.com
ScienceDirect
Remote Sensing of Environment
Remote Sensing of Environment
www.elsevier.com/locate/rse

Short-term assessment of burn severity using the inversion of the GeoSail model

Angela De Santis[1], Emilio Chuvieco[1], Patrick J. Vaughan[2]

[1]*Department of Geography, University of Alcalá, Alcalá de Henares, Spain*

[2]*Laboratorio de Espectro-radiometria y Teledetección Ambiental*

CCHS-CSIC, Madrid, Spain

Received 27 March 2008; under review

Abstract

Accurate estimations of burn severity and its distribution in post fire scenarios are critical for short term mitigation and rehabilitation treatments. The use of remote sensing techniques, coupled with radiative transfer models (RTMs) can improve the accuracy, precision (in terms of number of classes) and cost-effectiveness of burn severity estimation. In this paper, an improved simulation model that combines PROSPECT and GeoSail, was tested in three Mediterranean forest fires. Results are presented in terms of GeoCBI, a new version of the CBI index, that takes into account two relevant parameters: leaf area index (LAI) and the vegetation fraction of cover (FCOV). Model inversion results were accurate (RMSE between 0.18 and 0.21) and uniform in all three sites (107 field plots in total) throughout the full GeoCBI range (0-3).

Keywords: Forest fires; Burn Severity; RTM inversion; PROSPECT; GeoSail; GeoCBI; Landsat TM; SPOT-HRV; local Sensitivity Analysis.

1. Introduction

Forest fires are a major cause of environmental disturbance in Mediterranean ecosystems, producing principally vegetation biomass loss, soil degradation (Doerr *et al.*, 2006), and greenhouse gas emissions (Andreae and Merlet, 2001).

Post-fire management is normally focused on minimizing post-fire erosion effects (mitigation) and shortening ecosystem recovery times (rehabilitation) (Miller and Yool, 2002). In large forest fires, both post-fire mitigation and rehabilitation treatments can be costly and cumbersome due to the extension of the area affected.

In addition, summertime forest fires are generally followed by autumn rains, which are often torrential and cause erosion and soil degradation. Consequently, treatments must be completed within weeks after the fire. In this context, it is critical to target the efforts on high priority locations to reduce erosion risks in a cost effectively approach (Miller and Yool, 2002).

Both short- and long-term post-fire effects on vegetation and soil, as well as other subsequent processes, can be estimated in terms of "burn severity" (Chuvieco *et al.*, 2006; De Santis and Chuvieco, 2007; Key and Benson, 2005; Lentile *et al.*, 2006; van Wagtendonk *et al.*, 2004; White *et al.*, 1996). Detailed knowledge of the level of damage and its distribution throughout the burnt area (burn severity map) is a key factor to quantify the impact of fires on landscapes (van Wagtendonk *et al.*, 2004), to select and prioritize treatments applied on site (Bobbe *et al.*, 2001; Patterson and Yool, 1998), to plan and monitor restoration and recovery activities and, finally, to provide baseline information for future monitoring (Brewer *et al.*, 2005).

Different methods of burn severity estimation have been applied using post-fire field evaluation of soil and vegetation conditions (Moreno and Oechel, 1989; Pérez and Moreno, 1998). Since field surveys are costly and time consuming and do not provide a good spatial coverage, remote sensing imagery has been proposed as a sound alternative.

For instance, Interagency Burned Area Emergency Rehabilitation (BAER) teams use a semi-automatic estimation of burn severity from satellite images on a nationwide scale, applying techniques developed by the Remote Sensing Applications Center - RSAC of the USDA Forest Service. The field assessment method used by BAER is based on the widely used Composite Burn Index (CBI) (Key and Benson, 2005), which takes continuous values ranging from 0 (unburned) to 3 (completely burned). However, in most studies dealing with burn severity estimation from satellite imagery, damage levels are normally grouped into only four severity classes: unburned, low, moderate and severe (Kokaly *et al.*, 2007; Cocke *et al.*, 2005; Epting *et*

al., 2005; Hyde *et al.*, 2007; Lentile *et al.*, 2006; Miller and Thode, 2007; Patterson and Yool, 1998; van Wagtendonk *et al.*, 2004; Wang, 2002). Moreover, Rogan and Franklin (2001), having analyzed 71 different publications, observed that, as the number of burn severity classes considered increases, the accuracy of burn severity estimation decreases from 80% (for two classes: burned/not burned) to only 35% (for five classes).

To solve this limitation in accuracy and precision, recent studies (Chuvieco *et al.*, 2006; 2007; De Santis and Chuvieco, 2007) have proposed the use of Radiative Transfer Models (RTMs) to simulate the continuum interval of burn severity levels measured in CBI. RTMs simulate spectral signatures from a set of input parameters from leaf and canopy characteristics. In the forward simulation mode, RTMs are used to analyze the effects of such plant parameters on spectral reflectance, whereas, in the inverse mode, spectra (from remotely sensed data) are used as an input to estimate some of those plant parameters (output).

The first of these studies (Chuvieco *et al.*, 2006), used combinations of the main variables which define burn severity as input data to simulate CBI values. In a second approach (De Santis and Chuvieco, 2007), an inversion process was carried out, where the simulated spectra were compared to the spectral signature of each pixel from a post-fire image. The most similar simulated spectrum was selected, and its corresponding CBI value was assigned to that pixel.

RTMs used in both studies performed better than the traditional empirical fitting (De Santis and Chuvieco, 2007) especially in the extreme values of burn severity. However, in the intermediate range, burn severity was not correctly estimated, due to the high *vertical* contrast between the understory, which was highly affected by the fire, and the less affected overstory (Chuvieco *et al.*, 2007; De Santis and Chuvieco, 2007). In these studies, the simulation was carried out linking two models: PROSPECT (Jacquemoud, 1990), a widely used leaf level model, and a canopy model developed by Kuusk (Kuusk, 2001), which considers each vegetation stratum as a homogeneous layer composed of a turbid medium. These models are simple to compute and fit well into the structure of the field index used. However the assumption of a uniform turbid medium composition is not often the case in many forested areas, composed of non homogeneous vegetation layers that are unevenly distributed. An alternative to solve these problems is using geometric RTMs, which take into account the canopy structure and the illuminated/shadowed elements in the plot

Therefore, the main objective of this paper is to test the performance of a geometric RTM in order to improve the estimation of burn severity, based on inversion techniques and in the context of a short-term post-fire management. The validation will be carried out in terms of

GeoCBI (De Santis and Chuvieco, 2008), a new version of the original CBI field index, that is better adapted to the use of remotely sensed data.

2. Data and Methods

2.1 Test sites

The main study area is located in central Spain (site 1, table 1). This area was affected by a large forest fire on July 16th 2005, which lasted four days and burned 13,000 ha of pine forest (*Pinus pinaster*) mixed with semi-deciduous oaks (*Quercus pyrenaica* and *Quercus faginea*).

In order to verify the applicability of the methodology developed in this study, two additional test sites were included.

The north-western region of Spain (Galicia) underwent a severe fire season in August 2006, when a total of 103,728 ha were burned. A small cluster of these fires (site 2, table 1) was selected for this study. Unlike the other two sites, in this area of Galicia forest landcovers are highly fragmented and mixed. The main tree species is eucalyptus (*Eucalyptus globulus*) followed by pine trees (*Pinus pinaster*) and oaks (*Quercus robur)* with a thick understory of gorse (*Ulex europeaus)* shrubs.

Finally, the third area was located in north-eastern Portugal (site 3, table 1). In this case, the forest fire started in July 9th, 2006 near Famílaçao da Serra and burned a total of 568 ha, mainly composed of pine trees (*Pinus pinaster*) mixed with semi-deciduous oaks and Mediterranean shrubs.

Table 1. An overview of the test sites: description, field data and satellite imagery used.

TEST SITES LOCATION

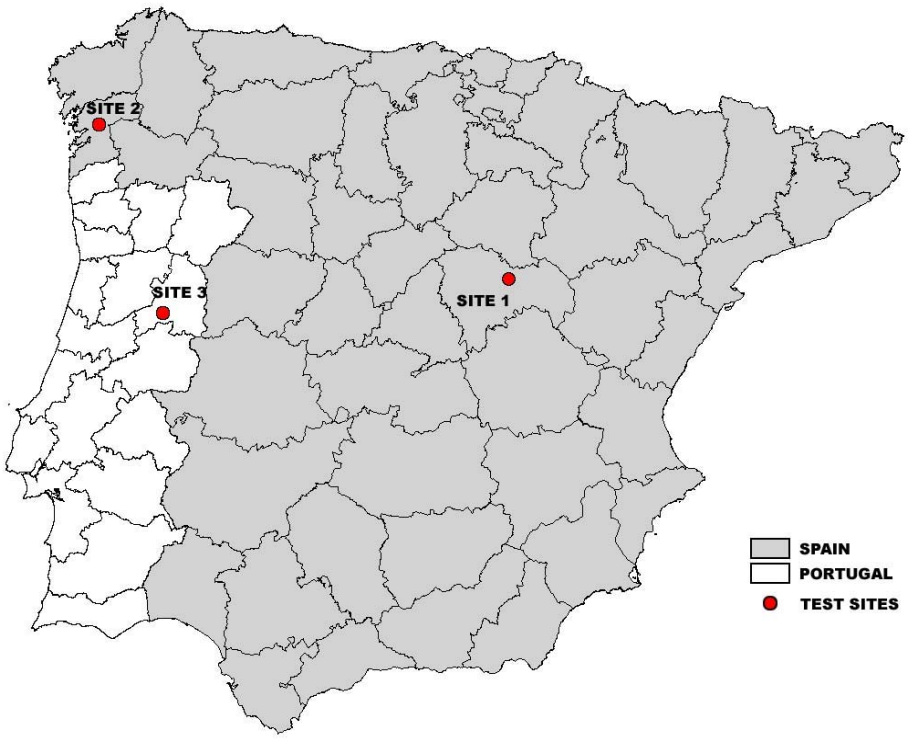

SITE #	FIRE NAME (province)	FIRE DATE (dd/mm/yyyy)	BURNT AREA (ha)	FIELD WORK		SENSOR	IMAGE DATE (dd/mm/yyyy)
				DATE (dd/mm/yyyy)	# PLOTS		
1	Riba de Saelices (Guadalajara)	16/07/2005	12,892	From 18/08/2005 to 28/09/2005	83	Landsat 5 TM	05/08/2005
2	Serrapio (Pontevedra)	4/08/2006	3,360	06/10/2006	10	SPOT 5 HRG	06/09/2006
3	Familaçao da Serra (Guarda)	09/07/2006	568	From 17 to 19/08/2006	14	Landsat 5 TM	05/09/2006

2.2 Field data

Depending on the weather conditions, burn severity was estimated in the field between one and two months after the fire (table 1), in terms of the GeoCBI index (*Geometrically structured* Composite Burn Index, De Santis and Chuvieco, 2008). This index is a modification of the original CBI (Key and Benson, 2005), which has been adjusted to calibrate and validate remote sensing methods. In accordance with Key and Benson (2005), average conditions of soil and plant communities were visually examined in 30m-diameter field plots, and the vegetation was considered to be composed of five strata, organized in a hierarchical structure (field estimation, table 2).

Table 2. Hierarchical structure of the GeoCBI and its adaptation to the GeoSail simulation model.

<table>
<tr><th colspan="3">FIELD ESTIMATION</th><th></th><th>GeoSail SIMULATION</th></tr>
<tr><td rowspan="3">GeoCBI of TOTAL PLOT</td><td rowspan="2">UNDERSTORY</td><td>A: Substratum</td><td>⇨</td><td>SUBSTRATUM</td></tr>
<tr><td>B: Herbs, low shrubs and trees < 1m</td><td rowspan="2">⇨</td><td rowspan="2">UNDERSTORY</td></tr>
<tr><td>C: Tall shrubs and trees = 1 to 5 m</td></tr>
<tr><td rowspan="2">OVERSTORY</td><td>D: Intermediate trees = 5 to 20 m</td><td rowspan="2">⇨</td><td rowspan="2">OVERSTORY</td></tr>
<tr><td>E: Large trees > 20 m</td></tr>
</table>

The main field variables assessed to estimate GeoCBI were litter and fuel consumption, changes in soil colour, foliage alteration, canopy mortality and char height. These attributes are rated in numerical scores ranging from 0 (unburned) to 3 (completely burned). The numerical rating derived for each attribute was obtained from a consensus of two field observers.

Two new variables per stratum were added to the original CBI field form:

1. the percentage of changes in the Leaf Area Index (LAI= Leaf area/Canopy area);
2. the fraction of coverage (FCOV) of each vegetation stratum, with respect to the total extension of the plot.

In agreement with the original variables of CBI, the percentage of changes in LAI was also scaled from 0 to 3 and was estimated for strata C, D and E (table 2). However, FCOV was quantified from 0 to 1 for strata B, C, D and E (table 2) since it is used as a weighting factor: strata with higher FCOV have a greater weight in the computation of the CBI of the total plot.

Consequently, the GeoCBI was computed as follows:

$$GeoCBI = \frac{\sum_{m_1}^{m_n} (CBI_m * FCOV_m)}{\sum_{m_1}^{m_n} FCOV_m} \quad (1)$$

where *m* is the identification of each stratum and *n* is the number of strata.

Field plots were selected within areas with homogeneous burn severity levels and gentle slopes, as recommended by Key and Benson (2005). In each field plot the new field form was filled in, digital photographs were taken and its centre coordinates were recorded using a GARMIN 12 GPS (5-10 m of error in x and y).

In site 1 (table 1), due to the rugged terrain conditions, all plot coordinates were later checked using a post-fire aerial orthophoto with a 50 cm-pixel resolution (provided by TRAGSA Group, Spain), as well as field notes and photographs. Out of the original 103 plots marked in the field, 20 plots were discarded for having an offset above 20 m.

In the remaining sites, field sampling was reduced to 10 plots in the Serrapio fire (site 2, table 1), and 14 plots in Familaçao (site 3, table 1), given their relatively small size. Table 3 shows the plot distribution in the three areas.

2.3 Remotely sensed data

In consistency with the field plot size (30 m), a post-fire Landsat 5 Thematic Mapper (TM, 30 m pixel) image was selected for site 1 and 3, whereas for site 2 a SPOT 5 HRG (10 m pixel) was provided by the Spanish National Geographic Institute (IGN) (table1).

Image data sets were radiometric and geometrically corrected as indicated in table 3. In the case of the TM image of site 1, an illumination correction was also carried out due to the ruggedness of the terrain (table 3).

Table 3. Field plot distribution (yellow dots) and image pre-processing description (DNs= digital numbers; GCPs= Ground control points; b=band; UL= upper left; LR= lower right).

SITE#	RGB-IMAGE AND FIELD PLOTS LOCATION	CORNERS AND PROJECTION	TYPE OF CORRECTION		
			RADIOMETRIC	GEOMETRIC	ILLUMI-NATION
1	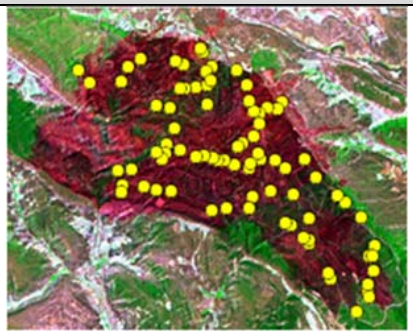 **LANDSAT TM; RGB=b7-b4-b1**	**UL:** 555030.00 4542540.00 **LR:** 575070.00 4526490.00 UTM, European 1950 mean, 30 N	**DNs to RADIANCE:** Chander and Markham Method (2003) **RADIANCE to REFLECTANCE:** Dark object Method (Chavez, 1996)	GPCs using a Landsat 7 ETM+ (CORINE Land Cover, 2000) ortho-image as reference	Method proposed by Civco (1989) using a digital elevation model (10m-pixel)
2	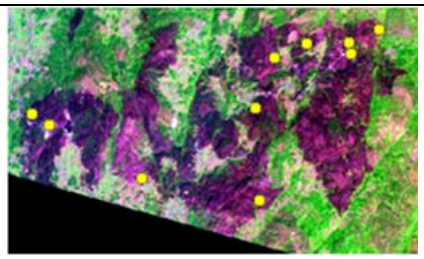 **SPOT 5 HRG; RGB=b4-b3-b1**	**UL:** 528820.70 4711016.66 **LR:** 547760.70 4799646.66 UTM, European 1950 mean, 29 N	**DNs to RADIANCE:** Gain and bias correction using metadata information. **RADIANCE to REFLECTANCE:** Dark object Method (Chavez, 1996)	Corrected by IGN	--------
3	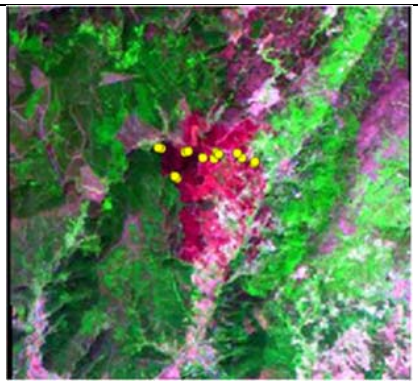 **LANDSAT TM; RGB=b7-b4-b1**	**UL:** 631462.01 4482033.79 **LR:** 640462.01 4473753.79 UTM, European 1950 mean, 29 N	**DNs to RADIANCE:** Chander and Markham Method (2003) **RADIANCE to REFLECTANCE:** Dark Object Method (Chavez, 1996)	GPCs using a Landsat 7 ETM+ (24-06-2000) ortho-image as reference from Global Land Cover Facility (http://glcfapp.umiacs.edu)	--------

2.4 Methodological workflow

Once all the field data was obtained and the post-fire images were processed, three consecutive phases were carried out: simulation, classification and validation (figure 1).

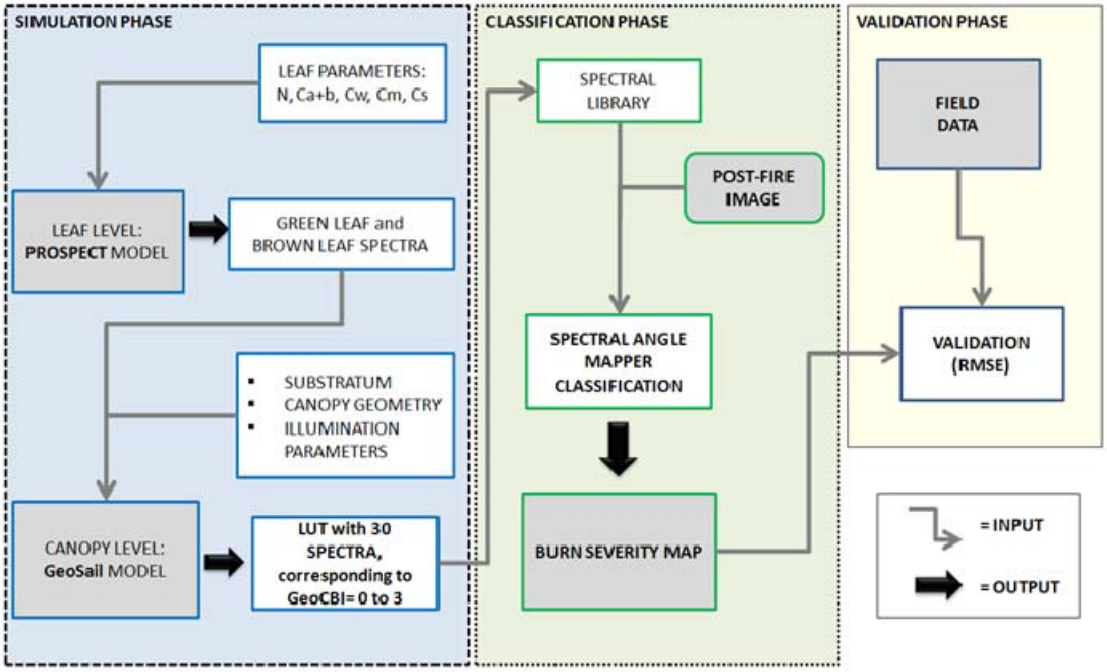

Figure 1. Methodological workflow used in this study.

Burn severity simulation (simulation phase in the figure 1) was accomplished by scaling up from leaf to canopy level, combining two RTMs: PROSPECT and GeoSail.

At leaf level, PROSPECT uses five biophysical leaf parameters (inputs) and the outputs are spectra of leaf reflectance and transmittance. These spectra, together with a series of canopy parameters (substratum type, geometry and illumination parameters), are used as inputs for the canopy level model (GeoSail). The canopy model output is converted into a Look-up Table (LUT) in which each reflectance spectrum corresponds to a given burn severity value. The LUT is then turned into a spectral library using ENVI™ 4.3 (Research Systems, Inc., www.rsinc.com). The post-fire image is then classified applying the Spectral Angle Mapper algorithm (Debba *et al.*, 2005; Kruse *et al.*, 1993) in ENVI, which uses, as reference, the spectral library of simulated spectra computed in the previous phase. The result of the classification phase is a Burn Severity Map.

Finally, the validation is performed computing the Root Mean Square Error (RMSE) between classified and observed (field plots) burn severity values (figure 1).

2.5 RTM selection

The simulation of burn severity levels was focused on pine trees, the dominant tree species of the main study area (site 1). To reproduce the combination of different factors that compose the field burn severity index (GeoCBI), two widely used RTMs were linked: the PROSPECT model (Jacquemoud, 1990) at leaf level and the GeoSail model (Huemmrich, 2001) at canopy level.

PROSPECT simulates both leaf reflectance and transmittance in the optical domain using five input parameters (in the version distributed by the Center for Spatial Technologies and Remote Sensing - CSTARS): leaf structure parameter N, chlorophyll a+b content (Ca+b), equivalent water thickness (Cw), dry matter content (Cm) and brown pigments content (Cs). PROSPECT assumes the leaf is composed by a set of stacked layers with several absorption components (Ca+b, Cs, Cw and Cm).

Although other RTM models are better adapted to simulate needle reflectance and transmittance (e.g. LIBERTY developed by Dawson *et al.*, 1998), they are not as operative as PROSPECT since they require more input variables with more complex parameters. Moreover, PROSPECT has been successfully used by several authors (Cheng *et al.*, 2006; Kötz *et al.*, 2004; Kötz *et al.*, 2003; Zarco-Tejada *et al.*, 2004) to simulate the response of conifers.

At canopy level, the use of a geometric model is more appropriate than a turbid medium model, due to the complex structure of Mediterranean forests and the importance of estimating of both LAI and FCOV per stratum in the GeoCBI computation.

Out of the canopy RTMs reviewed, the GeoSail model was selected, because it provides a more realistic description of canopy characteristics even if it is computationally simple (Huemmrich, 2001). In fact, GeoSail combines a geometric model with the SAIL model (Verhoef, 1984) that computes the reflectance and transmittance of the tree crowns. The geometric model determines the fraction of the illuminated and shadowed scene components as a function of canopy coverage, crown shape and illumination angle. The model assumes trees are identical, do not overlap, and they are relatively small in size compared to the size of the pixel (Huemmrich, 2001). This model was successfully used in coniferous forests (Kötz *et al.*, 2004, 2003; Hall *et al.*, 1997). Moreover, the structure of the GeoSail, which can simulate several vegetation strata, fits well into the structure of the GeoCBI index (table 2).

2.6 Sensitivity Analysis

Since the performance of simulation models greatly depends on their assumptions and the accuracy of input parameters (Liang, 2004), a simple sensitivity analysis (SA) was performed. In simulation studies, SA helps understand the importance of each input parameter and, consequently, the accuracy required to estimate these parameters.

The selected method was a local SA (Bicheron and Leroy, 1999; Bowyer and Danson, 2004), which assesses the local impact of the input parameters on the model output. Each parameter is perturbed (varied) in turn keeping all other model parameters fixed at their reference values (base-case) (Asner *et al.*, 2000). A "pseudo" merit function F' is used as the measure of the relative importance of each parameter for causing variations in reflectance (Bicheron and Leroy, 1999):

$$F' = \sum_{j=1}^{n} \frac{(\rho_0^j - \rho_{pert}^j)^2}{\rho_0^j} \quad (2)$$

where ρ_0^j and ρ_{pert}^j are the reflectance values in band *j* for the base-case and the perturbation respectively.

The local SA assesses the effects of the inputs of both RTMs (PROSPECT and GeoSail) on the reflectance output of the GeoSail. Table 4 shows the base-case of an unburned pine tree and the range of the perturbations, which simulates changes in the plant due to the fire.

Table 4. Parameters considered in the sensitivity analysis. (*) Specific leaf weight (SLW) = dry weight/leaf area.

INPUT PARAMETERS		UNIT	BASE-CASE	RANGE OF PERTURBATIONS
LEAF	**Ca+b**	µg/cm^2	70	10-70
	Cs	%SLW*	0.2	0.2-5
	N	--	2.5	1-4
	Cw	g/cm^2	0.048	0.001-0.06
	Cm	g/cm^2	0.035	0.01-0.06
CANOPY	**CROWN SHAPE**	--	CONE	CONE; CYLINDER
	FCOV	--	0.7	0-1
	LAI	--	2	0.1-2.5

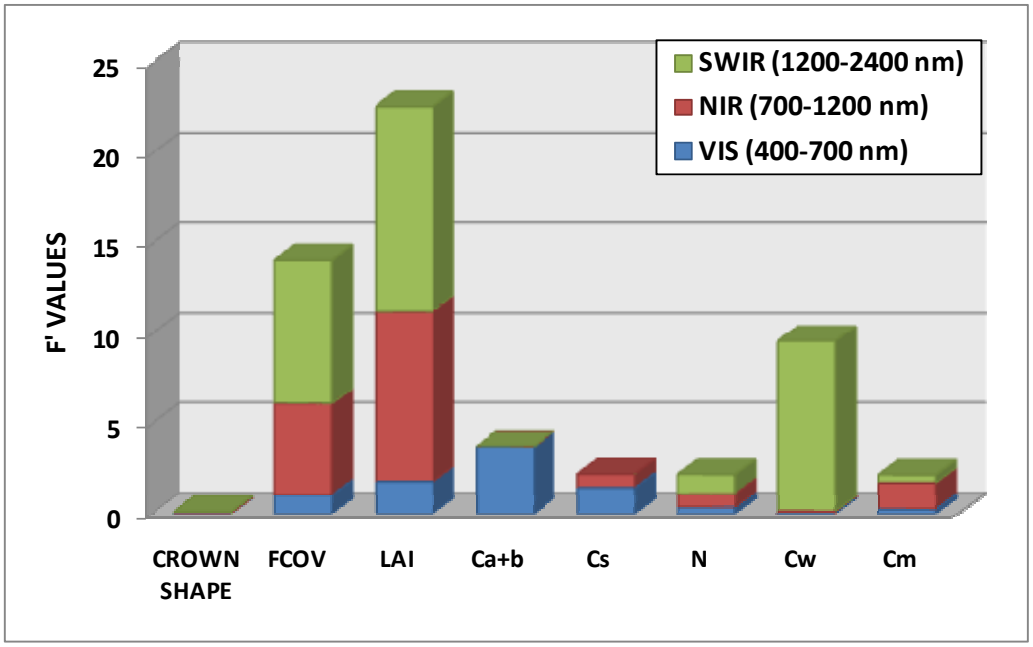

Figure 2. Results of the local SA in three wavelength ranges.

The results of the function merit F' (figure 2) show that the critical parameters are:

- ✓ Ca+b, followed by the LAI and Cs, in the visible (VIS);
- ✓ LAI and FCOV, in the near infrared (NIR);
- ✓ Cw, LAI and FCOV, in the short wave infrared (SWIR).

Therefore, the parameters which require a more careful selection of values (for parameterization purposes) are: water content (Cw) and chlorophyll (Ca+b), at leaf level, and LAI and FCOV, at canopy level. In addition, parameterization is simplified by identifying less relevant parameters.

2.7 Parameterization of the model at leaf level

In the GeoCBI field form the leaves were evaluated in terms of percentage of green and brown leaves present on the canopy. Therefore, the PROSPECT model was used in forward mode to simulate only one representative spectrum for each of these two reference leaf types (green and brown). In the case of green needles, the input parameters were derived from reference literature (table 5).

Table 5. Input parameter values for the simulation at leaf level using the PROSPECT model.

PARAMETERS	GREEN NEEDLE		BROWN NEEDLE
	VALUES	REFERENCES	
N	2.5	(Kötz et al., 2004; Kötz et al., 2003; Zarco-Tejada et al., 2004)	2.5
Ca+b (μg/cm^2)	70	(Kötz et al., 2004; Kötz et al., 2003)	20
Cw (g/cm^2)	0.048	(Kötz et al., 2004; Kötz et al., 2003; Zarco-Tejada et al., 2004)	0.0008
Cm (g/cm^2)	0.035	(Kötz et al., 2004; Kötz et al., 2003)	0.035
Cs (%SLW)	0.2	(Lang, 2005)	1.5

For the brown needles (table 5), no parameter values were found in the literature, therefore values were selected considering possible needle deterioration due to the fire. In this way:

- ✓ Ca+b was reduced, while the Cs increased.
- ✓ Cw was based on field samples of site 1.
- ✓ Since the dry matter content was calculated as the ratio between the dry weight (g) and the leaf area (cm^2), the Cm was kept fixed, because no leaf area variations in scorched needles were observed in the field (site 1) after the fire.
- ✓ N was also kept constant because the SA (figure 2) shows that its influence on the output reflectance of the canopy model is very low, and no values of N in scorched needles were found in the literature.

Finally, these simulated spectra were used as inputs for the canopy model (figure 1).

2.8 Parameterization of the canopy simulation model

There are generally two ways to carry out a simulation: (1) to combine input parameters freely obtaining all possible combinations, both realistic and unrealistic, and then try to filter out the latter; (2) to use only supervised (i.e. realistic) combinations of inputs.

As observed by Chuvieco *et al.* (2007), better results in burn severity estimation were obtained when a supervised simulation was performed because it reduces the noise introduced by unrealistic combinations when random ranges of inputs are considered. In short-time assessment of burn severity, field experience helped to select realistic combinations of damage levels between the different vegetation strata, which depend on vegetation type and both fire behaviour and intensity. For these reasons, only supervised

combinations of inputs were used to perform the simulation at canopy level, where the following assumptions were made (table 2):

1. The soil substratum (stratum A, table 2) of the GeoCBI was taken as the background layer of GeoSail. To reproduce the conditions found a few weeks after the fire, three reference spectra for the background layer were considered: soil, dark charcoal (DCH) and light charcoal (LCH, a mixture of charcoal and ashes). The soil spectrum was measured from a medium-moisture sandy soil, while both dark and light charcoal spectra were acquired from a recently burnt shrubland area. For the lower burn severity levels (from 0.5 to 1.5), two linear combinations of soil and dark charcoal were considered (table 4). All spectra were measured using a GER 2600 field spectroradiometer (Geophysical & Environmental Research Corporation, Millbrook, NY) calibrated against a Spectralon^{TM} white reference.

2. The first two vegetation strata of the GeoCBI (B and C, table 2) were merged and simulated as the understory layer of the model. In this simulation scenario, for the areas with a high burn severity (GeoCBI = 2.6 – 3), the understory was considered to be completely burnt.

3. Finally, the two strata which correspond to the intermediate and large trees in the GeoCBI (D and E, table 2), were simulated in GeoSail as one unified overstory layer.

All simulations were performed from 400 to 2400 nm, at 10 nm band sampling (201 spectral bands). The number of the simulation cases was reduced by fixing the following variables:

- ✓ Leaf angle distribution = spherical (according to Kötz *et al.*, 2004).
- ✓ Crown height to width ratio (Rv to Rh) = 2.36, derived from field measurements in the test-area 1.
- ✓ Sun zenith angle = 30^{o}, from the Landsat 5 TM post-fire image, site 1.
- ✓ Crown shape = cone, as suggested by Kötz *et al.* (2003) for pine forest.

The GeoCBI simulation was carried out in intervals of 0.05, for GeoCBI values from 2.3 to 3, because this is the most relevant range (moderate and high) of burn severity in the short-term post-fire assessment. In the remaining cases (GeoCBI from 0 to 2.2), the step varied between 0.1 and 0.5.

Table 6 shows an example of the combination of input parameters used for the simulation of the main GeoCBI values at canopy level (GeoSail model).

Table 6. Example of the combination of input parameters used for the simulation of the main GeoCBI values at canopy level (GeoSail model).

CASE	INPUT PARAMETERS						CASE DESCRIPTION
Geo CBI	UNDERSTORY		OVERSTORY		FCOV of both strata	Sub-stratum	
	LEAF TYPE	LAI	LEAF TYPE	LAI			
3	*No needles*	*0*	*Brown needle*	*0.05*	*0.4*	*DCH, LCH*	*Area affected by a high intensity fire. Combustion of the organic matter in the soil and all the vegetation strata. Presence of very few brown leaves on tree canopies. The substratum can be charcoal or ash depending on the burn efficiency.*
2.5	*Brown needle*	*1.8*	*Green needle*	*0.4*	*0.7*	*DCH*	*Rapid fire with low flame height. Total consumption of the organic matter in the soil. Understory with scorched leaves, overstory with low LAI and green canopies.*
2	*Brown needle*	*1.1*	*Green needle*	*1*	*0.75*	*DCH*	*Same as above except medium LAI in overstory.*
1.5	*Brown needle*	*0.8*	*Green needle*	*1.1*	*0.8*	*DCH*	*Rapid fire with low flame height. Total consumption of the organic matter on the soil. Higher percentage of green leaves on the canopies than brown leaves.*
1	*Brown needle*	*0.8*	*Green needle*	*1.2*	*0.8*	*50% Soil 50% DCH*	*Rapid fire with low flame height. Moderate consumption of the organic matter on the soil. Higher percentage of green leaves on the canopies than brown leaves. High FCOV of the vegetation.*
0.5	*Brown needle*	*0.3*	*Green needle*	*1.2*	*0.8*	*80% Soil 20% DCH*	*Rapid fire with very low flame height. Low consumption of the organic matter on the soil. Only indirect effects of the fire. Leaves in canopies are predominantly green.*
0	*Green needle*	*1.8*	*Green needle*	*2.5*	*0.8*	*Soil*	*Unburned areas.*

2.9 Model inversion strategy

The set of spectra obtained from the canopy level simulation, were matched with a look up table (LUT), where each GeoCBI value corresponds to a reflectance spectrum (figure 1). The LUT was turned into a spectral library (using ENVI 4.3) and convolved to Landsat 5 TM and SPOT 5 HRG bands. This spectral library was used as reference spectra (endmembers) to perform a Spectral Angle Mapper (SAM) supervised classification (figure 1). SAM is a pixel-based supervised classification technique that measures the similarity between spectra, in this

case between each pixel in the TM or SPOT images, and the simulated spectra included in the LUT. The similarity is computed from the spectral angle (in radians), when each spectrum is considered as an *m*-dimensional feature vector, with *m* being the number of spectral channels (Debba *et al.*, 2005; Kruse *et al.*, 1993). This angle is independent of the length of vector (Bakker & Schmidt, 2002), so it is insensitive to differences in illumination or albedo.

The result of this classification was a burn severity map, in which GeoCBI values were assigned to each pixel of the post-fire image.

The accuracy of the burn severity estimation was quantified in terms of the Root Mean Square Error (RMSE) between simulated GeoCBI (extracted from the burn severity maps) and that observed in the field.

3. Results

3.1 Simulation model results

The reference spectra used as input in the canopy level simulation are shown in figure 3. They consist of the two needle spectra (green and brown) obtained from the PROSPECT model and the different substratum types considered in this scenario.

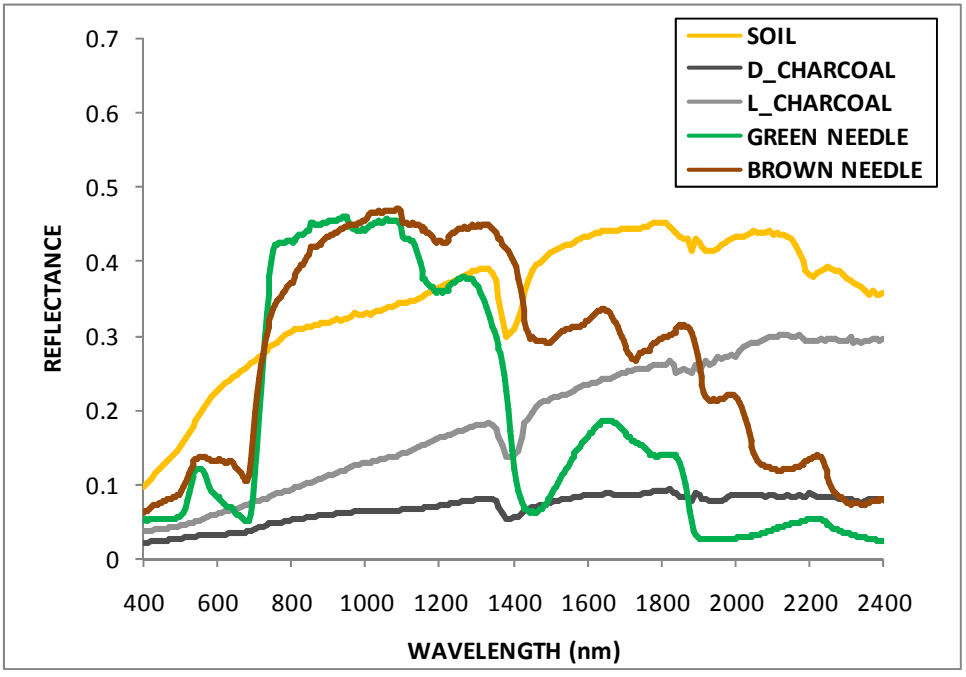

Figure 3. Reference spectra used as input for the simulation at canopy level.

The GeoSail simulation produced a total of 30 supervised spectra that corresponded to GeoCBI values from 0 to 3. Average spectra obtained for several ranges of GeoCBI are presented in figure 4. Simulation results showed the expected trends in reflectance for different values of burn severity (Chuvieco *et al.*, 1999; 2006; Key and Benson, 2005; Pereira *et al.*, 1999; Trigg and Flasse, 2000).

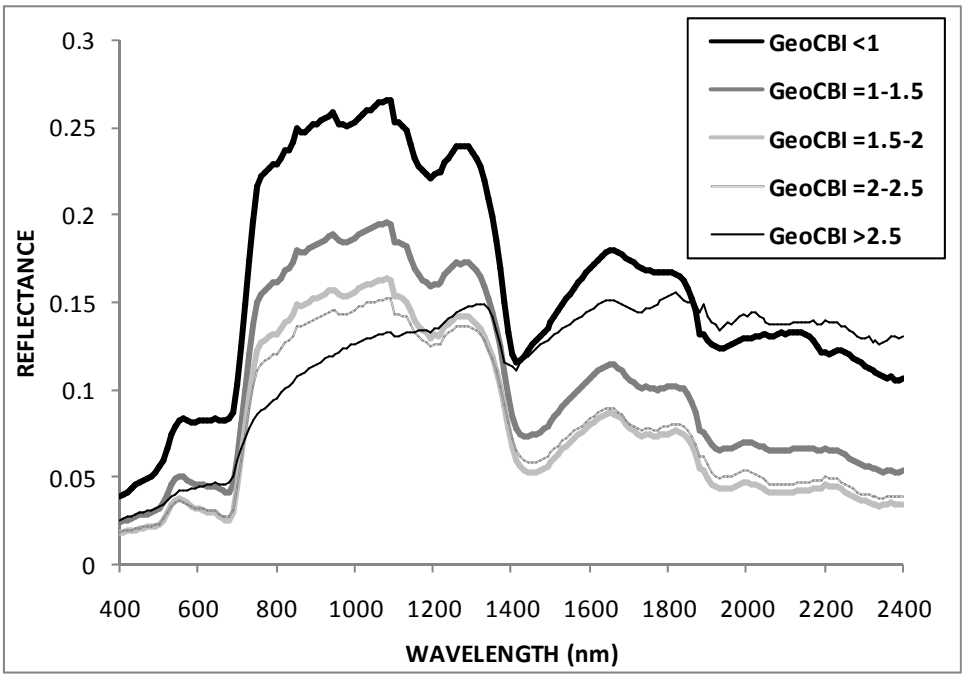

Figure 4. Average simulated reflectances, corresponding to the main intervals of GeoCBI.

Therefore, taking into account the main factors explained in table 7, the differences in the spectra per GeoCBI ranges (figure 4) depend on:

- ✓ variations in ground (substratum) visibility, which is directly proportional to the masking of the FCOV of the understory and overstory;
- ✓ variations in substratum (from "bright" soil to "dark" charcoal);
- ✓ needle type (from green to brown) and density (LAI) per stratum (understory or overstory).

To test the similarity between simulated and real data, Pearson correlation analyses were performed as follows: (1) *simulated* GeoCBI was correlated against simulated reflectances of the LUT and (2) *field* GeoCBI was correlated against Landsat TM reflectance corresponding to all the field plots in site 1 (figure 5). A strong negative correlation was observed in the 700-1300 nm range (r≈ -0.9) and, to a lower degree, in the green region (500-600nm) of the VIS

(r≈-0.7). According to the previous local SA, NIR-SWIR reflectance strongly depends on LAI and FCOV. Therefore, this result confirms that LAI and FCOV are the two most relevant factors in burn severity estimation. Instead, the green region is related, on the one hand, to both leaf damage and LAI and, on the other hand, to changes in the substrate from soil to char, as the severity level increases. In this region the correlation for *observed* data is not statistically significant due to the small number of field plots with moderate-low burn severity (i.e. plots where the presence of green canopies and soil is greater).

Figure 5 shows that the general trend of both correlations (*simulated* and *observed* data in site 1) is quite similar. Sites 2 and 3 also have similar correlation patterns, which suggest that the simulation model parameterization fits the field scenarios.

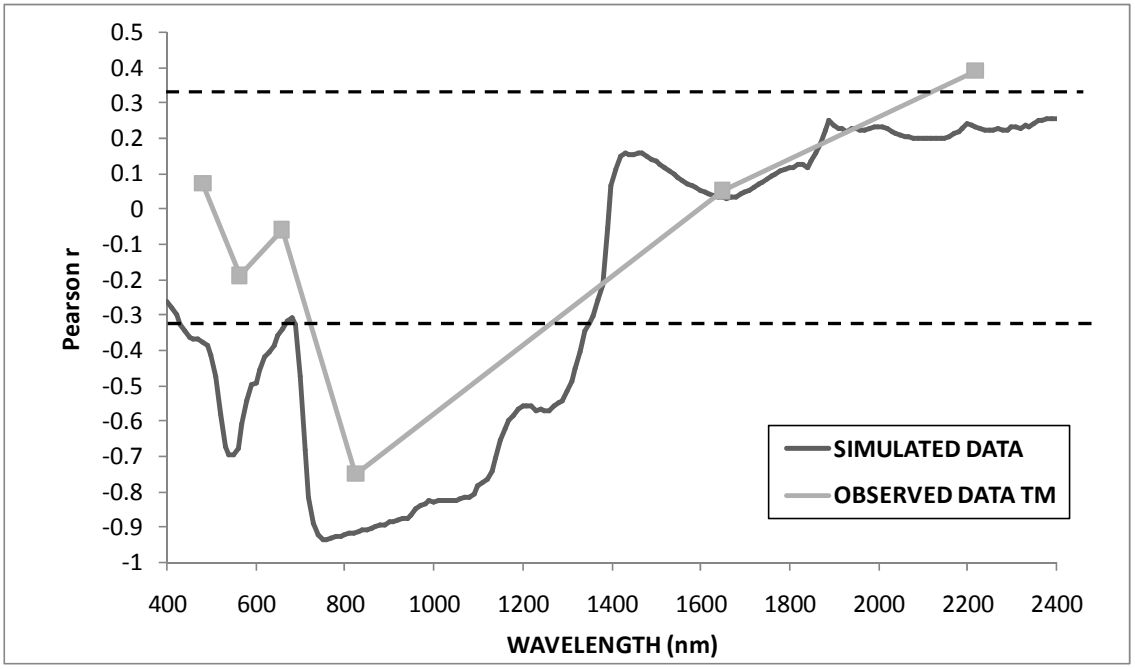

Figure 5. Pearson r coefficients for (1) *simulated* GeoCBI correlated against simulated reflectances of the LUT (black line) and (2) *field* GeoCBI correlated against Landsat TM reflectance corresponding to all the field plots of the test site 1(grey line). Dashed lines indicate the threshold of significance ($p<0.01$).

3.2 Burn severity estimation

Burn severity maps for each of the sites were produced using the SAM classification with simulated spectra (figure 6). Although GeoCBI is a continuous index, a non linear colour scale was used to emphasize differences from medium to high severity values, which are the most critical in the short-term assessment.

The map of site 1 (figure 6) shows three high severity areas separated by two NE-SW diagonal belts with lower GeoCBI values. The orthophoto (50cm resolution) in figure 7 shows two examples in these belts that confirm the presence of areas of medium-low burn severity (minor fire effects on tree crowns), surrounded by areas with a high burn severity. These intermediate levels are, therefore, correctly represented in the burn severity map.

Fires had a single ignition point both in site 1 (a barbecue) and 3. Instead, the map of site 2 shows an array of discontinuous burned areas, which is a typical fire occurrence pattern in Galicia, due to simultaneous ignition points. In site 2 the highest burn severity values are generally clustered in areas which were densely forested with pine and eucalyptus species. Moderate to high severity values are mainly located in areas with a lower FCOV of tree stratum and a thick gorse understory.

In the western part of the fire in site 3, burn severity values quickly shift from very high to very low, due to the efficiency in fire extinction tasks carried out by the fire-fighters, who had the advantage of dealing with a relatively small (i.e. more manageable) fire-front.

SITE #	BURN SEVERITY MAPS
1	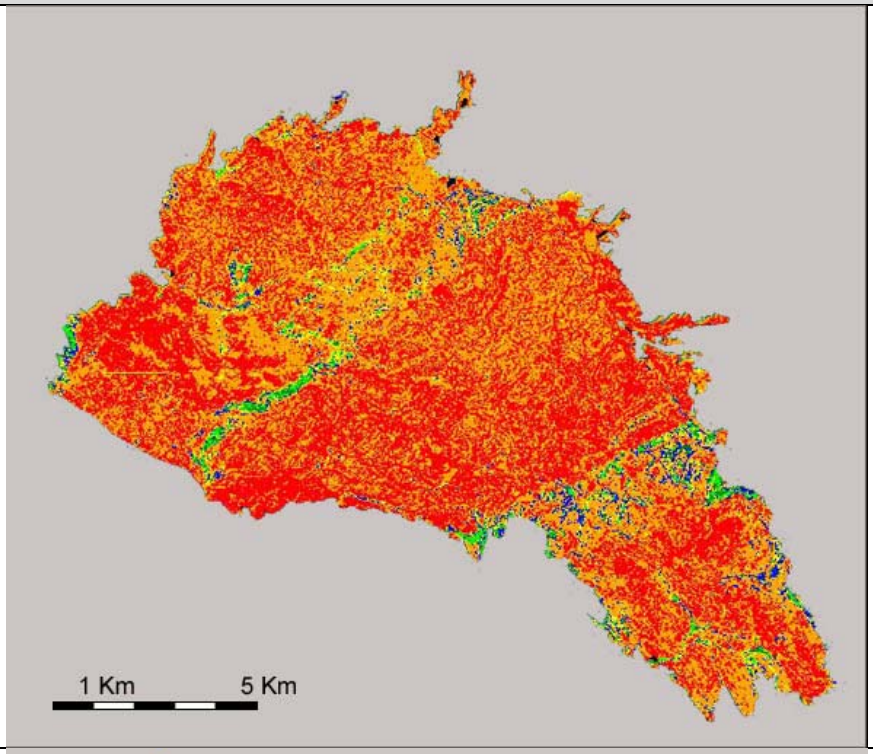
2	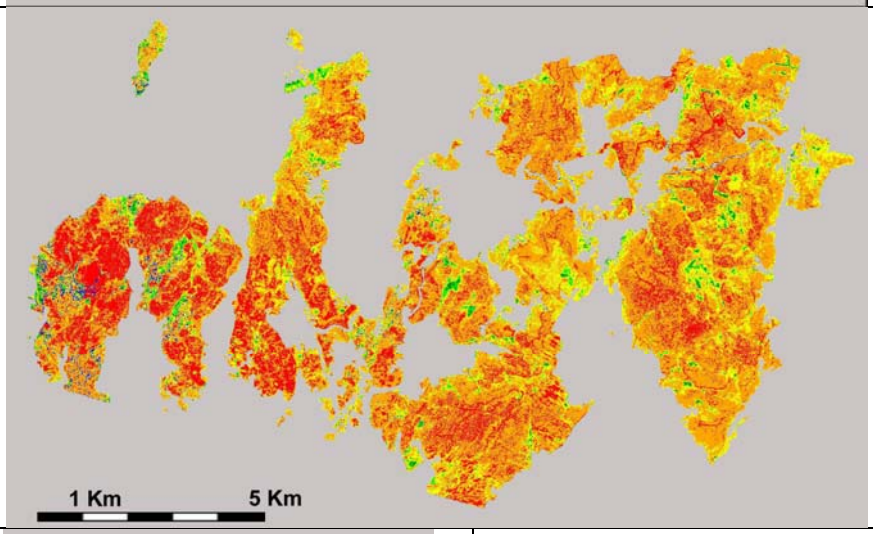
3	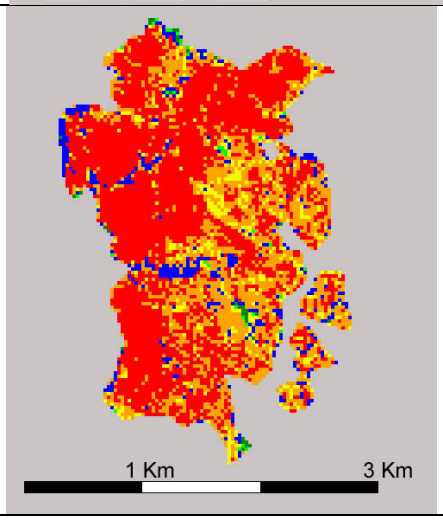 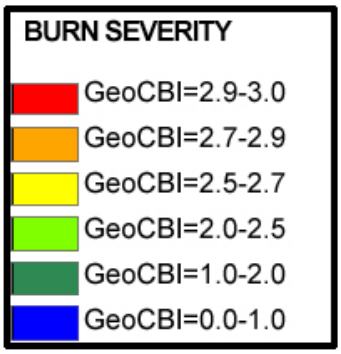

Figure 6. Burn severity maps obtained from the inversion of the simulation model.

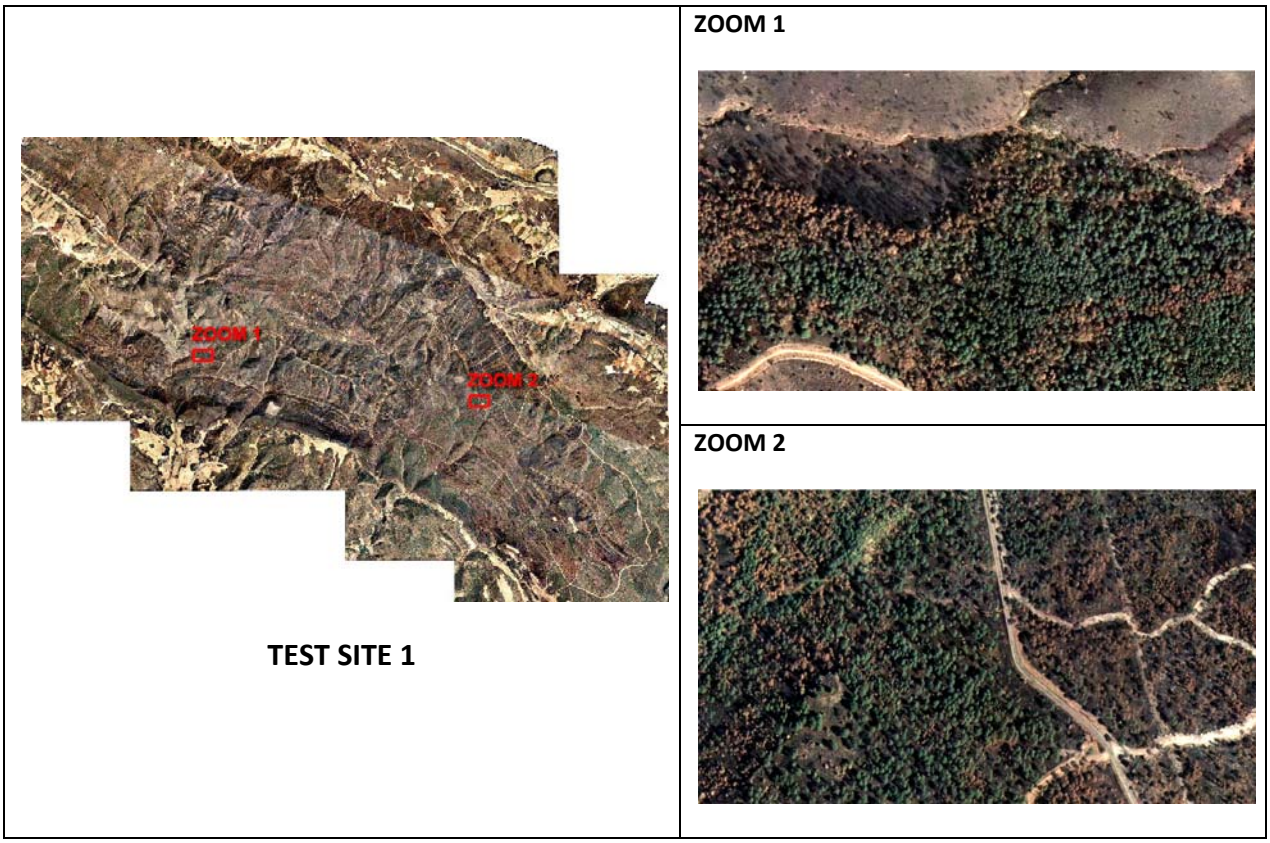

Figure 7. Post-fire orthophoto (true colour) of site 1.

3.3 Validation

The validation phase shows that the performance of the simulation model is similar in all test areas, and is almost equally accurate in all GeoCBI range values.

Details for each of the sites are as follows:

✓ Site 1: the correlation coefficient between observed and simulated GeoCBI values (table 7) was moderate-low (r^2=0.43), due to the short range of severity values found in this forest fire. However, the relationship is very close to a 1:1 linear fitting (slope ~1 and constant ~0) and the RMSE between simulated and observed GeoCBI values was also very low (RMSE=0.19) for all 83 plots. A comparison of observed and simulated values of GeoCBI (table 7) showed high estimation accuracies.

✓ Site 2: the correlation improves (r^2=0.69, table 7) and, more importantly, the RMSE is almost the same as in site 1 (RMSE= 0.18). Observed *versus* simulated burn severity are also closely matched, with only a slight overestimation in the first plot.

✓ Site 3: unlike the other two sites, the correlation coefficient was very high (r^2=0.96, table 7), due to the wide range of GeoCBI values. Again, the RMSE is very similar to sites 1 and 2 (RMSE=0.21), and so is the linear fitting, which is also near 1:1.

Table 7. Observed *versus* simulated GeoCBI values. All plots are ordered by their observed GeoCBI values from 0 to 3.

TEST SITE #	COMPARISON BETWEEN OBSERVED AND SIMULATED GeoCBI	
1	y = 0.963x+0.032 r^2=0.43 **RMSE=0.19**	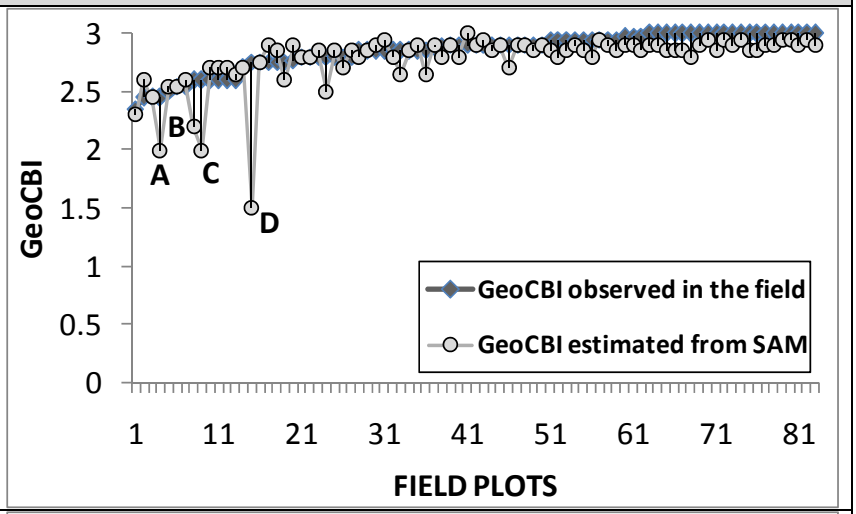
2	y= 0.495x+1.443 r^2=0.69 **RMSE= 0.18**	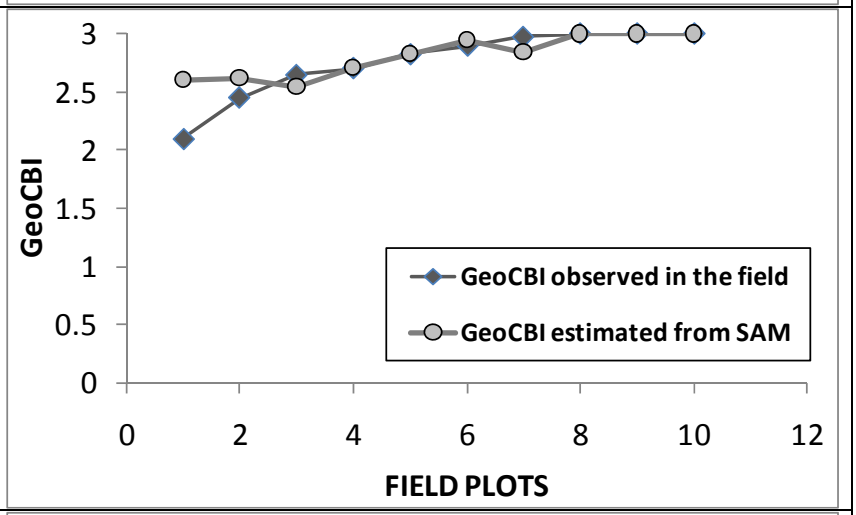
3	y= 1.046x-0.062 r^2= 0.96 **RMSE= 0.21**	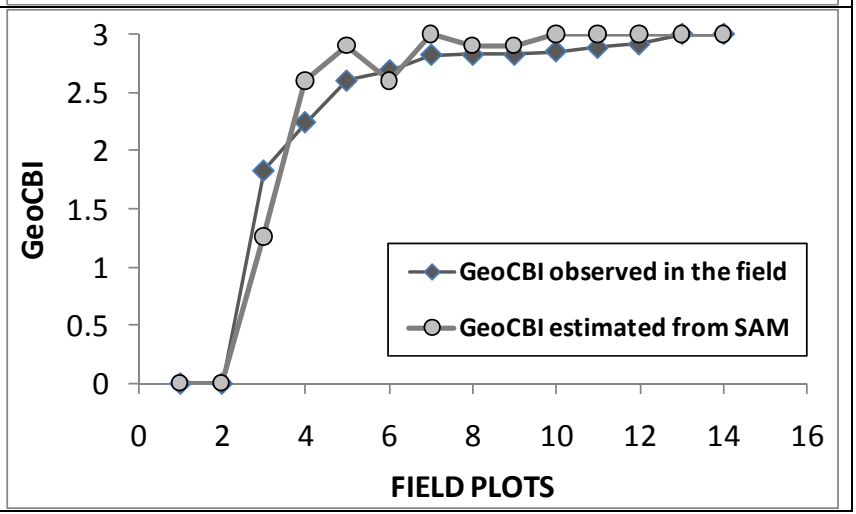

4. Discussion

4.1 Description of the plots with the highest estimation error

In site 1, the performance of the simulation model was uniform in all the ranges of burn severity observed, except for four plots (A, B, C and D in table 7, and table 8).

These four plots have two common features: (1) a high FCOV (FCOV > 60%, table 8) of the tree stratum (overstory); and (2) the burn severity of their overstory was lower than the burn severity of both their soil and understory. Therefore, the overstory partly masks the more severely affected understory, causing an underestimation of the GeoCBI of the total plot. This mask effect is an intrinsic limitation in optical remote sensing concerning vegetation studies. However, shortly after the fire, areas with green and thick canopies are less critical in terms of requiring rapid mitigation and rehabilitation treatments. Therefore, the slight underestimation in these plots was not a significant limitation of this estimation method, because these cases were infrequent and are less relevant from a forest management perspective.

Table 8. Description of the plots where burn severity was underestimated.

FIELD PLOT	DESCRIPTION	GeoCBI of TOTAL PLOT	
		OBSERVED	SIMULATED
PLOT A 	Tree strata: FCOV= 90% and CBI=1.2	2.45	2
PLOT B 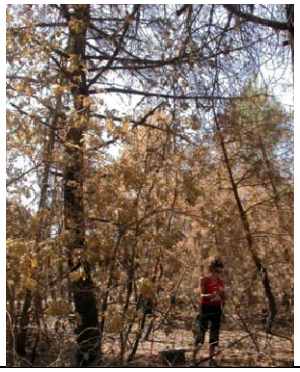	Tree strata: FCOV= 70% and CBI=1.95	2.6	2.2
PLOT C 	Tree strata: FCOV= 90% and CBI=2.2	2.6	2
PLOT D 	Tree strata: FCOV= 60% and CBI=2.4. Abundant dead needles litter.	2.75	1.5

5. Conclusions

In a post-fire scenario, a rapid and detailed knowledge of the level of damage and its distribution throughout the burnt area (burn severity map) is a key factor to quantify the impact of fires on landscapes and to plan efficiently both mitigation and rehabilitation treatments. In many cases, these treatments must be completed within weeks after the fire, to decrease severe erosion and soil degradation.

Since field estimation is time consuming and often spatially inaccurate, different remote sensing techniques have been proposed to estimate burn severity. Although burn severity is considered as a continuum (from unburned to completely burned), traditional techniques group the results in only three or four classes.

Compared to the traditional empirical fittings, previous studies showed that the use of RTMs improves the accuracy of burn severity estimation throughout the full range of severity (De Santis and Chuvieco, 2007). In this study, an improved simulation model was presented and its performance was tested in three different areas, in terms of GeoCBI (a new version of the CBI index).

The inversion of the new simulation model, which combines PROSPECT (at leaf level) and GeoSail (at canopy level), has improved significantly the accuracy in burn severity estimation. In addition, results were uniform in all GeoCBI ranges and in all test sites (RMSE between 0.18 and 0.21), despite their slightly different bioclimatic environments (Atlantic to inland Mediterranean). In the largest site (#1), only four plots out of 83 were underestimated, due to the presence of low affected canopies with a high FCOV that masks the signal of the highly affected understory. This is known limitation in optical remote sensing of vegetation studies.

The simulation model has been tested in Mediterranean areas and in fires that have mainly medium-high burn severity levels. Future studies will attempt to validate results in other ecosystems, trying to cover more homogeneously all the ranges of GeoCBI.

Acknowledgements

Special thanks to the Spanish Forest Service staff of Guadalajara and all team of the Geography Department of the University of Alcalá, who have been extremely helpful during the long fieldwork campaigns. The Spanish National Geographic Institute and the Department of Forestry of the Portuguese Agronomy Institute are acknowledged for providing the image data set corresponding to sites 2 and 3, respectively.

The Spanish Ministry of Science and Technology supports Angela De Santis within the FPU Programme framework. This project was founded by the EU Preview Project (www.preview-risk.com, EA21.CR/AC/03.064).

References

Andreae, M.O. and Merlet, P. (2001), Emission of trace gases and aerosols from biomass burning, *Global Biogeochemical Cycles*. 15(4): 955-966.

Asner, G.P., Wessman, C.A., Bateson, C.A. and Privette, J.L. (2000), Impact of tissue, canopy, and landscape factors on the hyperspectral reflectance variability of arid ecosystems, *Remote Sensing of Environment*. 74(1): 69-84.

Bakker, W. H., and Schmidt, K. S. (2002). Hyperspectral edge filtering for measuring homogeneity of surface cover type. *ISPRS Journal of Photogrammetry and Remote Sensing,56,*246-256.

Bicheron, P., Leroy, M. (1999), A Method of Biophysical Parameter Retrivial at Global Scale by Inversion of a Vegetation Reflectance Model, *Remote Sensing of Environment*. 67: 251-266.

Bobbe, T., Finco, M.V., Quayle, B., Lannom, K., Sohlberg, R., Parsons, A. (2001). Field Measurements for the Training and Validation of Burn Severity Maps from Spaceborne, Remotely Sensed Imagery, USDA Forest Service, Remote Sensing Applications Center, Salt Lake City, Utah.

Bowyer, P. and Danson, F.M. (2004), Sensitivity of spectral reflectance to variation in live fuel moisture content at leaf and canopy level, *Remote Sensing of Environment*. 92: 297-308.

Brewer, C.K., Winne, J.C., Redmond, R.L., Opitz, D. W., Mangrich, M.V. (2005), Classifying and Mapping Wildfire Severity: A Comparison of Methods, *Photogrammetric Engineering and Remote Sensing*. 71(11): 1311-1320.

Cheng, Y.B., Zarco-Tejada, P., Riaño, D., Rueda, C.A., Ustin, S. (2006), Estimating vegetation water content with hyperspectral data for different canopy scenarios: Relationships between AVIRIS and MODIS indexes, *Remote Sensing of Environment*. 105: 354-366.

Chuvieco, E. (Ed.) (1999). Remote Sensing of Large Wildfires in the European Mediterranean Basin. Springer-Verlag, Berlin.

Chuvieco, E., De Santis, A., Riaño, D., Halligan, K. (2007), Simulation approaches for burn severity estimation using remotely sensed images, *Fire ecology*. 3(1): 129-150.

Chuvieco, E., Riaño, D., Danson, F.M., Martín, P. (2006), Use of a radiative transfer model to simulate the postfire spectral response to burn severity, *Journal of Geophysical Research*. 111(G04S09): doi: 10.1029/2005JG000143.

Cocke, A.E., Fule, P.Z. and Crouse, J.E. (2005), Comparison of burn severity assessments using Differenced Normalized Burn Ratio and ground data, *International Journal of Wildland Fire*. 14: 189-198.

Dawson, T.P., Curran, P.J. and Plummer, S.E. (1998), LIBERTY - modeling the effects of leaf biochemical concentration on reflectance spectra., *Remote Sensing of Environment*. 65: 50–60.

Debba, P., van Ruitenbeek, F. J. A., van der Meer, F.D., Carranza, J. M., and Stein, A. (2005). Optimal field sampling for targeting minerals using hyperspectral data. *Remote Sensing of Environment, 99,* 373-386.

De Santis, A., Chuvieco, E. (2007), Burn severity estimation from remotely sensed data: performance of simulation versus empirical models, *Remote Sensing of Environment*. 108(4): 422-435.

De Santis, A., Chuvieco, E. (2008) GeoCBI: a modified version of the Composite Burn Index to estimate burn severity for remote sensing applications. *Remote Sensing of Environment,* under review.

Doerr, S.H., Shakesby, R.A., Blake, W.H., Chafer, C.J., Humphreys, G.S., Wallbrink, P.J. (2006), Effects of differing wildfire severities on soil wettability and implications for hydrological response., *Journal of Hydrology*. 319: 295-311.

Epting, J., Verbyla, D.L. and Sorbel, B. (2005), Evalation of remotely senses indices for assessing burn severity in interior Alaska using Landsat TM and ETM+, *Remote Sensing of Environment*. 96: 328-339.

Hall, F.G., Knapp, D.E., Huemmrich, K.F. (1997), Physicall based classification and satellite mapping of piophysical characteristics in the southern boreal forest, *Journal of Geophysical Research*. 102(D24): 29567-29580.

Huemmrich, K.F. (2001), The GeoSail model: a simple addition to the SAIL model to describe discontinuous canopy reflectance, *Remote Sensing of Environment*. 75: 423-431.

Hyde, K., Woods, S.W., Donahue, J. (2007), Predicting gully rejuvenation after wildfire using remotely sensed burn severity data, *Geomorphology*. 86(3-4): 496-511.

Jacquemoud, S. (1990), PROSPECT: a model to leaf optical properties spectra, *Remote Sensing of Environment*. 34: 74-91.

Key, C.H. and Benson, N. (2005), Landscape Assessment: Ground measure of severity, the Composite Burn Index; and Remote sensing of severity, the Normalized Burn Ratio. In: *FIREMON: Fire Effects Monitoring and Inventory System* (D.C. Lutes, R.E. Keane, J.F. Caratti, C.H. Key, N.C. Benson and L.J. Gangi, Eds.), USDA Forest Service, Rocky Mountain Research Station, Gen. Tech. Rep. RMRS-GTR-164, Ogden, UT, pp. CD:LA1-LA51.

Kokaly, R.F., Rockwell, B.W., Haire, S.L., King, T.V.V. (2007), Characterization of post-fire surface cover, soils, and burn severity at the Cerro Grande Fire, New Mexico, using

hyperspectral and multispectral remote sensing, *Remote Sensing of Environment*. 106 (3): 305-325.

Kötz, B., Schaepman, M., Morsdorf, F., Bowyer, P., Ittena, K. and Allgöwer, B. (2004), Radiative transfer modeling within a heterogeneous canopy for estimation of forest fire fuel properties, *Remote Sensing of Environment*. 92: 332-344.

Kötz, B., Schaepman, M., Morsdorf, F., Itten, K., Allgöwer, B., Bowyer, P., (2003). Multi-resolution Imaging Spectroscopy Resolving the Structure of Heterogeneous Canopies for Forest Fire Fuel Properties Mapping. In: I. International (Editor), Geoscience and Remote Sensing Symposium IGARSS '03, pp. 2869-2871.

Kruse, F. A., Lefkoff, A. B., Boardman, J. B., Heidebrecht, K. B., Shapiro, A. T., Barloon, P. J.,and Goetz, A. F. H. (1993). The spectral image processing (SIPS) - interactive visualization and analysis of imaging spectrometer data. *Remote Sensing of Environment,* 44*,* 145-163.

Kuusk, A. (2001) A two layer canopy reflectance model. *Journal of Quantitative Spectroscopy and Radiative Transfer*, 71, 1-9.

Lang, M., Nilson, T., Kuusk, A., Kiviste, A., Hordo, M., (2005). The performance of different leaf mass and crown diameter models in forming the input of a forest reflectance model: a test on forest growth sampleplots and Landsat ETM images, ForestSat 2005, Boras.

Lentile, L.B., Holden, Z. A., Smith, A.M.S., Falkowski, M. J., Hudak, A.T., Morgan, P., Lewis, S.A., Gessler, P.E., Benson, N. C. (2006), Remote sensing techniques to assess active fire characteristics and post-fire effects, *International Journal of Wildland Fire*. 15: 319-345.

Liang, S. (2004). *Quantitative remote sensing for land surface characterization*, Hoboken.

Miller, H.J. and Yool, S.R. (2002), Mapping forest post-fire canopy consumption in several overstory types using multi-temporal Landsat TM and ETM data, *Remote Sensing of Environment*. 82: 481–496.

Miller, J.D., Thode, A.E. (2007), Quantifying burn severity in a heterogeneous landscape with a relative version of the delta Normalized Burn Ratio (dNBR), *Remote Sensing of Environment*. 109: 66-80.

Moreno, J.M. and Oechel, W.C. (1989), A Simple Method for estimating fire intensity after a burn in California Chaparral, *Acta Ecologica (Ecologia plantarum)*. 10(1): 57-68.

Patterson, M.W. and Yool, S.R. (1998), Mapping Fire-Induced Vegetation Mortality Using Landsat Thematic Mapper Data: A Comparison of Linear Transformation Techniques, *Remote Sensing of Environment*. 65: 132-142.

Pereira, J.M.C., Sa, A.C.L., Sousa, A.M.O., Martín, M.P. and Chuvieco, E. (1999), Regional-scale burnt area mapping in Southern Europe using NOAA-AVHRR 1 km data. In: *Remote Sensing*

of Large Wildfires in the European Mediterranean Basin (E. Chuvieco, Ed.) Springer-Verlag, Berlin, pp. 139-155.

Pérez, B. and Moreno, J.M. (1998), Methods for quantifying fire severity in shrubland-fires, *Plant Ecology*. 139: 91-101.

Rogan, J. and Franklin, J. (2001), Mapping wildfire burn severity in Southern California Forests and shrublands using enhanced Thematic Mapper imagery, *Geocarto International*. 16(4): 89-99.

Trigg, S. and Flasse, S. (2000), Characterizing the spectral-temporal response of burned savannah using in situ spectroradiometry and infrared thermometry, *International Journal of Remote Sensing*. 21(16): 3161-3168.

van Wagtendonk, J.W., Root, R.R. and Key, C.H. (2004), Comparison of AVIRIS and Landsat ETM+ detection capabilities for burn severity, *Remote Sensing of Environment*. 92(3): 397-408.

Verhoef, W. (1984), Light scattering by leaf layers with application to canopy reflectance modeling: the SAIL model, *Remote Sensing of Environment*. 16: 125-141.

Wang, G.G. (2002), Fire severity in relation to canopy composition within burned boreal mixewood stands, *Forest Ecology and Management*. 163: 85-92.

White, J.D., Ryan, K.C., Key, C.C. and Running, S.W. (1996), Remote sensing of forest fire severity and vegetation recovery, *International Journal of Wildland Fire*. 6(3): 125-136.

Zarco-Tejada, P. *et al.* (2004), Needle chlorophyll content estimation through model inversion using hyperspectral data from boreal conifer forest canopies, *Remote Sensing of Environment*. 89(2): 189– 199.

V

Análisis comparativo de sensores espaciales para la cartografía de la severidad en el incendio de Riba de Saelices (Guadalajara)

Angela De Santis, Emilio Chuvieco

[1]*Departmento de Geografía*, *Universidad de Alcalá*, *Alcalá de Henares (Madrid)*
Recibido el 29 de noviembre de 2007; aceptado el 16 de abril de 2008.

Resumen

La severidad del fuego es un elemento clave para la estimación de los efectos a medio y largo plazo de los incendios forestales y consecuentemente para la previsión de la evolución ecológica de las áreas quemadas. Generalmente la severidad se evalúa en campo (a corto o medio plazo) o mediante ajustes empíricos a partir de imágenes de satélite, apoyados en parcelas de campo tomadas justo después del incendio. Pero, debido la escasa representatividad espacial del primer método y a la difícil generalización del segundo, se ha propuesto como alternativa el empleo de modelos de simulación (RTM). Los RTM estiman la reflectividad a partir de asunciones físicas y resultan ser más precisos que los métodos empíricos tradicionales. En este estudio la severidad se ha estimado a partir de dos modelos de simulación PROSPECT y GeoSail. El modelo desarrollado se ha aplicado a imágenes de cinco distintos sensores espaciales (SPOT HRV, Landsat TM, AWIFS, MERIS y MODIS), sobre la misma área de estudio (el incendio de Riba de Saelices, 2005), con el fin de comparar su precisión en la estimación de la severidad. La validación se ha realizado comparando los valores de severidad simulados para cada sensor, con los estimados en campo en 81 parcelas. Los resultados obtenidos muestran que el sensor Landsat TM es el que presenta el menor error en la estimación (RMSE=0.2) y su precisión es homogénea en todo el rango de GeoCBI analizado.

Palabras clave: Severidad del fuego, Modelos de simulación RTM, Teledetección, CBI, GeoCBI, PROSPECT, GeoSail.

Abstract

Burn severity is a key factor in both short and long term fire effects assessment and consequently in the estimation of the ecological evolution of the burnt areas. Traditionally, burn severity is estimated using field work or empirical fitting from remotely sensed data, based on field plots. However, due to the low spatial coverage of the first method and to the site- and data- specificity of the second one, alternative approaches have been proposed based on radiative transfer models (RTM). The RTM estimate reflectance using physical based assumptions and are more accurate than the empirical methods. In this study, burn severity was estimated using two RTM (PROSPECT and GeoSail). The developed model was applied to images of five different sensors (SPOT HRG, Landsat TM, AWIFS, MERIS y MODIS), and in the same study area (forest fire of Riba de Saelices, 2005), to compare their accuracy in the burn severity estimation. Validation was performed comparing simulated severity values for each sensor and burn severity values observed in 81 field plots. The results show that the Landsat TM has the lower error in the estimation (RMSE=0.2) and its accuracy is homogeneous in all range of GeoCBI analyzed.

Keywords: Burn severity, simulation models RMT, remote sensing, CBI, GeoCBI, PROSPECT, GeoSail.

1. Introducción

Los efectos de los incendios forestales sobre la cubierta vegetal y su impacto en la erosión del suelo son muy dependientes del nivel de severidad del fuego. Este concepto identifica los daños causados al ecosistema, principalmente en términos de biomasa quemada (materia seca en el suelo, hojas y troncos de especies a diferentes alturas). El análisis de los niveles de severidad del fuego resulta así un elemento clave para prever la evolución ecológica de las áreas afectadas, y los efectos a medio y largo plazo que el incendio supone sobre el ecosistema.

La severidad de un incendio está directamente relacionada con la intensidad y el tiempo de residencia del fuego. En incendios muy intensos, con una elevada liberación de energía en el frente de llamas, o en aquellos que se propagan lentamente y cuentan con periodos largos de quema, se destruyen buena parte de los elementos vitales de las plantas y de la materia orgánica del suelo, lo que supone una pérdida de protección del suelo y una regeneración posterior más lenta. Las estrategias de reproducción de las plantas son también claves en la evolución posterior al fuego: las germinadoras requieren disponer de un banco de semillas en buen estado y de condiciones meteorológicas favorables, mientras que las rebrotadoras están mejor adaptadas a fuegos periódicos, ya que pueden emitir nuevos brotes a partir de distintas partes de la planta justo después del incendio (Generalitat, 1988; Moreno y Oechel, 1991; Navarro *et al.*, 1996; Calvo *et al.*, 2003; Díaz-Delgado *et al.*, 2003).

Habitualmente, la severidad del fuego se evalúa según el grado de carbonización de los

diferentes estratos vegetales, y la proporción carbón/ceniza en la capa más superficial del suelo. Existen varios métodos de estimación disponibles en la literatura, principalmente apoyados en trabajo de campo (Moreno y Oechel, 1989; Pérez y Moreno, 1998; Key y Benson, 2005). El inventario de campo puede realizarse poco después del fuego (evaluación inmediata), o varios meses después (evaluación a medio plazo). La primera opción es útil para la gestión inmediata del área quemada, mientras que la segunda es más recomendable en diversos ecosistemas, al ofrecer un balance más riguroso de los daños reales del fuego y la regeneración potencial (Key y Benson, 2005). Además, en la evaluación inmediata pueden detectarse como persistentes, especies que pocos meses más tarde acaban muriendo a consecuencia de tener partes vitales seriamente dañadas.

La dificultad para abarcar un amplio territorio a partir de observaciones de campo, ha llevado a diversos autores a plantearse el empleo de imágenes de satélite en la cartografía de niveles de severidad, de cara a garantizar una cobertura actualizada y completa del territorio afectado (Díaz-Delgado *et al.*, 2003; van Wagtendonk *et al.*, 2004; Cocke *et al.*, 2005; Parra y Chuvieco, 2005). El principal reto en el empleo de la teledetección en los estudios de severidad del fuego es demostrar que los niveles de daño están asociados a la variación espectral que pueda recoger el sensor. Esto supone explorar la discriminabilidad teórica entre distintos niveles de severidad, por ejemplo usando modelos de transferencia radiativa (Chuvieco *et al.*, 2006). Una vez que se demuestra la sensibilidad teórica de las distintas bandas de reflectividad, habría que constatar si disponemos de sensores con el suficiente nivel de detalle (resolución espacial y espectral) para evaluar la severidad de una manera más o menos automática.

La mayor parte de los estudios de teledetección y severidad del fuego actualmente disponibles están basados en ajustes empíricos, apoyados en parcelas de campo tomadas poco después del incendio (Cocke *et al.*, 2005; Epting *et al.*, 2005; Miller y Yool, 2002; van Wagtendonk *et al.*, 2004). Los modelos empíricos son relativamente sencillos de calcular, pero tienen poca capacidad de generalización. La alternativa es emplear modelos de simulación (RTM, De Santis y Chuvieco, 2007), que intentan estimar la reflectividad procedente de una determinada cubierta a partir una serie de asunciones físicas. Variando las condiciones de entrada del modelo, puede simularse la reflectividad de un dosel, lo que ayuda a entender mejor la acción de esos factores (características bioquímicas de la hoja, cantidad, distribución geométrica, etc.), cuando se usan en modo directo; o a estimar los mismos factores de entrada, habitualmente manteniendo algunos constantes o extrayéndolos de otras fuentes, cuando se usan en modo inverso (Jacquemoud *et al.*, 2000). Hasta el momento, los modelos RTM no se han aplicado extensamente al análisis de áreas quemadas, orientándose los pocos

trabajos publicados a la determinación de quemado/no quemado (Roy *et al.* , 2002; Pereira *et al.*, 2004). Chuvieco *et al.* (2006) plantearon el uso de modelos de simulación en modo directo para la cartografía de niveles de severidad, mediante un enlace entre dos modelos, de hoja (PROSPECT) y de dosel (Kuusk), empleados para simular diversos escenarios de daño y señalando las potencialidades de los RTM. Posteriormente, De Santis y Chuvieco (2007) emplearon ese mismo modelo de simulación en modo inverso para estimar la severidad y comprobaron que los RTM resultaban más precisos que los métodos empíricos tradicionales, sobre todos en los valores extremos de severidad. Más recientemente, Chuvieco *et al.* (2007) extendieron la simulación a diversas condiciones de entrada. El escenario simulado seleccionando las combinaciones de parámetros de entrada, de acuerdo con la experiencia de campo, proporcionó los mejores resultados, aunque todavía se registraron importantes errores de subestimación. Finalmente, De Santis *et al.* (2008) mejoraron la estimación de la severidad a corto plazo utilizando el modelo PROSPECT para simular dos tipos de hoja (verde y quemada) y un modelo geométrico a nivel de dosel (GeoSail, Huemmrich, 2001). En este estudio obtuvieron un ajuste homogéneo en todo el rango de severidad analizado en tres áreas de estudio distintas, situadas en España y Portugal.

Ya que se ha identificado una técnica eficaz para cartografiar la severidad, ahora nos planteamos el problema de identificar que sensor espacial, entre los más comúnmente utilizado, es el más adecuado para este tipo de estudio. Con gran diferencia, las imágenes Landsat (TM o ETM+) han sido las más frecuentemente utilizadas en este contexto (White *et al.*, 1996; Kushla y Ripple, 1998; Patterson e Yool , 1998; Key y Benson, 1999; Rogan e Yool, 2001; Miller e Yool, 2002; Bobbe *et al.*, 2003; van Wagtendonk *et al.*, 2004; Brewer *et al.*, 2005; Bigler *et al.*, 2005; Cocke *et al.*, 2005; Epting *et al.*, 2005; Finney *et al.*, 2005; Sorbel y Allen, 2005; Hyde *et al.*, 2007; Kokaly *et al.*, 2007 ; Miller y Thode, 2007; Robichard *et al.*, 2007; De Santis y Chuvieco, 2007; Chuvieco *et al.*, 2007), pero también existen otros estudios que emplean otros sensores como SPOT, MERIS y MODIS (Isaev *et al.*, 2002; Chaefer *et al.*, 2004; Hudak *et al.*, 2004; Alleaume *et al.*, 2005; Chuvieco *et al.*, 2007; Roldan-Zamarrin *et al.*, 2006). Finalmente, la teledetección hiperespectral resulta particularmente adecuada para estas aplicaciones (van Wagtendonk *et al.*, 2004; Parra y Chuvieco, 2005).

Tratándose de una estimación que requiere una sola imagen post-incendio, el tiempo de revisita de los sensores no constituye una limitación, por esto nos centraremos en la comparación de las características espectrales y espaciales de cinco distintos sensores: SPOT 5 HRG, Landsat TM, AWIFS, MERIS y MODIS, utilizando la simulación presentada en De Santis *et al.* (2008) para la estimación de la severidad a corto plazo. La validación se llevará a cabo utilizando como referencia las medidas de severidad realizadas en campo.

2. Materiales y métodos

2.1 Área de estudio

El área de estudio está localizada en el NE de la provincia de Guadalajara (40-41 ^{o} N y 1-2 ^{o} W) (Figura 1). La topografía es rugosa con variaciones altitudinales entre 1100 y 1400 m. La precipitación promedio se sitúa entre 600-800 mm anuales, principalmente en Noviembre-Diciembre. La temperatura promedio es de 7.5 a 15^{o} C, según las zonas. La vegetación dominante está formada por pinares de pino resinero (*Pinus pinaster*) con mezcla de robledales mediterráneos de quejigo (*Quercus faginea*) y rebollo (*Quercus pyrenaica*), principalmente en la capa inferior del sustrato vegetal (< 5 m). El matorral está dominado por *Cistus ladanifer*, *Cistus albidus*, *Rosmarinus officinalis*, *Juniperus oxycedrus*, *Rosa canina*, *Cytisus scoparius*, y *Lavanda Pedunculata*.

El área fue afectada por un gran incendio en Julio de 2005, causado por una negligencia humana. Las condiciones de extrema sequía, alta temperatura y fuerte viento contribuyeron al crecimiento incontrolado del fuego, que duró 4 días, quemando 13.000 ha. El incendio fue tristemente célebre por la muerte de 11 bomberos forestales que trabajaban en la extinción, lo que causó un gran impacto en la opinión pública.

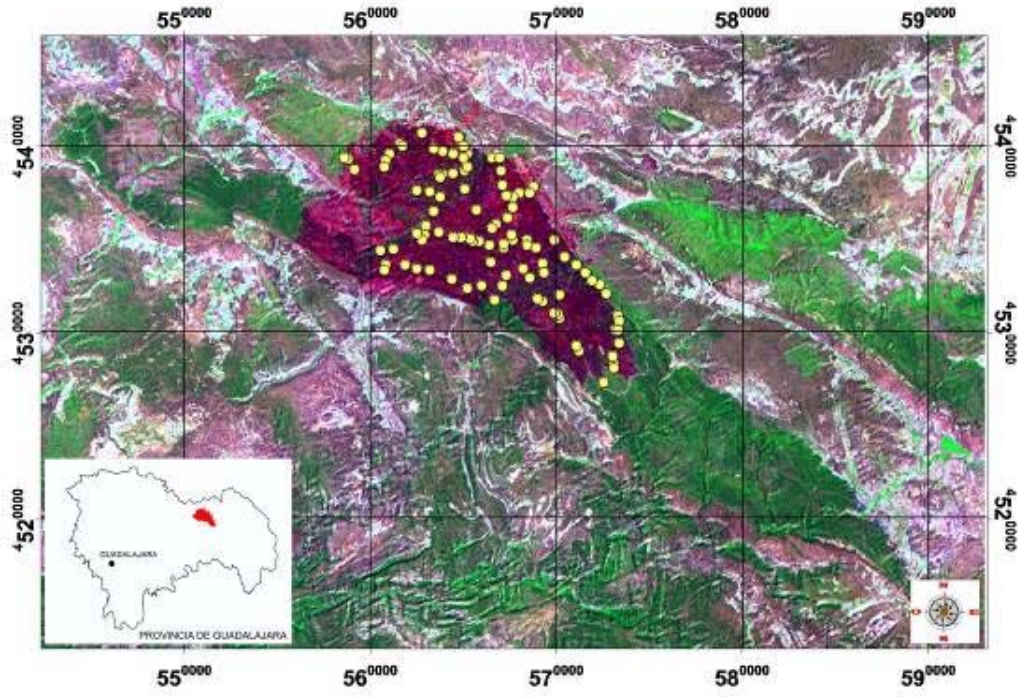

Figura 1. Localización del área de estudio sobre una imagen Landsat-TM. Los puntos amarillos identifican las parcelas muestreadas en campo.

2.2 Trabajo de campo

El análisis de la severidad en campo se basó, en líneas generales, en el método CBI (Composite Burned Index), desarrollado por el US Forest Service en el marco del proyecto FIREMON (Fire Effects Monitoring and Inventory Project: http://fire.org/firemon/: Key y Benson, 2005). La ventaja de este método es que facilita una estimación numérica de los niveles de daño, que se basa en variables fácilmente obtenibles en campo. La escala propuesta en el CBI va de 0 (sin daño) a 3 (máximo daño), y se basa en considerar el impacto del fuego sobre cinco estratos de vegetación (substrato, herbáceo, matorral y árboles pequeños, árboles intermedios y árboles grandes). Los tres primeros forman el sotobosque y sustrato, y los dos últimos el dosel.

Las variables que recoge el CBI hacen referencia al cambio causado por el fuego sobre la estructura vegetal, por lo que se recomienda analizar previamente zonas no quemadas en los alrededores para estimar las condiciones de partida. El CBI se calcula a partir de unas variables parametrizadas que describen distintos rangos de daño. Las más importantes son el cambio en el color del suelo, la presencia de materia orgánica, la pérdida de hojas, el cambio en el color de la hoja, la altura del carbón en los troncos, y la mortalidad de la vegetación (Key y Benson, 2005).

Para ajustar este índice de campo al análisis de imágenes de satélite, se consideró necesario introducir algunas modificaciones en el protocolo original (De Santis y Chuvieco, 2008). Dos nuevas variables fueron añadidas por cada estrato vegetal:

1- el porcentajes de cambios en el área foliar (*Leaf Area Index* ,LAI= área foliar por unidad de superficie de suelo; Ceccato *et al.*, 2002a).
2- la cabida cubierta de la vegetación (*Fraction of Cover*, FCOV= porcentaje de cabida cubierta respecto al total de la parcela).

De manera similar al CBI original, al porcentaje de cambios en el LAI se le asignaron valores entre 0 (no cambio, ausencia de daño) y 3 (100% de cambio, daño máximo). La FCOV, sin embargo, se utilizó para ponderar el peso de cada estrato en el cálculo del valor de severidad de toda la parcela. De este modo, se obtiene una mejor caracterización de la estructura y de la composición de las parcelas quemadas. El nuevo índice propuesto GeoCBI (*Geometrically structured Composite Burn Index,* De Santis y Chuvieco, 2008) tiene la siguiente formulación:

$$GeoCBI = \frac{\sum_{m_1}^{m_n} (CBI_m * FCOV_m)}{\sum_{m_1}^{m_n} FCOV_m} \quad (1)$$

donde *m* representa el estrato considerado y *n* es el numero de estratos.

Tres semanas después del incendio, se muestrearon 103 parcelas distribuidas en todo el área de estudio, siempre que las zonas resultaran razonablemente accesible. Cada parcela tenía un diámetro aproximado de 30 m y pretendía situarse en áreas homogéneas desde el punto de vista de la severidad. Las coordenadas de las parcelas se extrajeron de un navegador GPS (GARMIN 12). El trabajo de campo se realizó entre agosto y septiembre de 2005, poco después de ser extinguido el incendio. La figura 2 recoge un ejemplo de distintos niveles de severidad observados en el campo.

Figura 2. Ejemplos de diferentes valores de GeoCBI: (a) alto (GeoCBI=3), (b) moderado (GeoCBI=2.14) y (c) medio- bajo (GeoCBI= 1.5).

2.3 Imágenes de satélite

Para este trabajo se emplearon imágenes de 5 distintos sensores. La tabla 1 muestra un resumen de sus características espectrales y espaciales.

Tabla 1. Resumen de las características espectrales y espaciales de los sensores utilizados en este estudio.

SENSOR	SPOT 5 HRG	Landsat TM	AWIFS	MERIS	MODIS
RESOLUCIÓN ESPACIAL (m)	10	30	60	300	500
RESOLUCIÓN ESPECTRAL (nm)					
B1	500-590	450-515	520-590	407,5-417,5	620-670
B2	610-680	525-605	620-680	437-447	841-876
B3	780-890	630-690	770-860	485-495	459-479
B4	1580-1750	750-900	1550-1700	505-515	545-565
B5		1550-1750		555-565	1230-1250
B6				615-625	1628-1652
B7		2090-2350		660-670	2105-2155
B8				677,5-685	
B9				703,75-713,75	
B10				750-757,5	
B12				771,25-786,25	
B13				855-875	
B14				880-890	

La imagen SPOT 5 HRG1 se adquirió el 20 de Septiembre de 2005, y pertenece a la cubierta nacional preparada para el Plan Nacional de Teledetección (cortesía IGN). Lamentablemente, la imagen no cubre toda la superficie del incendio, a consecuencia de la traza del satélite y la cobertura de nubes, por lo que se seleccionó únicamente el sector más oriental. Para la corrección geométrica se utilizó como referencia con una ortofoto digital post-incendio (píxel de 50 cm), proporcionada por TRAGSA. Se empleó un modelo polinomial de primer grado (error < 0.5 pixel). La calibración radiométrica se basó en los coeficientes de cabecera de la imagen y en el método del objeto oscuro propuesto por Chavez (1996). Tras estas correcciones, se abordó una corrección de efecto de sombreado topográfico, empleando un modelo digital de elevaciones de alta precisión (10 m) y el método de corrección lambertiano propuesto por Civco (1989).

La imagen Landsat 5 Thematic Mapper (TM) (path 200, row 32) corresponde al 5 de Agosto de 2005 (10 días después de la extinción del incendio). Los valores brutos (niveles digitales) fueron convertidos a reflectividad (ρ) empleando los valores de calibración propuestos por Chander y Markham (2003) y el método de corrección atmosférica del objeto oscuro. La corrección geométrica se basó en un conjunto de puntos de control, empleando como

referencia la ortoimagen Landsat ETM+ utilizada en el proyecto CORINE 2000 (proyección UTM 30 T, datum Europeo Medio de 1950). Se usaron funciones polinómicas de primer grado. Los residuales medios están por debajo de 0.5 píxeles. Al igual que con la imagen SPOT, se aplicó la corrección de iluminación de Civco.

La imagen AWIFS fue adquirida el 22 de agosto de 2005, y fue corregida geométrica y radiométricamente siguiendo el mismo esquema de la imagen Landsat TM.

La imagen MERIS es del 12 de agosto de 2005, y se consiguió a través del servicio de distribución de datos de la Agencia Espacial Europea, en el marco del proyecto europeo Preview (www.preview-risk.com). Los datos fueron procesados por el UK-PAC (UK Multi-Mission Processing and archiving Centre), y distribuidos en formato FR-2P. Este formato, con resolución espacial de 300 m, se compone de 12 de las 15 bandas originales de MERIS, como datos de reflectividad, y 8 bandas adicionales de información (dos índices de vegetación, concentración de algas, concentración de materia orgánica e inorgánica en suspensión, albedo de las nubes, espesor óptico de las nubes y concentración de vapor de agua). La imagen entregada está corregida atmosférica y radiométricamente, y se presenta en la proyección UTM y datum WGS 84, por lo que hubo que reproyectarla a la proyección UTM 30 T, datum Europeo medio de 1950. Al observarse sucesivamente un ligero desplazamiento respecto a las imágenes Landsat y SPOT, se realizó la corrección geométrica tomando como referencia un mosaico de imágenes Landsat 7 del año 2000 (fuente CORINE 2000). Se utilizaron funciones polinómicas de segundo grado, y se obtuvieron residuales medios inferiores a 0,6 píxeles.

Finalmente se utilizó una imagen MODIS (a bordo de la plataforma TERRA) del 12 de agosto del 2005. Se trata de producto MOD 09 (MODIS Surface-Reflectance Product, http://modis.gsfc.nasa.gov/) que se calcula a partir del nivel 1B de MODIS, y corresponde a la reflectividad estimada al suelo para cada banda sin absorción o dispersión de la atmósfera. La imagen ha sido reproyectada a UTM 30 T, datum Europeo medio de 1950.

En la tabla 2 se muestra un resumen de todas las correcciones aplicadas a las cinco imágenes.

Tabla 2. Resumen de las correcciones aplicadas a las cinco imágenes.

SENSOR	TIPO DE CORRECCIÓN		
	RADIOMÉTRICA	**GEOMÉTRICA**	**TOPOGRÁFICA**
SPOT	Método del objeto oscuro (Chavez, 1996)	Puntos de control. Imagen de referencia: ortofoto (50 cm)	Método de Civco (1989)
LANDSAT TM	Método del objeto oscuro (Chavez, 1996)	Puntos de control. Imagen de referencia: Landsat 7 ETM+ (Corine Land Cover, 2000)	Método de Civco (1989)
AWIFS	Método del objeto oscuro (Chavez, 1996)	Puntos de control. Imagen de referencia: Landsat 7 ETM+ (Corine Land Cover, 2000)	Método de Civco (1989)
MERIS	UK-PAC (Agencia Espacial Europea)	UK-PAC + Puntos de control. Imagen de referencia: Landsat 7 ETM+ (Corine Land Cover, 2000)	----------
MODIS	NASA	NASA + reproyección	----------

2.4 Modelos de simulación

Entre los modelos de simulación de reflectividad de la vegetación que se vienen utilizando en los últimos años, los más comunes se basan en la ecuación de transferencia radiativa (RTM), que permite simular físicamente la reflectividad de una cubierta a partir de los factores que influyen en la absorción y dispersión de la radiación solar incidente.

Para este trabajo, la simulación de los niveles de severidad se ha centrado en la especie *Pinus pinaster* (especie dominante en la zona de estudio) y se ha llevado a cabo utilizando dos modelos (como en De Santis *et al.*, 2008): el PROSPECT (Jacquemoud, 1990) a nivel de hoja y el GeoSail (Huemmrich, 2001) a nivel de dosel.

El modelo PROSPECT simula la reflectividad y la transmisividad de la hoja a partir de cinco parámetros de entrada (parámetro estructural N, contenido de clorofila a+b, espesor equivalente de agua, materia seca y contenido de pigmentos marrones) y se ha utilizado ampliamente en teledetección. En este estudio se han simulado dos tipos de hojas, verde y

seca, fijando los parámetros de entrada en base a los valores de referencia encontrados en la bibliografía para acículas de pino (Kötz *et al.*, 2004; Kötz *et al.*, 2003; Zarco-Tejada *et al.*, 2004; Lang, 2005).

Sucesivamente, a nivel de dosel se ha empleado el modelo GeoSail, que permite simular distintos estratos de vegetación, más un sustrato y que considera condiciones de observación e iluminación, parámetros geométricos de la copa y el efecto de las sombras.

Puesto que resultaba muy complejo simular todas las variables medidas en campo, se seleccionaron para la simulación las siguientes:

- ✓ Cambios de sustrato: se consideraron tres espectros de referencia correspondientes a los tipos de sustrato más comunes pocas semanas después del incendio (suelo, carbón y ceniza);
- ✓ Cambios en el sotobosque: que corresponde a los dos primeros estratos de vegetación considerados en el GeoCBI (hasta 5 m de altura);
- ✓ Cambios en el dosel: que corresponde a los últimos dos estratos de vegetación del GeoCBI (vegetación arbórea > 5m).

Todas las simulaciones se llevaron a cabo entre 400 y 2400 nm (con intervalos de 10 nm) y los espectros a nivel de hoja generados con el PROSPECT fueron utilizados como parámetros de entrada para el GeoSail, juntos a las siguientes variables, que fueron fijadas para reducir el número de simulaciones:

- ✓ Distribución angular de las hojas (*Leaf Angle Distribution*, LAD)= esférica (Kötz *et al.*, 2004);
- ✓ Proporción entre alto y ancho de la copa = 2.36 (medido en campo en la zona de estudio);
- ✓ Ángulo cenital solar = 30^{o} (derivado de la imagen Landsat 5 TM);
- ✓ Forma del dosel = cónica (Kötz *et al.*, 2003).

Los espectros simulados con PROSPECT+GeoSail, cada uno correspondiente a un determinado valor de GeoCBI, se utilizaron para formar una librería espectral de referencia (De Santis *et al.*, 2008). Para extraer qué espectro incluido en esta librería resultaba más similar a cada píxel de la imagen, utilizamos el clasificador angular (Spectral Angle Mapper, SAM), disponible en ENVI. El algoritmo SAM minimiza el ángulo espectral entre el espectro observado (extraído de la imagen) y el simulado (de la librería espectral) y es insensible a las condiciones de iluminación y efectos de albedo (Bakker y Schmidt, 2002).

2.5 Validación

En primer lugar, para identificar las bandas más significativas a la hora de estimar la severidad, se calculó, para cada sensor, la correlación de Pearson entre las firmas espectrales extraídas en correspondencia de las parcelas de campo y su correspondiente valor de severidad observado.

Debido a que la imagen SPOT no cubre todo el incendio y para evitar el solape entre parcelas en el caso de las imágenes con píxel de 300 y 500 m, se seleccionó una sub-muestra de 81 parcelas, de las 103 marcadas en campo.

Sucesivamente, el ajuste de las estimaciones fue cuantificado en términos de error cuadrático medio (*Root Mean Square Error*, RMSE) entre GeoCBI simulado y observado en campo, en la misma sub-muestra.

Es importante tener en cuenta que, debido a la alta intensidad del incendio de Guadalajara, el rango de GeoCBI observado en campo está comprendido entre 2.35 y 3, lo que dificulta extrapolar las conclusiones de este estudio a zonas que presentan valores inferiores a estos.

3. Resultados

La figura 3 muestra la correlación entre las bandas de los sensores y la severidad observada en correspondencia de la sub-muestra de las parcelas de campo. Destaca la alta correlación negativa de las bandas correspondientes al infrarrojo cercano (IRC, tabla 1) ($r > -0.45$), siendo la banda 4 de Landsat la que registra el valor más alto ($r = -0.65$), seguida por la banda 3 de SPOT ($r = -0.57$), las bandas de MERIS de 10 a 13 ($r = -0.55$) y finalmente la banda 3 de AWIFS ($r = -0.54$). En el IRC la reflectividad depende especialmente de la cantidad de biomasa vegetal y de su estado de vigor. Esto confirma que el LAI y la FCOV son los factores predominantes en la determinación de los niveles de severidad.

Por otro lado, la banda 7 de Landsat, correspondiente al infrarrojo de onda corta (SWIR 2, tabla 1) muestra una alta correlación positiva ($r = 0.51$), superior a la que se observa para la banda 5 del mismo sensor y a las bandas 4 de SPOT y AWIFS centradas en el SWIR 1.

Esta capacidad del SWIR 2 debería relacionarse con su sensibilidad para distinguir distintos tipos de substratos y contenido de humedad.

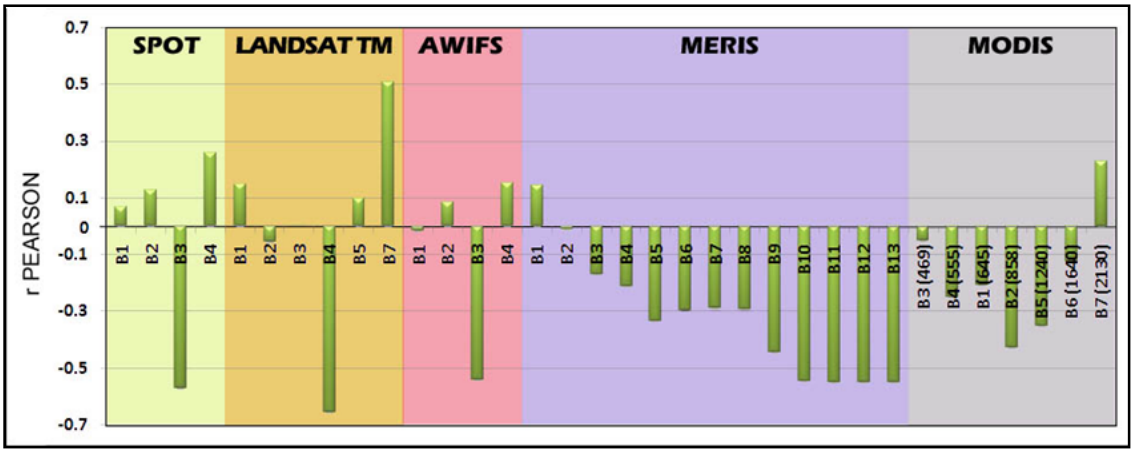

Figura 3. Correlación entre las bandas de los sensores y la severidad de las parcelas observada en campo (para mayor claridad, las bandas de MODIS han sido ordenadas según las longitudes de onda correspondientes).

3.1 Validación

La figura 4 muestra los errores cuadráticos medios por cada sensor. Para analizar mejor la precisión de las estimaciones, el RMSE ha sido dividido en tres grupos, además de considerar su valor total: GeoCBI entre 2.35 y 2.5, 2.5-2.7, 2.7-3.

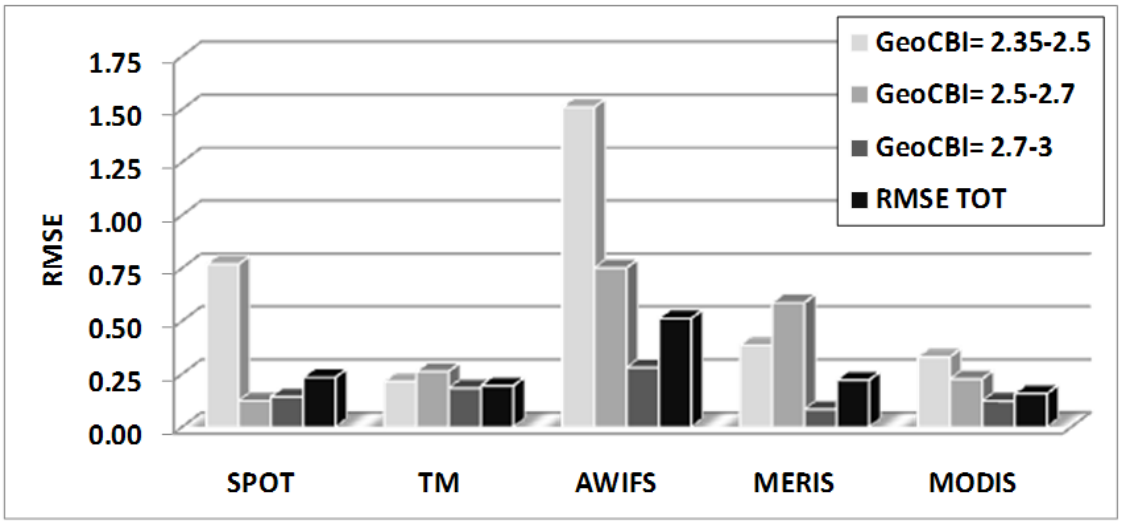

Figura 4. Error cuadrático medio calculado para cada sensor y cada rango de GeoCBI analizado.

El primer intervalo considera valores severidad intermedios, que corresponden normalmente a zonas con alta heterogeneidad en los efectos del fuego en los distintos estratos de la vegetación. Para este rango, el error más bajo se registra para Landsat TM

(RMSE= 0.21, tabla 2). MERIS y MODIS muestran una precisión parecida (RMSE=0.39 y RMSE=0.33, respectivamente) mientras que SPOT (RMSE= 0.77) y sobre todo AWIFS (RMSE=1.51) presentan errores muy elevados y no aceptables, ya que corresponden a una incertidumbre mayor que 25% del rango total del GeoCBI.

En el segundo intervalo, que corresponde a valores de severidad medio-altos (menor grado de heterogeneidad en la distribución del daño en la parcela), SPOT presenta el menor error (RMSE=0.12), seguido por MODIS y Landsat TM (RMSE=0.23 y RMSE=0.26, respectivamente). MERIS muestra un error más elevado respecto al intervalo anterior (RMSE=0.59), mientras que AWIFS, aunque mejore ligeramente, sigue presentando un error no aceptable (RMSE=0.75).

En el último intervalo, correspondientes a áreas muy quemadas y por tanto más homogéneas, MERIS destaca por su error muy reducido (RMSE=0.08), seguido por MODIS, SPOT y TM (RMSE entre 0.12 y 0.18) y, finalmente, también AWIFS presenta un error bajo (RMSE=0.28).

Si consideramos el RMSE total, los errores son muy parecidos para SPOT, Landsat TM, MERIS y MODIS (RMSE entre 0.16 y 0.23), mientras que AWIFS presenta el error más alto (RMSE = 0.51).

En la tabla 3, se muestra también el ajuste lineal entre GeoCBI observado y simulado.

Tabla 3. Error cuadrático medio (RMSE) y ajuste lineal entre GeoCBI observado y simulado, calculados para cada sensor.

SENSORES	Rangos de GeoCBI			RMSE TOTAL	Ajuste lineal entre GeoCBI observado y simulado	R^2
	2.35-2.5	2.5-2.7	2.7-3			
SPOT	0.77	0.12	0.14	0.23	y = 1.466x - 1.341	0.522
TM	0.21	0.26	0.18	0.20	y = 0.981x - 0.020	0.426
AWIFS	1.51	0.75	0.28	0.51	y = 2.25x - 3.639	0.368
MERIS	0.39	0.59	0.08	0.22	y = 0.556x + 1.296	0.152
MODIS	0.33	0.23	0.12	0.16	y = 0.229x + 2.209	0.117

Analizando las ecuaciones, solo Landsat TM muestra un ajuste muy cercano a la relación 1:1 (pendiente ≈1 y constante ≈ 0). SPOT y AWIFS presentan una subestimación acusada para GeoCBI<2.5, mientras que MERIS y MODIS sobrestiman en el mismo rango.

Finalmente, el r^2 disminuye a medida que aumenta la resolución espacial del sensor (desde 0.522 para SPOT hasta 0.117 para MODIS).

3.2 Cartografía de resultados

La figura 5 muestra los mapas de niveles de severidad resultantes de la inversión del modelo de simulación, aplicada a todas las imágenes.

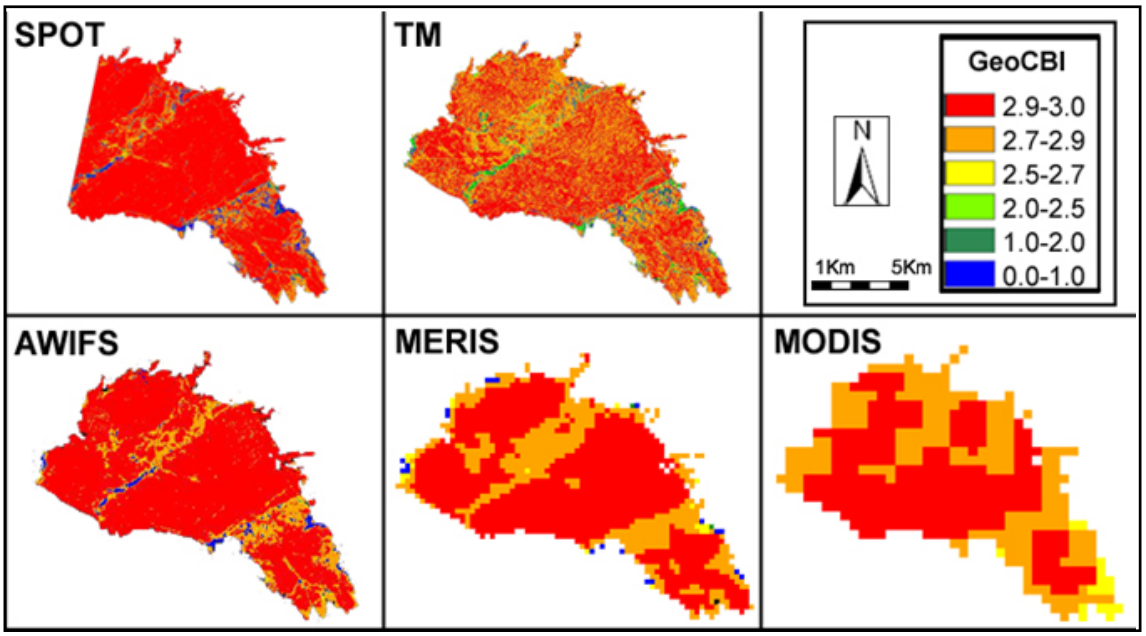

Figura 5. Mapas de severidad resultantes para cada sensor.

En todos los mapas se observa la presencia de dos franjas (orientadas NE-SO) menos afectadas por el fuego, rodeadas por áreas que presentan valores de severidad muy altos. En estas últimas, hay mayor acuerdo entre los sensores, aunque se observa una mayor homogenización a medida de que aumenta el tamaño del píxel del sensor.

En las franjas diagonales, si tomamos como referencia el mapa del Landsat TM, más preciso a la hora de estimar los valore de GeoCBI<2.5, se confirma la tendencia a la sub-estimación de SPOT y AWIFS en contraposición a la sobre-estimación de MERIS y MODIS.

4. Discusión de resultados

La correcta estimación de la severidad se basa en la correcta caracterización espectral y espacial del área quemada.

Desde el punto de vista espectral, Landsat TM y MODIS son los únicos sensores que presentan bandas en las dos regiones del espectro más importantes para discriminar los niveles de severidad: el IRC (750-1000 nm) y el SWIR2 (2000-2500 nm). El IRC es especialmente sensible a los cambios en el LAI, en la FCOV y en el estado de vigor de la vegetación, mientras que el SWIR 2 es más sensible al contenido de humedad y a las variaciones en el tipo de substrato.

Como cabe esperar, la mejor resolución espacial del Landsat TM (30 m frente a 500 m, tabla1) mejora ampliamente los resultados. En el caso de SPOT y AWIFS se nota claramente la perdida de precisión en la estimación de valores de severidad entre 2.35 y 2.5 debido a la falta de información en el SWIR2 y al escaso número de bandas. En el caso de MERIS, la falta de datos en el SWIR se ve ligeramente compensada por una alta resolución espectral (tabla 1) en el visible-NIR.

Como se nota claramente en los mapas (figura 5), SPOT y AWIFS tienden a subestimar los valores medios y bajo de GeoCBI, aunque conservan una buena descripción de la variabilidad espacial de la severidad. Por el contrario, dado que las zonas menos afectadas del incendio están localizadas en dos franjas relativamente estrechas y rodeadas por áreas con severidad máxima, los dos sensores de más baja resolución espacial (MERIS y MODIS) sobre-estiman los valores de GeoCBI<2.5.

En conclusión, el mejor compromiso entre resolución espectral y espacial para la estimación de la severidad resulta ser el sensor Landsat TM, que además asegura un comportamiento homogéneo en todos los rangos de GeoCBI. El resto de sensores podría ser empleado en áreas muy afectadas por el fuego (más homogéneas) y en las que se quiere distinguir la severidad en rangos más generales (severidad baja, media, alta).

5. Conclusiones

En este trabajo se comparan estimaciones de niveles de severidad del fuego obtenidas con cinco sensores sobre el mismo incendio. En todos los casos se ha seguido la misma metodología basada en la inversión de un modelo de simulación, ya que en trabajos anteriores hemos demostrado que permite una discriminación mejor respecto a los modelos empíricos tradicionales.

Los resultados obtenidos señalan el Landsat TM como el sensor más adecuado, porque tiene una resolución espacial idónea y bandas en los rangos del espectro más significativos en este tipo de estudios. Su precisión es homogénea en todo el rango de GeoCBI analizado y no presenta tendencias marcadas a la sobre- o subestimación. El resto de sensores presenta niveles de precisión desiguales, con mayores errores en correspondencia de los valores medios y bajos de GeoCBI.

Debido a que los datos de campo cubren un rango de GeoCBI comprendido entre 2.35 y 3, los resultados obtenidos no se pueden extrapolar directamente a valores inferiores a estos.

De cara al futuro, la puesta en órbita de nuevos sensores hiperespectrales (como el EnMAP, Kaufmann et al, 2006) permitirá una mejor descripción de la variabilidad espectral y espacial del área quemada.

Referencias

Alleaume, S., Hely, C., Le Roux, J., Korontzi, S., Swap, R.J., Shugart, H.H, Justice, C.O. (2005). Using MODIS to evaluate heterogeneity of biomasa burning in southern African savannahs: a case study. *International Journal of Remote Sensing.* Vol. 26, 4219- 4237.

Bakker, W. H., Schmidt, K. S. (2002). Hyperspectral edge filtering for measuring homogeneity of surface cover types. *ISPRS Journal of Photogrammetry & Remote Sensing*, Vol.56, 246–256.

Bigler, C., Kulakowski, D., Veblen, T.T. (2005). Multiple disturbance interactions and drought influence fire severity in rocky mountain subalpine forests. *Ecology*. Vol. 86, 3018-3029.

Bobbe, T., Finco, M.V., Quayle, B., Lannom, K. Sohlberg, R., Parsons, A. (2003). Field measurements for the training and validation of burn severity maps from spaceborne remotely sensed imagery. 18 pp. Salt lake City, Utah, USDA Forest Service.

Calvo, L., S. Santalla, S., Marcos, E., Valbuena, L., Tárrega, R., Luis, E. (2003). Regeneration after wildfire in communities dominated by Pinus pinaster, an obligate seeder, and in others dominated by Quercus pyrenaica, a Typical resprouter. *Forest Ecology and* Management, Vol. 184, 209-223.

Ceccato, P., Gobron, N., Flasse, S., Pinty, B., Tarantola, S. (2002a). Designing a spectral index to estimate vegetation water content from remote sensing data: Part 1 Theoretical approach. *Remote Sensing of Environment*. 82, 188-197.

Chafer, C.J., Noonan, M., Macnaught, E. (2004).The post-fire measurement of fire severity and intensityin the Christmas 2001 Sydney wildfires. *International Journal of Wildland Fire*. Vol.13, 227-240.

Chander, G., Markham, B. (2003). Revised Landsat-5 TM Radiometric Calibration Procedures and Postcalibration Dynamic Ranges. *IEEE Transactions on Geoscience and Remote Sensing*, Vol. 41(11), 2674-2677.

Chavez, P. S. (1996). Image-based atmospheric corrections. Revisited and improved. *Photogrammetric Engineering and Remote Sensing*, Vol. 62(9), 1025-1036.

Chuvieco, E., D. Riaño, D., Danson, F.M., Martín, P. (2006). Use of a radiative transfer model to simulate the post-fire spectral response to burn severity. *Journal of Geophysical Research - Biosciences* , Vol. 111(G04S09): doi: 10.1029/2005JG000143.

Chuvieco, E., De Santis, A., Riaño, D., Halligan, K. (2007), Simulation approaches for burn severity estimation using remotely sensed images, *Fire ecology*, Vol. 3(1), 129-150.

Civco, D. L. (1989). Topographic Normalization of Landsat Thematic Mapper Digital Imagery. *Photogrammetric Engineering and Remote Sensing***,** Vol. 55(9), 1303-1309.

Cocke, A. E., P. Z. Fule, Crouse, J.E. (2005). Comparison of burn severity assessments using Differenced Normalized Burn Ratio and ground data. *International Journal of Wildland Fire* , Vol. 14, 189-198.

De Santis, A., Chuvieco, E. (2007). Burn severity estimation from remotely sensed data: performance of simulation versus empirical models. *Remote Sensing of Environment*, Vol.108(4), 422-435.

De Santis, A., Chuvieco, E. (2008). GeoCBI: a modified version of the Composite Burn Index to estimate burn severity for remote sensing applications. *Remote Sensing of Environment*, en revisión.

De Santis, A., Chuvieco, E., Vaughan, P. J.(2008). Short-term assessment of burn severity using the inversion of the GeoSail model. *Remote Sensing of Environment*, en revisión.

Díaz-Delgado, R., Lloret, F., Pons, X. (2003). Influence of fire severity on plant regeneration by means of remote sensing imagery. *International Journal of Remote Sensing,* Vol. 24(8), 1751-1763.

Generalitat Valenciana (1988). Respuesta y adaptación de la vegetación al fuego. *Los incendios forestales en la Comunidad Valenciana.* Valencia, Generalitat Valenciana, Conselléria d'agricultura, 49-55.

FINNEY, M.S., Mchugh, C.W., GRENFELL, I.C. (2005). Stand- and landscape-level effects of prescribed burning on two Arizona wildfires. *Canadian Journal of Forest Research.*Vol.35, 1714-1722.

Huemmrich, K.F. (2001). The GeoSail model: a simple addition to the SAIL model to describe discontinuous canopy reflectance. *Remote Sensing of Environment*, Vol. 75, 423-431.

Hudak, A.T., Robichaud, P.R., Evans, J.B., Clark, J., Lannom, K., Morgan, P., Stone, C. (2004). Field validation of Burned Area Reflectance Classification (BARC) products for post-fire assessment. *Proceeding of Remote Sensing for field users-Tenth Forest Service Remote Sensing Applications Conference,* Salt Lake City, Utah, April 5-9, 2004.

Hyde, K., Woods, W.W., Donahue, J. (2007). Predicting gully rejuvenation after wildfire using remotely sensed burn severity data. *Geomorphology.* Vol.86, 496-511.

Isaev, A.S., Korovin, G.N,, Bartalev, S.A., Ershov, D.V., Janetos, A., Kasischke, E.S., Shugart, H.H., French, N.H., Orlick, B.E., Murphy, T.L. (2002). Using remote sensing for assessment of forest wildfire carbon emissions. *Climate change.*Vol.55 (1-2), 231-255.

Jacquemoud, S. (1990). PROSPECT: a model to leaf optical properties spectra. *Remote Sensing of Environment*, Vol. 34, 74-91.

Jacquemoud, S., C. Bacour, Poilve, H., Frangi, J.P. (2000). Comparison of Four Radiative Transfer Models to Simulate Plant Canopies Reflectance: Direct and Inverse Mode. *Remote Sensing of Environment*, Vol. 74, 471-481.

Kaufmann, H. Segl, K. Chabrillat, S. Hofer, S. Stuffler, T. Mueller, A. Richter, R. Schreier, G. Haydn, R. Bach, H. (2006). EnMAP. A Hyperspectral Sensor for Environmental Mapping and Analysis. In: *Geoscience and Remote Sensing Symposium IGARSS '06*, 1617-1619. doi: 10.1109/IGARSS.2006.417

Key, C.H., Benson, N. (1999). Datos no publicados presentados en la siguiente pagina web: http://www.nrmsc.usgs.gov/research/dnbr.htm.

Key, C.H., Benson, N. (2005). Landscape Assessment: Ground measure of severity, the Composite Burn Index; and Remote sensing of severity, the Normalized Burn Ratio. In: *FIREMON: Fire Effects Monitoring and Inventory System* (D.C. Lutes, R.E. Keane, J.F. Caratti, C.H. Key, N.C. Benson and L.J. Gangi, Eds.), USDA Forest Service, Rocky Mountain Research Station, Gen. Tech. Rep. RMRS-GTR-164, Ogden, UT, pp. CD:LA1-LA51.

Kokaly, R.F., Rockwell, B.W., Haire, S.L., King, T.V.V. (2007). Characterization of post-fire surface cover, soils and burn severity at the Cerro Grande Fire, New Mexico, using hyperspectral and multispectral remote sensing. *Remote Sensing of Environment*. Vol. 106, 305-325.

Kötz, B., Schaepman, M., Morsdorf, F., Bowyer, P., Ittena, K. And Allgöwer, B. (2004). Radiative transfer modeling within a heterogeneous canopy for estimation of forest fire fuel properties. *Remote Sensing of Environment*. Vol.92, 332-344.

Kötz, B., Schaepman, M., Morsdorf, F., Itten, K., Allgöwer, B., Bowyer, P. (2003). Multi-resolution Imaging Spectroscopy Resolving the Structure of Heterogeneous Canopies for Forest Fire Fuel Properties Mapping. In: I. International (Editor), *Geoscience and Remote Sensing Symposium IGARSS '03*, 2869-2871.

Kushla, J.D., Ripple, Z.A., Smith, A.M.S, Falkowski, M.J., Hudakl, A.T., Morgan, P., Lewis, S.A., Gessler, P.E., Benson, N.C. (2006). Assessing wildfire effects with Landsat Thematic Mapper data. *International Journal of Remote Sensing.* Vol.19, 2493-2507.

Lang, M., Nilson, T., Kuusk, A., Kiviste, A., Hordo, M. (2005). The performance of different leaf mass and crown diameter models in forming the input of a forest reflectance model: a test on forest growth sample-plots and Landsat ETM images. *ForestSat 2005*, Boras.

Miller, A.B, Yool, S.R. (2002). Mapping forest post-fire canopy consumption in several overstory types using multitemporal Landsat. *Remote Sensing of Environment.* Vol.82, 481-496.

Miller, J.D., Thode, A.E. (2007). Quantifying burn severity in a heterogeneous landscape with a relative version of the delta Normalized Burn Ratio (dNBR). *Remote Sensing of Environment.* Vol.109, 66-80.

Moreno, J. M., Oechel, W. C. (1989). A Simple Method for estimating fire intensity after a burn in California Chaparral. *Acta Ecologica (Ecologia plantarum)*. Vol. 10(1), 57-68.

Moreno, J. M., Oechel, W. C. (1991). Fire intensity effects on germination of shrubs and herbs in southern California chaparral. *Ecology* **,** Vol.72(6), 1993-2004.

Navarro, R. M., Navarro, C., Salas, F.J., González, M.P., Abellanas, B (1996). Regeneración de la Vegetación después de un Incendio. Aplicación de Imágenes Landsat-TM a su caracterización y seguimiento: propuesta metodológica y desarrollo parcial. *Seminario sobre Nuevas Tecnologías contra Incendios Forestales*, Madrid, ICONA.

Parra, A., Chuvieco, E. (2005). Assessing burn severity using Hyperion data. *Proceedings of the 5th International Workshop on Remote Sensing and GIS applications to Forest Fire Management: Fire Effects Assessment.* J. Riva, F. Pérez-Cabello y E. Chuvieco. Paris, Universidad de Zaragoza, GOFC-GOLD, EARSeL**,** 239-244.

Patterson , M.W., Yool, S.R. (1998). Mapping Fire-Induced Vegetation Mortality Using Landsat Thematic Mapper Data- Rincon Mountain Wilderness, Arizona, USA. *Remote Sensing of Environment.* Vol. 65, 132-142.

Pereira, J. M. C., Mota, B., Privette, J.L., Caylor, K.K., Silva, J.M.N., Sa, A.C.L. And Ni-Meister, W. (2004). A simulation analysis of the detectability of understory burns in miombo woodlands. *Remote Sensing of Environment*. Vol. 93, 296-310.

Pérez, B., Moreno, J. M (1998). Methods for quantifying fire severity in shrubland-fires. *Plant Ecology* . Vol.139, 91-101.

Robichaud, P.R., Lewis, S.A., Laes, D.Y.M., Hudad, A.T., Kokaly, R.F., Zamudio, J.A. (2007). Post fire soil burn severity mapping with hyperspectral image unmixing. *Remote Sensing of Environment.*Vol.108, 467-580.

Roy, D., P. E. Lewis, Justice, C.O. (2002). Burned area mapping using multi-temporal moderate spatial resolution data—a bi-directional reflectance model-based expectation approach. *Remote Sensing of Environment*. Vol. 83(1-2), 263-286.

Rogan, J., Yool, S.R. (2001). Mapping fire-induced vegetation depletion in the Peloncillo Mountains, Arizona and New Mexico. *International Journal of Remote Sensing.*Vol.16, 3101-3121.

Roldan-Zamarron, A., Merino-De-Miguel, S., Gonzales-Alonso, F., Garcia-Gigorro, S., Cuevas, J.M (2006). Minas de Riotinto (south Spain) forest fire: burned area assessment and fire

severity mapping using Landsat 5-TM, Envisat-MERIS and Terra-MODIS post-fire images. *Journal of Geophysical Research.* Vol. 111, Art.nº. G04S11.

Sorbel, B., Allen, J. (2005). Space-based burn severity mapping in Alaska's Nat. Parks. *Alaska Park Science*, 4-11.

van Wagtendonk, J.W., Root, R.R, Key, C.H. (2004). Comparison of AVIRIS and Landsat ETM+ detection capabilities for burn severity. *Remote Sensing of Environment* . Vol. 92**(**3), 397-408.

White, J.D., Ryan, K.C., Key, C.C., Running, S.W.(1996). Remote Sensing of forest fire severity and vegetation recovery. *International Journal of Wildland Fire.* Vol.6, 125-136.

Zarco-Tejada, P. J., Miller, J. R., Harrona, J., Hub, B., Nolandd, T. L., Goele, N., Mohammedd, G. H., Sampsond, P. (2004). Needle chlorophyll content estimation through model inversion using hyperspectral data from boreal conifer forest canopies. *Remote Sensing of Environment*. Vol.89(2), 189– 199.

La correcta estimación a corto plazo de los niveles de severidad de grandes incendios forestales representa una herramienta muy útil para ayudar a los gestores:

- ✓ a identificar las zonas prioritarias, que necesitan una intervención rápida para intentar reducir la erosión del suelo;
- ✓ a planificar las intervenciones destinadas a la recuperación del ecosistema dañado.

De hecho, la integración del mapa de severidad con los datos de pendiente y tipos de vegetación presentes antes del incendio, pueden ofrecer tanto una estimación de la erosionabilidad de suelo, como del potencial de regeneración de la vegetación.

En este contexto, la técnica de estimación de la severidad desarrollada en esta tesis doctoral representa una mejora significativa en precisión y aplicabilidad respecto a las técnicas tradicionales. Sin embargo, para seguir afinando en el modelo de simulación utilizado, pensamos que sería conveniente profundizar en las siguientes líneas de investigación.

1. En primer lugar, dado que las áreas de estudio analizadas presentaban en su gran mayoría valores medio-altos de severidad, se intentará validar el modelo en otras áreas que cubran todo el rango de GeoCBI con una distribución más homogénea de valores.

2. Por otro lado, se validará el modelo en otros ecosistemas siguiendo dos líneas paralelas de estudio:

- ✓ una experimentación de laboratorio a nivel de hoja para cuantificar los parámetros biofísicos (en hojas verdes y quemadas) de las especies más comunes de ecosistemas no mediterráneos, que representan los parámetros de entrada del modelo PROSPECT.
- ✓ La validación en otros incendios con datos de campo.

3. También, se estudiará la aplicabilidad de los modelos de simulación para la estimación de la severidad a medio y largo plazo (a partir de un año después del incendio). Para abarcar este último punto, habrá que ampliar el rango de simulaciones incluyendo otros tipos de substratos, ya que las cenizas y el carbón tienden a perderse rápidamente después del incendio. Además, se intentará colaborar con el servicio forestal de Estados Unidos que cuenta con una larga experiencia en este campo.

4. Por último, se considerará la utilización de otras fuentes de datos como los sensores hiperespectrales y lidar.